DESIGN STUDY OF A SPACE MOTION SIMULATOR

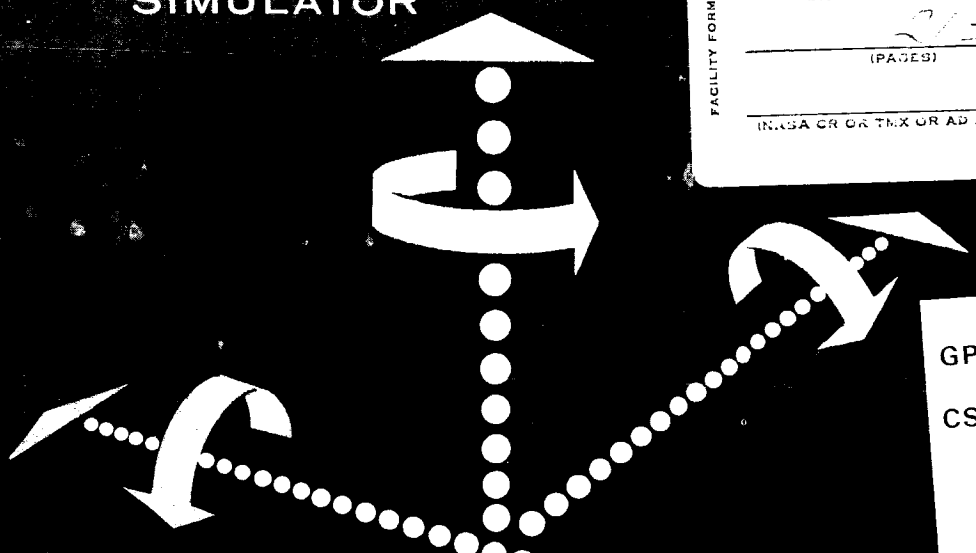

FINAL REPORT----- ER-3377

ON CONTRACT NAS9-1416

for the NASA

MANNED SPACECRAFT CENTER

by

COCKEYSVILLE
MARYLAND

MARCH 1964
Report No. ER-3377

DESIGN STUDY

OF A SPACE MOTION SIMULATOR

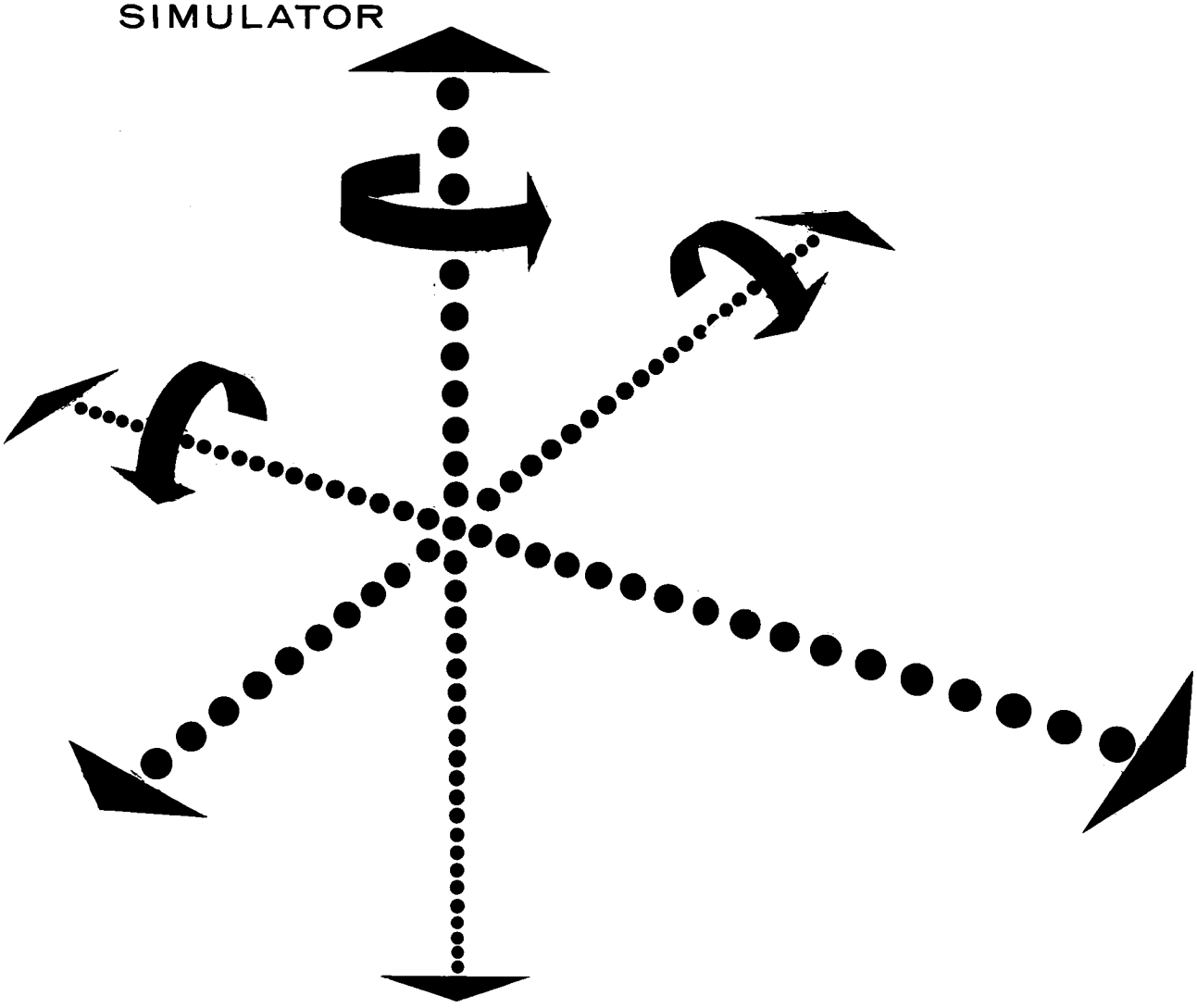

FINAL REPORT----- ER-3377

ON CONTRACT NAS9-1416

for the NASA

MANNED SPACECRAFT CENTER

by

AAI

COCKEYSVILLE
MARYLAND

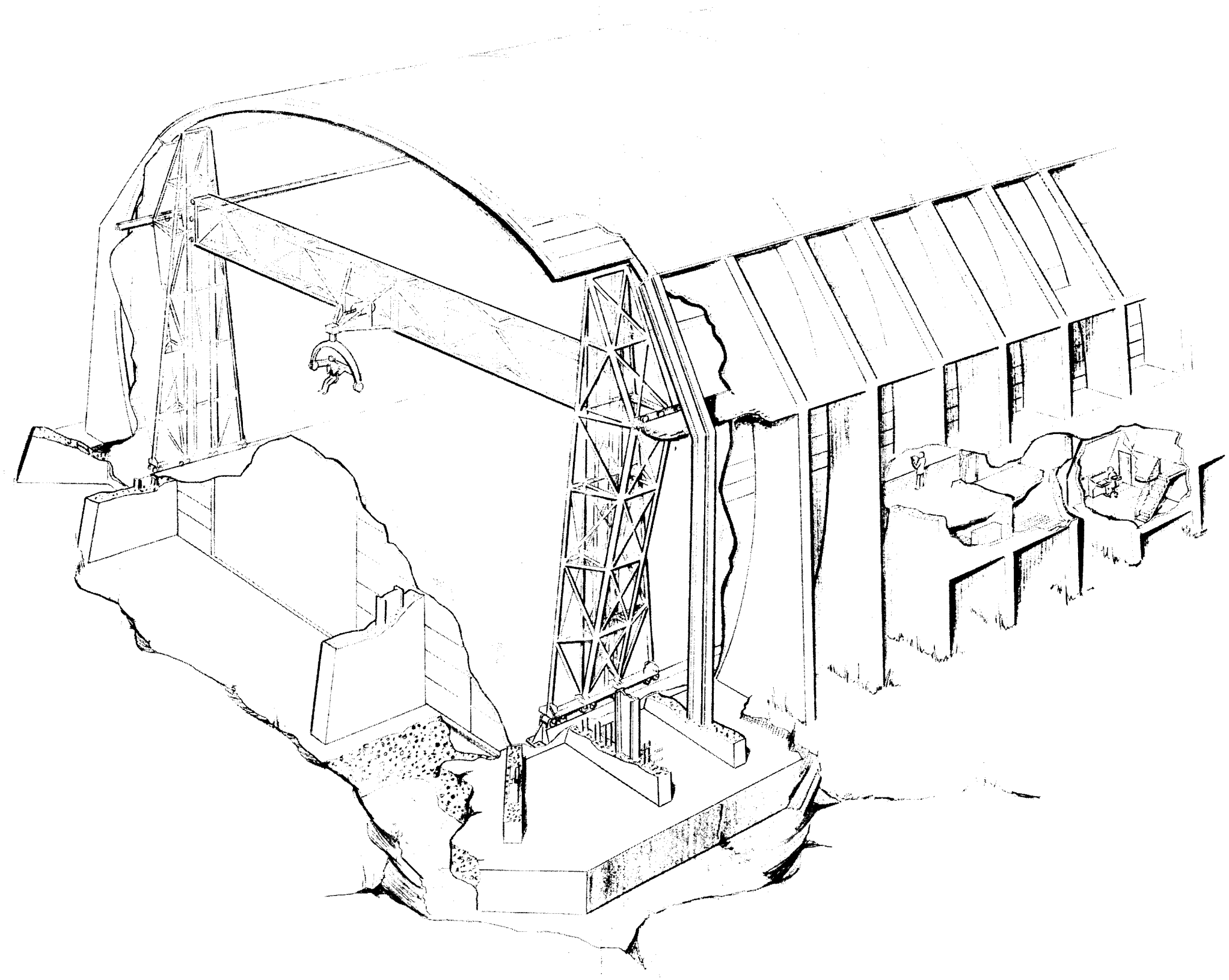

TABLE OF CONTENTS

TABLE OF CONTENTS (Continued)

TABLE OF CONTENTS (Continued)

ACKNOWLEDGEMENTS

The authors wish to acknowledge the direction of Messrs. A. Assadourian and H. I. Johnson in this design study.

In addition to the listed authors, various staff members at AAI and Barry Controls contributed substantially to the study and wrote contributing portions of this report. AAI personnel included G. J. Granros, who performed the majority of the analog simulation and wrote Section 2.4; L. M. McClernan and M. P. Ranc, Jr., who directed most of the testing and modifications of the support harness, conceived and developed the fiberglass support harness, and wrote the majority of Section 3; R. G. Sanford and M. S. Hess, who contributed substantially to the structural analysis in Section 2.1 and Appendix A; F. E. Flesher, who performed the conceptual design of the support harness for a man in a back-pack propulsion unit and made many of the line drawings in the report; S. Dutton, who acted as a test subject for the experiments described in Sections 3 and 4; and G. Cook, who contributed a majority of the art work. The analysis presented in Section 2.2 was prepared by Mr. J. E. Ruzicka, of Barry Controls, Inc., under sub-contract to AAI.

PREFACE

In a previous design study for the Manned Spacecraft Center of the National Aeronautics and Space Administration, AAI considered the problems which one would encounter in building a large device to simulate the motion of an astronaut while under conditions of zero or reduced gravity.[1*] As a result of that study, we concluded that such a device could be built, but it must be completely driven in all motions; it would require sophisticated structural design; it must incorporate a complex sensing, drive and control system; and a large digital computer would probably be required as a part of the device. We also recommended that additional work be accomplished in three critical areas, prior to detailed design.

This report constitutes an extension to the original design study, and presents at least partial solutions to those problems which we considered to be most critical in preliminary design of the simulator. In addition to providing a quantity of useful design data, the current work has strengthened our conviction that this device is indeed feasible.

---

* Superscript numbers denote references in Section 6.

1. INTRODUCTION

The work reported herein has been accomplished for the Manned Spacecraft Center of the National Aeronautics and Space Administration under Contract NAS 9-1416. It consists of three phases, each related to one of the three areas which were recommended for further design study in reference 1. These phases are:

I. Redesign of simulator structure and computation of its vibratory response to external forces, in damped and undamped configurations.

II. Further design and experimentation on harnesses to hold test subjects in the simulator.

III. Acquisition of data on maximum angular accelerations which humans can achieve under their own muscle power, to more accurately define the upper limits of rotational motion for the simulator.

In Phase I, the work has been divided into the following tasks:

1. Redesign the simulator structure, using the 75' x 75' x 200' size and the general configuration recommended in reference 1, but reducing the overall fundamental structural frequency from 10 cps to 4 cps, and employing viscoelastic damping in the structure. Employ more exact analytical techniques in the vibration analysis to investigate the possibility of markedly reducing structural weight with or without the addition of damping.

2. Reassess motor drive powers and weights, based on structural changes in 1.

3. Make comparative computations of response of structure, drive and control systems for the lightly-damped high-frequency structure, and the heavily-damped low-frequency structure.

4. Make budgetary estimates of total cost of the simulator, exclusive of the computer, for three sizes from 50' x 50' x 200' to 100' x 100' x 200', assuming a damped structure with a 4 cps frequency. For one size, estimate cost for a 10 cps, undamped structure.

The results of our work on this phase are given in Section 2 of this report.

For the work in Phase II, the following tasks are delineated:

1. Construct a test rig for evaluating the existing man-support harness, modify the harness so that it comfortably supports a man in any static position or rotational mode while he is dressed in conventional clothing.

2. Devise a method for supporting a man in the simulator while he is wearing a back-pack propulsion unit.

3. Make and test a harness for supporting the man in the simulator while he is encased in a pressurized space suit.

Results of work on these tasks are described in detail in Section 3.

In Phase III, the tasks are outlined as:

1. Build an air-bearing support device which allows unlimited freedom of rotation about the vertical axis, as well as freedom of translation on a level floor.

2. Conduct tests to determine maximum angular accelerations and velocities which a man can achieve under his own muscle power.

3. On completion of tests, deliver rotational air-bearing platform to NASA-MSC. Section 4 contains a description of our efforts on these tasks.

The remainder of the report contains a brief summary of the program (Section 5), a list of references (Section 6), and appendices (Section 7) which contain supporting analyses and data which are too voluminous or too detailed for inclusion in the body of the report.

2. NEW STRUCTURAL DESIGN

In this section, we will report our efforts on Phase I of the contract. We will first describe in some detail our improved techniques for analysis of the vibrations of the simulator structure, under the assumption that no artificial damping has been added, and will estimate new weights and moments of inertia of the undamped structure for several fundamental vibration frequencies. Next, we will report on the feasibility of inclusion of viscoelastic damping in the simulator structure, and will discuss recommended techniques for application of this damping material. Based on the revised structural weights, we will reassess the requirements for driving equipment, computing new powers and weights. The effectiveness of the structural damping technique will be determined by analog computer studies of response to transient force input of the relatively stiff, undamped structure and the relatively limber, damped structure, plus the drive and control system. The section will be completed by a budgetary cost estimate for detail design and construction of the simulator in several sizes, and by recommendations on structural design.

2.1 Structural Vibrations

2.1.1 General

As discussed in reference 1, one of the major design problems associated with the design of a dynamic simulator is the determination of a simulator structure that is compatible with the drive system. The power of the drive system is directly related to certain physical characteristics of the simulator, primarily the mass and moments of inertia

of the moving parts of the structure. From the standpoint of drive system design, the system that requires the minimum power is the optimum one. A minimum power drive system therefore dictates a light weight and low interia structure for the moving parts of the simulator. While a design based on low drive power requires a low weight and inertia structure, these characteristics must be tempered by the requirement that, to insure reasonable accuracy of response, the simulator's overall fundamental structural frequency should lie well above the highest forcing frequency of the drive system. Based on these two requirements, the design approach is to achieve a structure which is stiff enough to meet the fundamental frequency requirement and yet is sufficiently low in mass and moment of inertia to be driven by an available drive system. The basic structure is shown in Figure 1.

Because the structure of this simulator is complex in its makeup and its vibration response as a dynamic system this investigation can only produce approximate results. To accurately obtain the vibration characteristics of the simulator structure and verify the analytical investigation, the construction and testing of a small scale dynamic model is necessary. The technique of dynamic modeling provides an inexpensive technique for verifying the vibration characteristics of a complex structure prior to the construction of the full scale structure.

The vibration analyses reported in reference 1 contained many conservative assumptions of boundary and loading conditions. It was also tacitly assumed that the structure was lightly damped, and therefore the

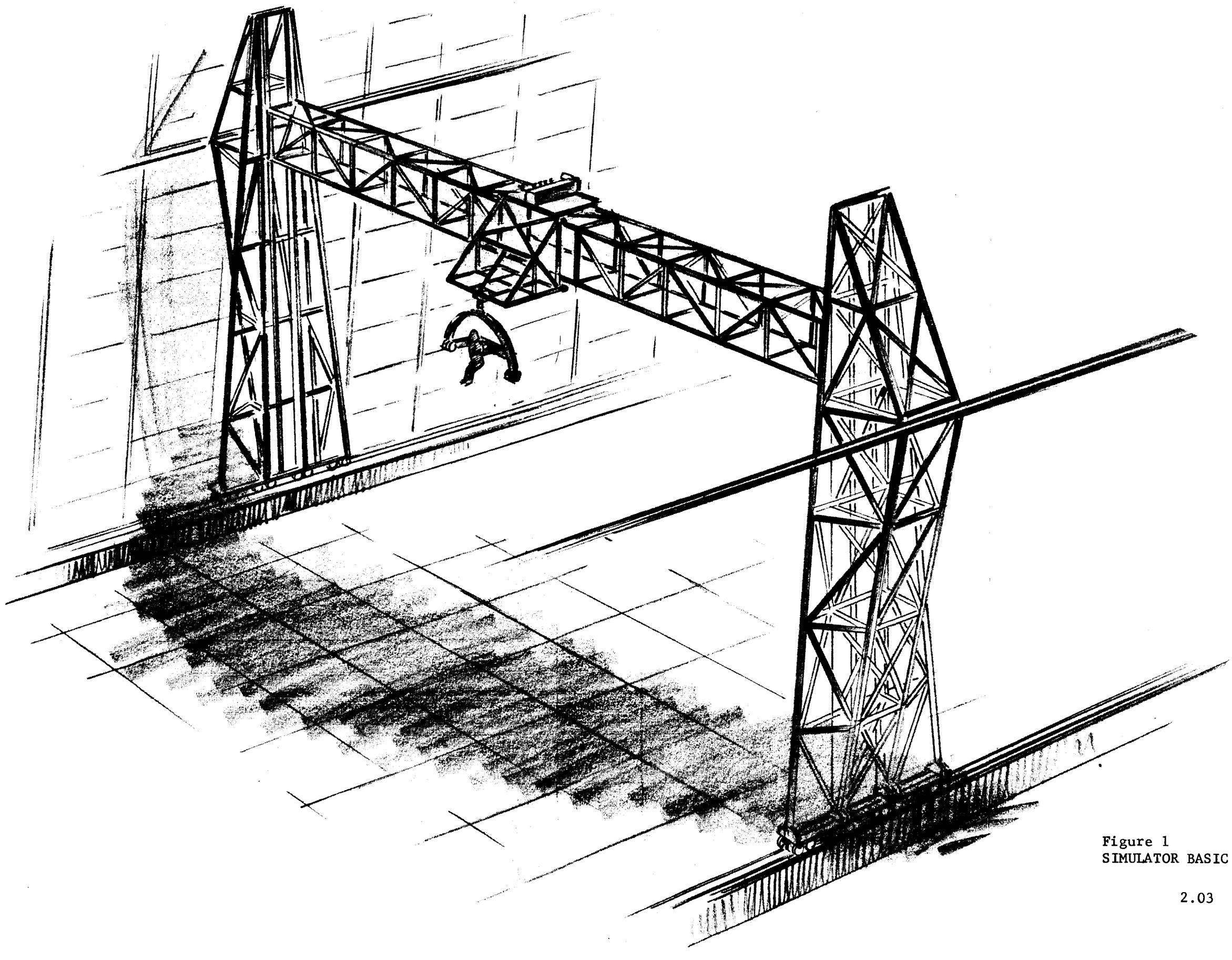

Figure 1
SIMULATOR BASIC STRUCTURE

fundamental frequency of the structure should lie well above the greatest forcing frequency of the drive system.

In the current study a new vibration analysis was derived utilizing more realistic boundary and loading conditions. Once again, some conservative assumptions were made to simplify the analysis. The frequencies of the various arms of the gimbal system were combined to obtain overall frequency for the gimbal system. The frequencies of the Cross Span Dolly, Cross Span and Vertical Trusses were obtained by considering each as a separate element. In order to allow for the coupling effect of the various elements of the simulator each element was designed for a 5 cps frequency to insure that the overall frequency of the simulator was near 4 cps. The justification for using a fundamental design frequency of 5 cps for each element of the simulator can be proven by the following brief analysis. Considering the cross span and gimbal system as a two degree of freedom system, with M_1, the mass of the gimbal system, cross span dolly, cross span and drive system hardware and M_2, the mass of the simulator payload the system can be shown schematically as follows:

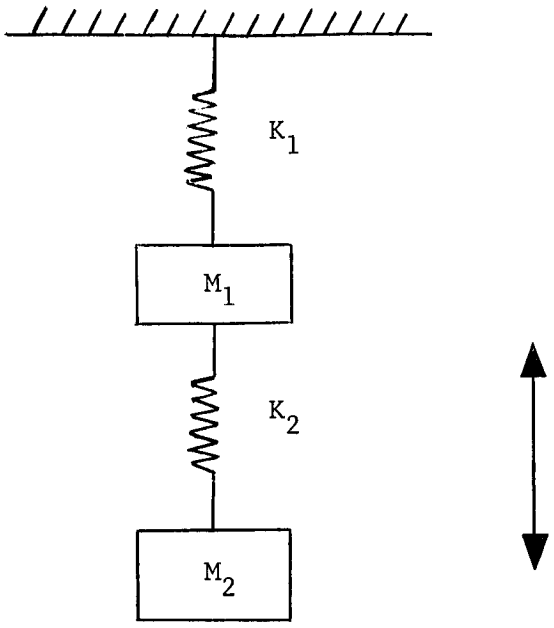

The circular frequency equation for this elastic system with two degrees of freedom is given by the following equation.[3]

$$\omega^2 = \frac{1}{2}\left[\frac{K_1 + K_2}{M_1} + \frac{K_2}{M_2} \pm \left[\frac{(K_1 + K_2)^2}{M_1^2} + \frac{2K_2(K_2 - K_1)}{M_1 M_2} + \frac{K_2^2}{M_2^2}\right]^{\frac{1}{2}}\right] \quad \ldots(1)$$

The lower frequency is given by the minus sign. From this equation let us determine the values of $\frac{K_1}{M_1}$ and $\frac{K_2}{M_2}$ which will give a lower natural frequency of $f = \frac{\omega}{2\pi} = 4$ cps. Assuming $K_2/M_2 = K_1/M_1$ we get

$$2\omega^2 = \frac{K_1}{M_1}\left[2 + \frac{M_2}{M_1} - \left[\left(\frac{M_2}{M_1}\right)^2 + 4\frac{M_2}{M_1}\right]^{\frac{1}{2}}\right] \quad \ldots(2)$$

Now, $\omega_1^2 = \frac{K_1}{M_1}$ is the circular vibration frequency for a single degree of freedom system. Since $\frac{K_2}{M_2} = \frac{K_1}{M_1}$, $\omega_2^2 = \omega_1^2$. Since we wish to determine this frequency for a fixed value of ω and various values of the mass ratio $M_2/M_1 = R$ equation (2) now becomes

$$\left(\frac{\omega_1}{\omega}\right)^2 = \frac{2}{\left[2 + R - \left[R^2 + 4R\right]^{1/2}\right]} \qquad \ldots(3)$$

In our system M_2, the mass of the payload, is always considerably less than M_1 the mass of the gimbal system, cross span dolly and cross span. For example if M_1 = 6000 lbs and M_2 = 600 lbs R will equal (.10). ω_1 will then equal

$$\left(\frac{\omega_1}{\omega}\right)^2 = \frac{2}{2 + .1 - \left[(.1)^2 + 4 \times (.1)\right]^{1/2}}$$

$$= \frac{2}{2.10 - .64}$$

$$= 1.37$$

$$\omega_1 = \omega\sqrt{1.37}$$

$$\omega_1 = 4 \times 1.17$$

$$\omega_1 = 4.68 \text{ cps}$$

Thus the designing of each element of the simulator structure for 5 cps will insure that the overall frequency of the simulator will be equal to at least twice the 2 cps operating frequency of the simulator drive system.

Designing the simulator structure for a 4 cps fundamental frequency will greatly reduce its weight.

Selection of this low design frequency was made on the assumption that heavy damping could be incorporated into the structure through the use of viscoelastic damping material. The introduction of this material in the structure will reduce the amplification of the structural vibrations caused by the drive system operation. The incorporation of viscoelastic damping material into the structure while

increasing the damping capacity of the structure will at the same time increase the weight of the structure. If this increase in weight causes the total structure weight to exceed the weight of a higher frequency undamped structure then, from the standpoint of producing a minimum weight simulator, viscoelastic damping is not an adequate technique.

Details of the techniques and feasibility of applying viscoelastic damping to the simulator structure will be discussed in greater detail in Section 2.2.

2.1.2 Gimbal System

The gimbal system consists of the Roll Arm, Pitch Arm and Yaw Arm. These arms are connected together to allow the test subject to have a full 360^{o} of rotation about three axes. The clearance envelope of the gimbal system was modified from the one established in the first phase since the requirement of a full 360^{o} pitch maneuver of the spacecraft was relaxed. The new clearance envelope is shown in Figure 2. This clearance envelope is primarily[1] dictated by the functional reach limits of a 95th percentile man performing extravehicular maintenance tasks utilizing hand tools up to 24 inches in length. Using the clearance envelope, a gimbal configuration as shown in Figure 3 was established. The stiffness of each arm was determined and combined to form a series spring network with an equivalent mass.

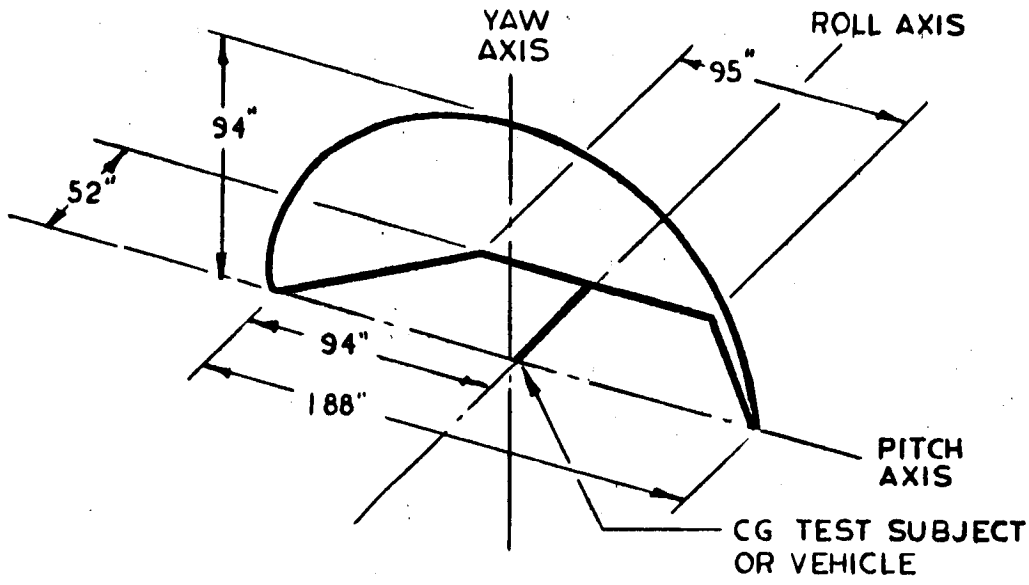

GIMBAL CLEARANCE ENVELOPE

FIGURE 2

The Gimbal System was analyzed for both fore and aft and vertical modes of vibration. The vertical mode consists of the gimbal payload vibrating in the vertical plane with the pitch arm oriented at 90^{o} to the vertical or lying in the horizontal plane. The fore and aft mode consists of the gimbal payload vibrating in the horizontal plane when the pitch arm is rotated 90^{o} clockwise from the horizontal plane or lying in the vertical plane. These modes are shown graphically in Figure 4. The fore and aft mode was found to be the controlling mode because of contributions of bending of the yaw arm out of its plane of curvature and of the torsional deflection of the arm. The spring network was then analyzed as a single degree of freedom system with no damping. The stiffness expressions for each arm were determined by applying a unit load at the payload location. The equivalent mass consisted of the payload mass and one third of the gimbal mass. The addition of one third of the gimbal mass was made to account for the fact that the mass of the gimbal arms is a significant portion of the payload mass. The factor of one third was selected by considering the gimbal system to be analogous to a single degree of freedom cantilever beam of significant mass with a payload at the free end.[4]

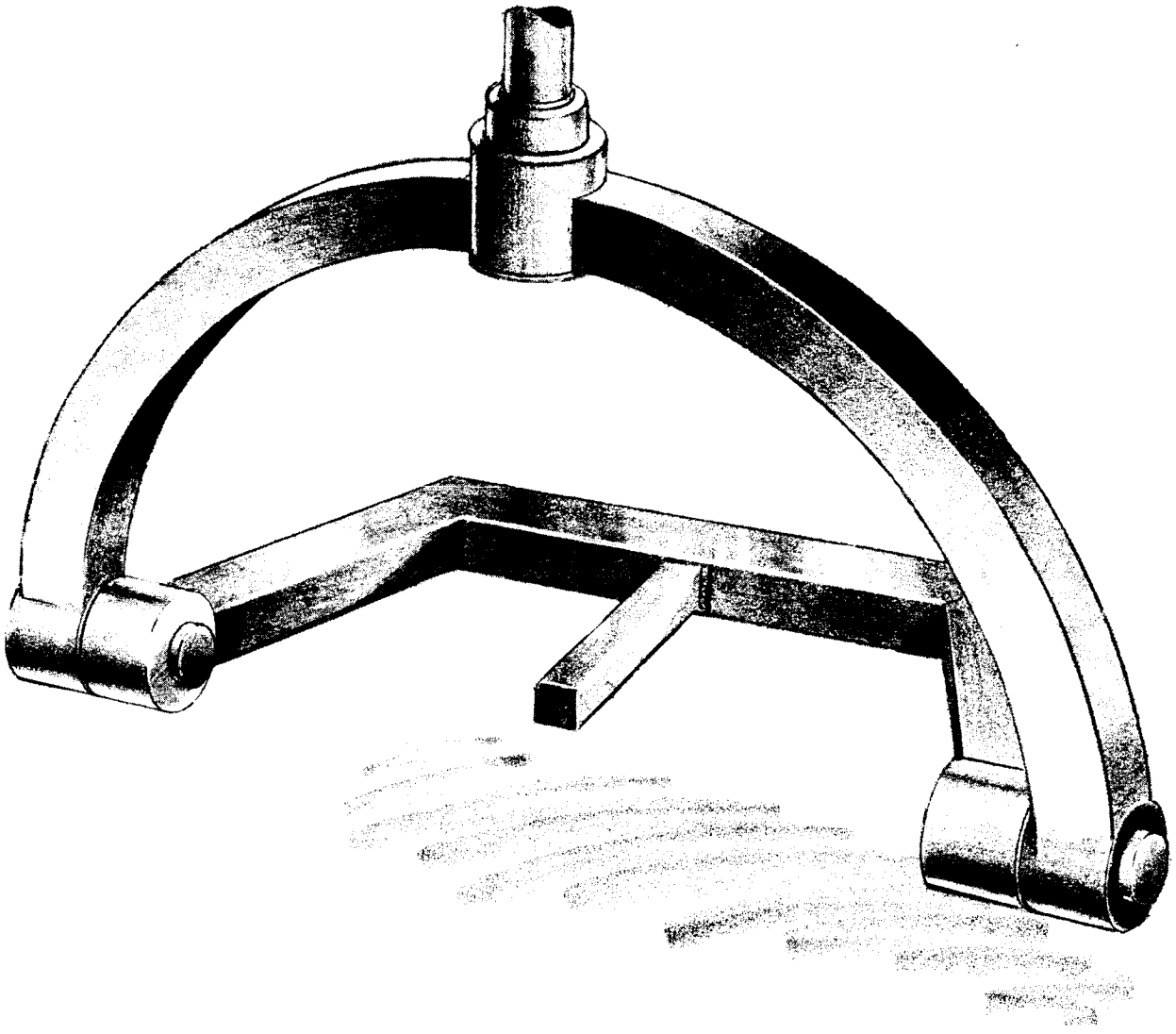

Figure 3
GIMBAL CONFIGURATION

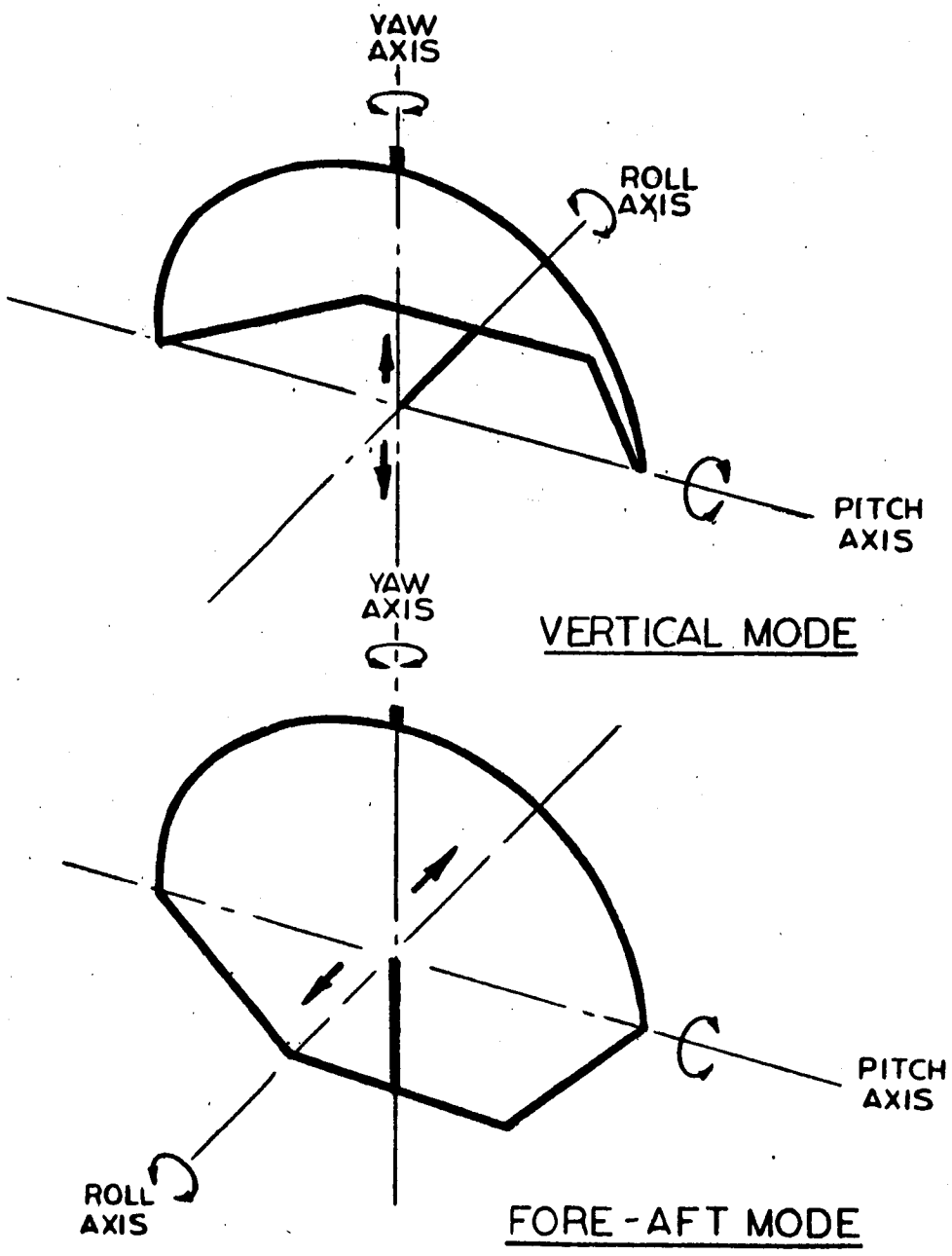

GIMBAL SYSTEM VIBRATION MODES

FIGURE 4

Since it also was necessary to design a gimbal system that was light in weight the stiffness equation

$$\delta_t = \delta_{roll} + \delta_{pitch} + \delta_{yaw}$$

$$= \frac{A''}{I_{roll}} + \frac{B''}{I_{pitch}} + \frac{C''}{I_{yaw} + K_{yaw}}$$

where δ = deflection or $\frac{1}{K}$, K being the spring constant of the member or system must be related in some manner to the gimbal system weight expression

$$W_{\substack{gimbal \\ system}} = W_{\substack{roll \\ arm}} + W_{\substack{pitch \\ arm}} + W_{\substack{yaw \\ arm}} .$$

This was done by considering the loading conditions of each arm and arriving at a structure cross section or shape that would most efficiently supply the structure strength required. In order to simplify the analysis somewhat, it was decided to use a similar section, a hollow square box, for each arm. Although the hollow square box is not as efficient in bending as a hollow rectangular box, the larger weight of the rectangular box does not warrant the increase in stiffness over the square box. The section properties and weight of a hollow square box arm can be related approximately by the following expressions.

$$I = \frac{2}{3} S^3 t, \text{ in}^4.$$

$$K = \frac{3}{2} I = S^3 t, \text{ in}^4.$$

$W = 4St\ L\rho$, lbs where

L equals the length of the arm,

$\rho = .1\#/\text{in}^3$ (Alum.)

From these expressions we can obtain the following relationship for the section inertia of each arm, I, in terms of the arm's weight.

$$I = W \frac{S^2}{6L\rho}$$

To further optimize the gimbal design and to obtain structurally realistic sizes for each arm, an S/t ratio for each arm was established. This ratio was obtained by considering the buckling of the sides of each arm. The sides were considered to be long flat plates loaded in compression, with all edges simply supported. For long flat aluminum plates in compression the Euler Equation[5] is

$$f_c = \frac{102 \times 10^6}{(K' \frac{S}{t})^2}$$

where f_c = buckling stress of plate., psi.

K' = Factor based on length and width of plate and conditions of support.

The buckling stress of the plate, f_c, for each arm was taken as four times the maximum stress in the arm. The maximum stress in each arm of the gimbal system was estimated based on the results of earlier preliminary gimbal analyses. By using the S/t ratio (R) obtained from the buckling stress, the weight of each arm could be expressed in the following manner.

$$W = \frac{4S^2L\rho}{R}$$

Using this and expression for the arm section inertia in terms of its weight we can obtain the total deflection equation for the gimbal system in terms of the weights of each arm. In final form this equation is

$\delta_t = \frac{A}{W_r^2} + \frac{B}{W_p^2} + \frac{C}{W_y^2}$. Combining this equation and the total gimbal system weight equation we can obtain expressions for the minimum weight of each arm in terms of gimbal system geometry and the desired deflection. In general these minimum gimbal arm weights are arrived at mathematically minimizing a function of three variables, $W_g = f(W_r, W_p, W_y)$. Once these expressions are obtained and added together we have an expression for the minimum gimbal system weight in terms of δ_t. Since the frequency of the gimbal system is expressed by

$$f = \frac{1}{2\pi} \sqrt{\frac{K_t}{M_e}}$$

where $K_t = \frac{1}{\delta_t}$, gimbal system spring constant

$$me = \frac{W_{pl} + \frac{W_{gs}}{3}}{g}$$, equivalent mass of gimbal system

consists of gimbal payload and one third of gimbal system structure weight. We can obtain an equation for δ_t in terms of the gimbal system weight and the desired frequency. Equating this to the minimum gimbal system equation solved for δ_t gives us an equation for the minimum gimbal system weight in terms of the gimbal configuration and desired frequency Then from the gimbal system weight the individual arm weights and sizes can be determined. The details of this method of analysis and a sample solution are found in Appendix A of this report.

The gimbal configuration was evaluated for design frequencies of 5, 10 and 15 cps and the results of these evaluations are shown in Table I. The arm mass moments of inertia were calculated in the manner

GIMBAL CONFIGURATIONS

5 CPS GIMBAL SYSTEM

Arm	Weight (lbs)	S (inches)	I (inches^4)	Mass Moment of Inertia (in. lb sec^2)		
				J_R	J_P	J_Y
Roll	25	10.40	87	2	65	65
Pitch	140	10.60	122	—	626	1545
Yaw	240	11.82	191	—	—	2750
Total Gimbal Weight	= 405 lbs					

10 CPS GIMBAL SYSTEM

Arm	Weight (lbs)	S (inches)	I (inches^4)	Mass Moment of Inertia (in. lb sec^2)		
				J_R	J_P	J_Y
Roll	47	18.80	538	14	110	110
Pitch	218	17.95	546	—	1001	2421
Yaw	370	19.95	830	—	—	4225
Total Gimbal Weight	= 635 lbs					

15 CPS GIMBAL SYSTEM

Arm	Weight (lbs)	S (inches)	I (inches^4)	Mass Moment of Inertia (in. lb sec^2)		
				J_R	J_P	J_Y
Roll	63	27.20	1489	40	147	147
Pitch	316	23.40	1339	—	1432	3548
Yaw	537	27.40	2522	—	—	6810
Total Gimbal Weight	= 916 lbs					

TABLE I

shown in Appendix A. From the results shown in Table I it can be seen that the yaw arm has the most inertia and weight of the gimbal arms. This led to an investigation of a tapering yaw arm with the hope of significantly reducing the yaw arm inertia and weight. An expression was established to allow the section moment of inertia of the yaw arm to vary linearly from a minimum value at the pitch arm attachment point to a maximum at the cross span dolly attachment point. The expression chosen was $I = I_o (1 + T \phi)$. The constant T was varied from zero to $\frac{14}{\pi}$ in value(*). The results of this investigation showed that for each design frequency the tapering produced a maximum of 15 to 20 pounds reduction in weight and a maximum of 20% reduction in the mass moment of inertia of the yaw arm. Although the reduction in mass moment of inertia is significant, consideration must be given to the fact that, in the actual calculation of the yaw arm mass moment of inertia for drive power requirements, the inertia of the pitch arm drive motors must be added. Since these motors are relatively heavy in weight and located at a great distance from the yaw axis their effect on the mass moment of inertia is considerable. Their effect when added to the 20% reduction due to tapering causes the inertia to practically remain the same as that of a constant section yaw arm. This coupled with the

(*) Since $I = 2/3\ S^3 t$ the expression for the maximum section side for each value of T becomes

$$S = S_o \sqrt[3]{1 + \frac{T\pi}{2}}$$

For $T = 14/\pi$ then the sides of the section are twice as big at the yaw axis end as at the pitch arm attachment end.

increased cost of manufacturing does not warrant using a tapered yaw arm in the final gimbal configuration.

It should be noted that, although the gimbal configurations shown in Table I represent arms that are staticaly stressed to very low levels due to being stiffness designed, some structural weight will be added to account for local strengthening of the arms in the areas of drive motor attachment and control system component mounts.

2.1.3 Translation System

The translation system of the simulator consists of the Cross Span dolly, Cross Span Truss and Vertical Trusses. The purpose of these elements is to provide the gimbal system and payload with translational motion in three directions.

The cross span dolly is a cantilevered truss that is mounted on wheels. It is shown conceptually in Figure 5. The wheels roll along tracks on the front face and top of the cross span truss. The wheels are provided with slipper assemblies to resist the moments caused by the gimbal system. For analysis purposes the dolly was considered a single degree of freedom cantilever beam with a payload at the free end undergoing symmetric bending. To minimize the weight of dolly the cross section of dolly varied along its length of 50 inches according to the following approximate relationship.

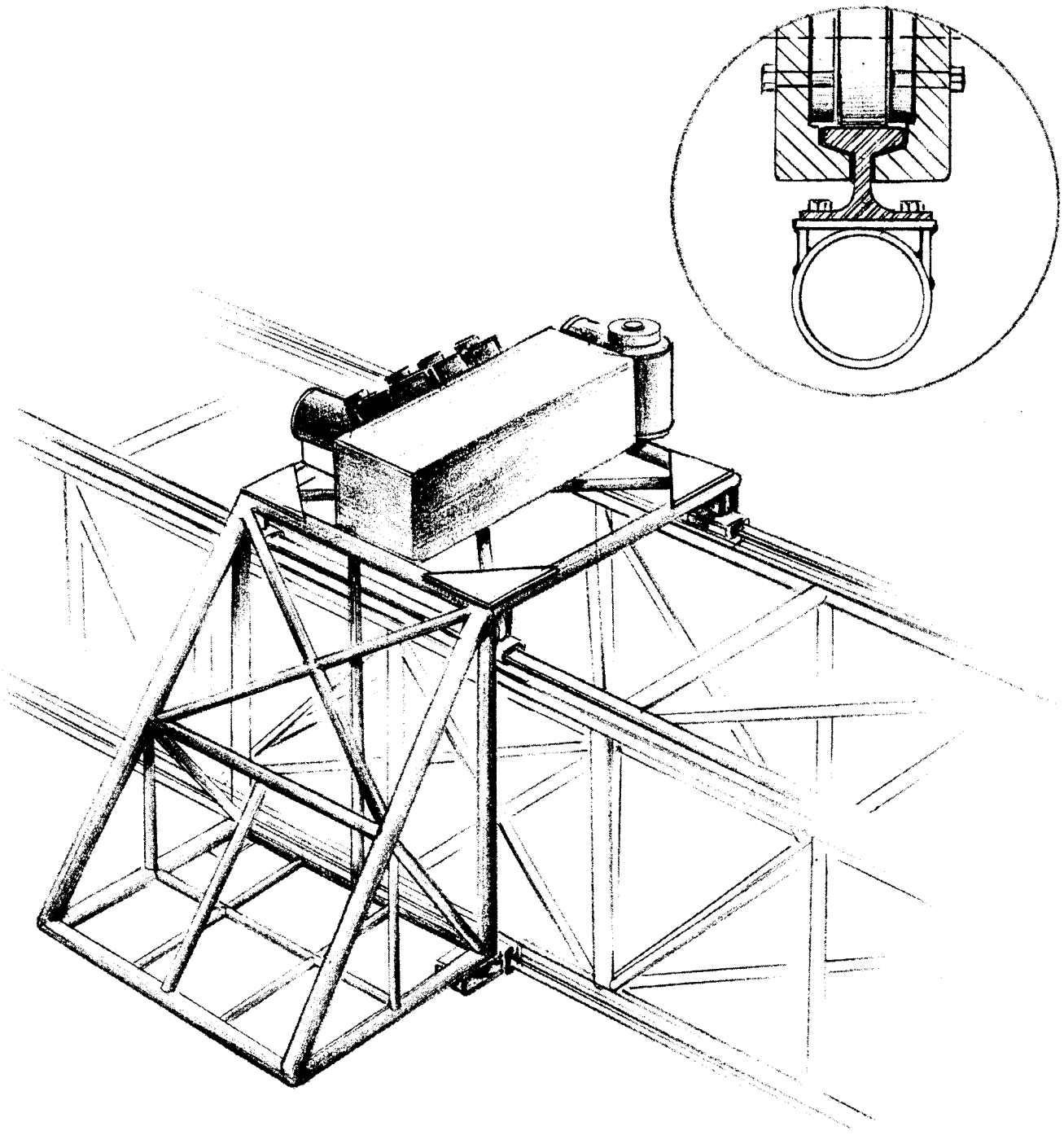

Figure 5
CROSS SPAN DOLLY

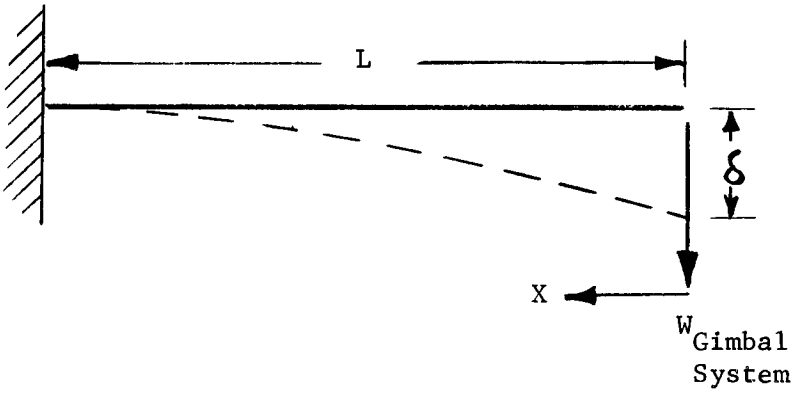

$$I(X) = I_o \left(\frac{X}{L}\right)^2$$

where I_o is the section moment of inertia of the dolly at the base. Using this relationship and the method of unit loads, a stiffness equation for the dolly was derived. With this equation and the frequency equation, $f = \frac{1}{2\pi}\sqrt{\frac{K}{m}}$, where m^* equals the payload at the free end of the beam, a value for I_o was determined for a given frequency. Results of the analysis showed that designing the dolly for a frequency greater than five times the design frequency of the other elements of simulator produced a very stiff structure for a small amount of weight. The section moment of inertia and the weight of the cross span dolly truss were calculated using the following relationships.

---

* No portion of dolly weight is included since the mass of the dolly is small in comparison to the mass of the payload.

$I = \frac{1}{2} Ad^2$, inches^4

d = depth of truss, inches

$A/_2$ = cross sectional area of each longitudinal member of truss

$W = 2AL\rho K$

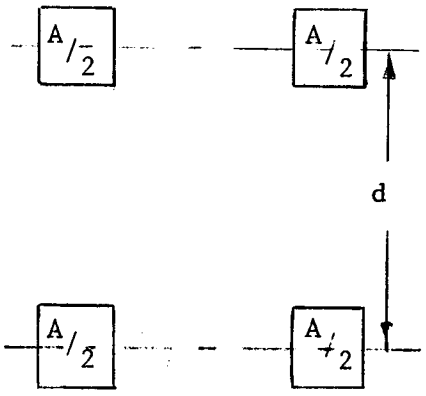

Beam Cross-Section
Dumbbell

L = length of truss, inches

ρ = .1#/in^3 (Aluminum)

$K \overset{(*)}{=} 3$ = weight factor for shear members of the truss.

The complete analysis of the cross span dolly truss and a sample solution are found in Appendix A of this report. Again it is emphasized that the weight determined in Appendix A for the dolly do not include allowance for local strengthening of the dolly for mounting the drive and control components.

(*) This factor was increased from the 1.5 used in first preliminary analysis to insure that the shear deflection of the truss is low and thereby make the beam frequency calculations valid.

The cross span truss is analyzed as a uniform beam undergoing bending vibrations. This beam has a concentrated mass at the center and is supported at the ends by springs which oppose rotation of its ends. Schematically, this can be shown as follows.

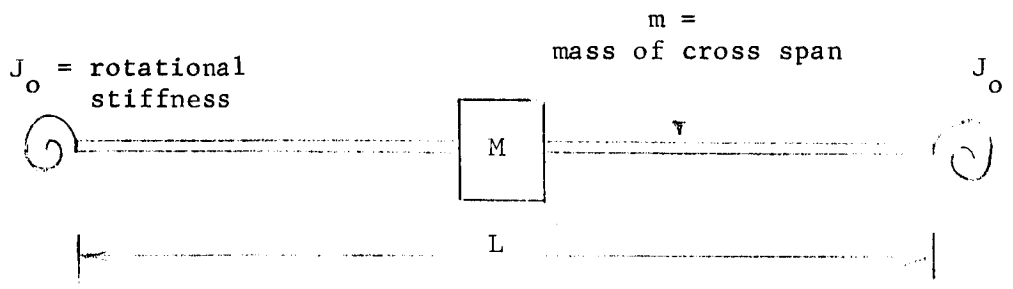

The analysis was conducted to determine the fundamental frequency for both the symmetric and asymmetric bending mode of vibration. The rotational stiffness, J_o, is provided by the vertical trusses on which the cross span is mounted. To physically obtain this rotational stiffness in the simulator, the wheels on the cross span would be provided with slipper assemblies. These slippers would engage with the rails mounted on the vertical trusses. The cross span and its slipper assemblies are shown conceptually in Figure 6.

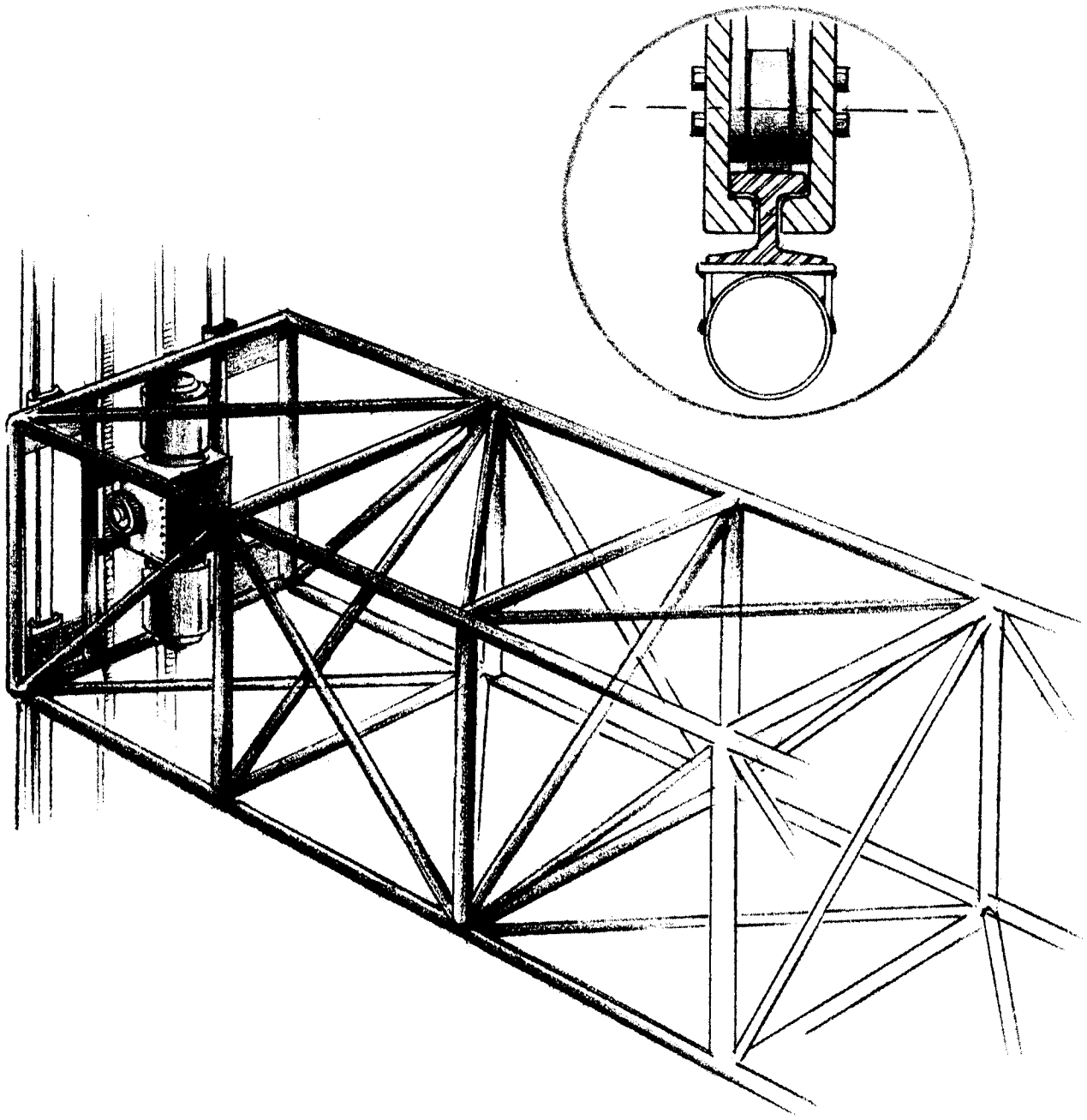

Figure 6
CROSS SPAN TRUSS

The mass at the center, M, consists of the mass of the cross span dolly and equipment, gimbal system and equipment and the simulator payload. For a 5 cps simulator these values are as follows:

Gimbal Structure	= 405 lbs
Gimbal Equipment(*)	= 1233 lbs
Gimbal Payload (mockup of spacecraft)	= 600 lbs
Cross Span Dolly Structure	= 150 lbs
Cross Span Dolly Equipment	= 3814 lbs
TOTAL (M)	= 5602 lbs

The solution of the frequency equations for symmetric and asymmetric bending for the first root, λ_1, was obtained for various values of the parameters $\frac{JoL}{2EI_{c.s}}$, $\frac{M}{m}$ and $\frac{4N}{mL^2}$. The parameter $\frac{JoL}{2EI_{c.s}}$ represents the relative value of rotational constraint provided by the vertical trusses. A value of zero for this parameter corresponds to a simple supported beam and a value of infinity to a beam with fixed end conditions. Since it is not feasible to physically obtain a value of ∞, we selected a value of 5 which we feel can be obtained without excessive cost and complexity. The parameter $\frac{M}{m}$ is the ratio of the mass at the center of the cross span to the mass of the cross span. This ratio and a value of $\frac{JoL}{2EI_{c.s}}$ will give one root, λ_1, of the symmetric bending frequency equation. The parameter $\frac{4N}{mL^2}$ is a parameter that relates the

(*) For detailed breakdown of this weight see Section II of Appendix A.

effect of the mass moment of inertia, N, of the center mass, M, to the asymmetric mode of vibration. With a value of this parameter and $\frac{JoL}{2EI_{c.s}}$ one root, λ_1, of the asymmetric bending frequency can be obtained. Thus, once a value of λ_1 is established based either on the symmetric or asymmetric mode, a value of the beam frequency can be obtained.

Using the equations

$$\omega = 2\pi f_1 = \frac{\lambda_1^2}{L} \sqrt{\frac{EI_{c.s}}{ML}}$$

$$I = \frac{1}{2} Ad^2$$

$$M = \frac{2\, AL\rho\, K}{g}$$

See page 2.23 for definition of these terms

a relationship for λ_1 can be obtained.

This relationship is

$$\lambda_1 = \frac{4\pi f L^2}{d} \sqrt{\frac{\rho K}{E g}} .$$

Thus by picking a depth of the cross span, d, the beam frequency, beam material and length a value for λ_1 can be determined. By using this value and the selected value of $\frac{JoL}{2EI_{c.s}}$ the size and weight of the cross section truss can be determined for either symmetric or asymmetric mode of vibration. A comparison of the results between the symmetric and asymmetric mode indicates that the symmetric mode of vibration is of lower frequency. It should be noted that this comparison is based on an approximate calculation of the mass moment of inertia of the cross span center mass. Also because the structure is complex, the use of dynamic modeling to prove that the symmetric mode is the governing mode is desirable.

With the cross span configuration established the rotational stiffness, J_o, of vertical trusses can be determined. Using J_o, the size and weight of vertical trusses can be determined by considering the loading conditions of the vertical trusses. The vertical trusses can vibrate in the bending modes shown below.

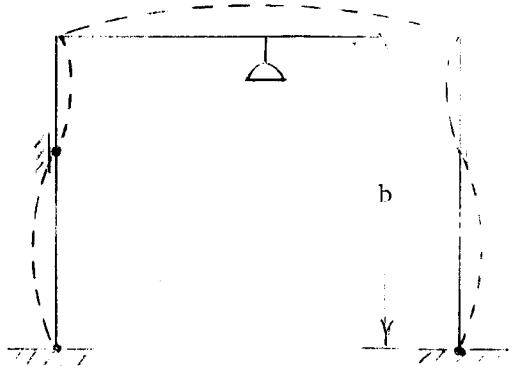

Symmetric Mode

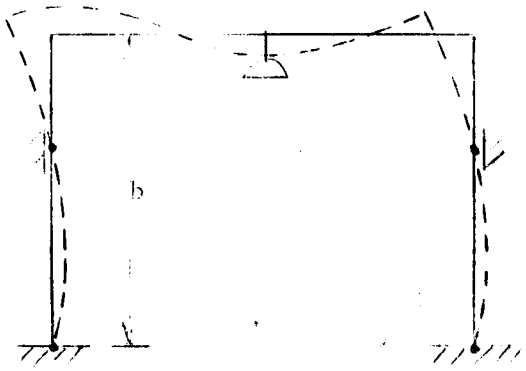

Asymmetric Mode

Since the loading conditions of the vertical truss vary with the position of the cross span, several conditions for each mode of vibration were analyzed. The results indicate that when the vertical position (b) of the cross span on the vertical truss is greater or equal to one half the length of the vertical truss (L) the rotational stiffness, J_o, is a minimum and therefore the designing condition. For these conditions J_o is equal to $\frac{3EI_{vt}}{b}$ where I is the section inertia of vertical truss. Using this criterion and the triangular truss configuration established in the first phase of the study program the weight and stiffness of the vertical trusses were determined. It should be pointed out that the analysis of the vertical trusses was accomplished by using a relatively simple analysis with many assumptions. These assumptions were necessary

because of the complex nature of the structure. The configuration of the vertical truss has been envisioned as a variable depth member supported at the base and at two thirds of its height. Some other configuration may be preferable. Actual determination of the type of beam cross section and support points will be made in detail design, after evaluation of the dynamic modeling results. The action of the vertical trusses under torsional vibrations is another condition that must be accounted for. To offset these many unknowns the weight of the vertical truss has been estimated in a conservative manner. The vertical truss weight was determined by selecting b in the J_o expression to be equal to two thirds the length of the truss. This selection will result in a truss whose stiffness and consequently weight will be between the maximum obtained for $b = \frac{L}{2}$ and the minimum for b = L. Using the stiffness determined by

$$J_o = \frac{3EIvt}{b} \quad \text{where } b = 2/3\ L,$$

we estimate the weight for the truss by using the dumbbell model for its cross section. In using this model we are considering the truss to be a constant cross section beam. Again the shear member weight factor was taken as 3 to keep the shear deflection low.

To show the net result of designing the simulator for a lower fundamental frequency, Table II is provided. It shows the structural weights for a 5, 10, and 15 cps simulator of the 75' x 75' x 100' configuration. The detailed analysis of the cross span and vertical trusses is found in Section III of Appendix A.

TABLE II

SIMULATOR STRUCTURE WEIGHT BREAKDOWN

5 CPS - 75 ' x 75' x 100'

Gimbal Structure	- 405 lbs	
Cross Span Dolly	- 150 lbs	
Cross Span	- 3000 lbs	60" x 5.6 in^{2*}
Vertical Trusses	- 5918 lbs	90" x 5.5 in^2
Total Simulator Structure Wt.	= 9,473 lbs	

10 CPS - 75' x 75' x 100'

Gimbal Structure	- 635 lbs	
Cross Span Dolly	- 275 lbs	
Cross Span	- 6720 lbs	90" x 12.5 in^2
Vertical Trusses	- 16800 lbs	120" x 15.6 in^2
Total Simulator Structure Wt.	= 24,430 lbs	

15 CPS - 75' x 75' x 100'

Gimbal Structure	- 916 lbs	
Cross Span Dolly	- 400 lbs	
Cross Span	- 10,940 lbs	120" x 20.3 in^2
Vertical Trusses	- 31,320 lbs	150" x 29.0 in^2
Total Simulator Structure Wt.	= 43,576 lbs	

* Denotes depth of beam (d) and one half cross sectional area (A) of beam (see page 2.23)

2.2 Techniques for Damping of Simulator Structure

In this section we will give the results of a feasibility study performed by Barry Research and Development generally dealing with structural vibration problems that have been anticipated with regard to a facility to simulate the dynamic environment encountered under conditions of reduced or zero gravity. We will first present a general discussion concerning modern viscoelastic damping concepts, with particular emphasis placed on structural fabrications employing viscoelastic shear-damping mechanisms. The effect of vibration frequency on the loss factor of viscoelastic shear-damped structures is presented qualitatively for arbitrary structural members and experimentally for rectangular cross-section beams. Primary structural members of the space motion simulator described in Reference 1 are analyzed and means of incorporating viscoelastic shear-damping mechanisms in the structural members are discussed. Estimates of the loss factors of the damped primary structural members are made. In a later section, recommendations are made for further research work that should be carried out prior to applying the recommended viscoelastic damping techniques to the structural members of the space motion simulator.

2.2.1 General

In section 2.1 of this report, we initially determined the weight and flexural rigidity properties of structural members based on stiffness requirements rather than strength requirements. On the basis that primary structural members of the simulator structural assembly would be lightly damped, it was deemed necessary to ensure that the elastic-body structural

resonances were substantially higher than predominant excitation frequencies. The control system to be employed in the space motion simulator was assumed to have a maximum excitation frequency of 2 cps; hence, structural members were designed so that the fundamental resonant frequency of primary structural members occurred in the 10-15 cps region. By maintaining a high fundamental resonant frequency of the structure (compared to the maximum excitation frequency of the control system), an attempt was made to apply the vibration control concept of detuning in order to minimize the effect of resonant structural vibrations on the performance of the control system. While primary structural members have been designed on the basis of attaining a specified stiffness and fundamental resonant frequency, it can be expected that the structure is overdesigned with regard to strength and the structure weight will be relatively high.

The general nature of the investigation performed by Barry Research and Development is concerned with the application of viscoelastic structural damping concepts in an effort to satisfy the need for vibration control while simultaneously reducing the weight of the over-all structure. Hence, the feasibility study performed by Barry was aimed at determining satisfactory means of incorporating high degrees of damping in primary structural members of the space motion simulator so that the fundamental structural resonant frequencies of these members could be allowed to be considerably closer to the maximum excitation frequency of the control system. Barry Controls has been engaged to assist Aircraft Armaments in determining

the best means of applying viscoelastic damping concepts in the design and fabrication of primary structural members of the space motion simulator.

The scope of work reported in this section includes the following:

1. Investigate the feasibility of introducing viscoelastic damping materials in the primary structural members of the space motion simulator described in Reference 1.

2. Recommend techniques for incorporating viscoelastic damping materials in primary structural members of the space motion simulator.

3. Estimate the loss factor for the viscoelastic-damped primary structural members of the space motion simulator having a nominal fundamental resonant frequency of 5 cps.

4. Delineate any further study or research which would be required prior to applying the recommended viscoelastic damping techniques to the primary structural members.

2.2.2 Viscoelastic Damping Concepts

While the damping characteristics of structural systems have been investigated by scientists and engineers for well over a century, early investigators focused their attention on the internal damping properties of structural materials. More recent investigations have been concerned with the damping properties of composite structures because of the need for a substantial increase in the damping property of structural fabrications. The most successful approaches developed to

incorporate high-energy dissipating mechanisms in structural fabrications involve the use of viscoelastic damping materials (See References 6 through 15).

The comparative damping properties of conventional structures and viscoelastic-damped structures are indicated by the steady-state structure vibration response plotted as a function of excitation frequency, as illustrated in Figure 7. The conventional-structural response is indicative of the type of motion experienced by a structural member that relies on the inherent damping of the structural material and the energy dissipation at conventionally fabricated structural joints to control the amplification of vibration at structural resonances. The response curve for the viscoelastic-damped structure indicates the typical reduction in resonant and near-resonant vibrations that can be obtained under certain circumstances by appropriate incorporation of viscoelastic materials in the structural fabrication.

Structural fabrications may be damped by viscoelastic damping materials employed either as unconstrained layers applied to surfaces of structural members or as constrained layers interposed between the surfaces of members comprising a structural composite. An unconstrained viscoelastic layer experiences primarily cyclic tension-compression strains when applied to a structural member undergoing flexural vibrations, whereas a constrained viscoelastic layer experiences primarily cyclic shear strains when incorporated in a structural composite. Therefore, unconstrained viscoelastic-damped structural configurations rely predominantly on a shear-damping mechanism. It generally is necessary to use

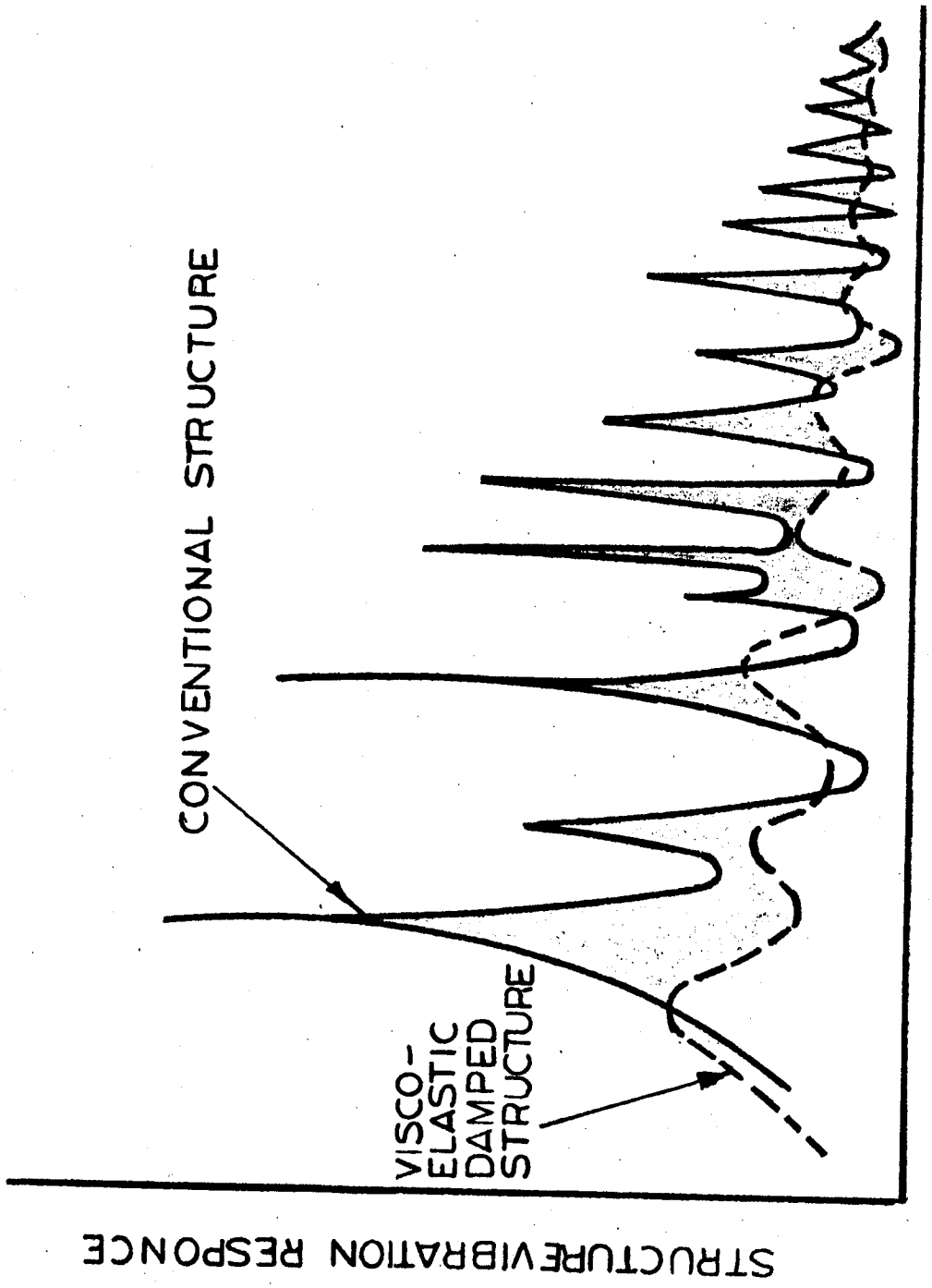

EFFECT OF DAMPING ON STRUCTURAL RESPONSE

FIGURE 7

relatively thick layers of damping material in unconstrained viscoelastic-damped structural configurations while relatively thin layers are usually adequate in constrained viscoelastic-damped structural configurations.

Over certain frequency and temperature ranges, viscoelastic damping materials are capable of dissipating energy several hundred times greater than that dissipated by typical structural materials. Either unconstrained or constrained layers of viscoelastic materials may be employed to damp structural members undergoing flexural vibrations; however, the most satisfactory results have been obtained by using constrained viscoelastic-damped structural configurations involving a shear-damping mechanism. Studies have shown that structures which properly incorporate constrained viscoelastic layers provide more damping with less added weight than structures damped by use of unconstrained viscoelastic layers.[13]

The high damping energy of viscoelastic shear-damping materials is of practical use only when these materials are appropriately incorporated in structural fabrications. A number of special design configurations have been developed which incorporate viscoelastic shear-damping mechanisms in typical structural members such as plates and beams.[11,12]. Satisfactory approaches to damping structural members include designs employing laminated sheets and cell-insert configurations*. Cross-section configurations of typical damped structural plates and structural shapes involving laminated sheets are illustrated in Figure 8; cross-section configurations of typical cell-insert beams are illustrated in Figure 9.

* Patented by Barry Controls

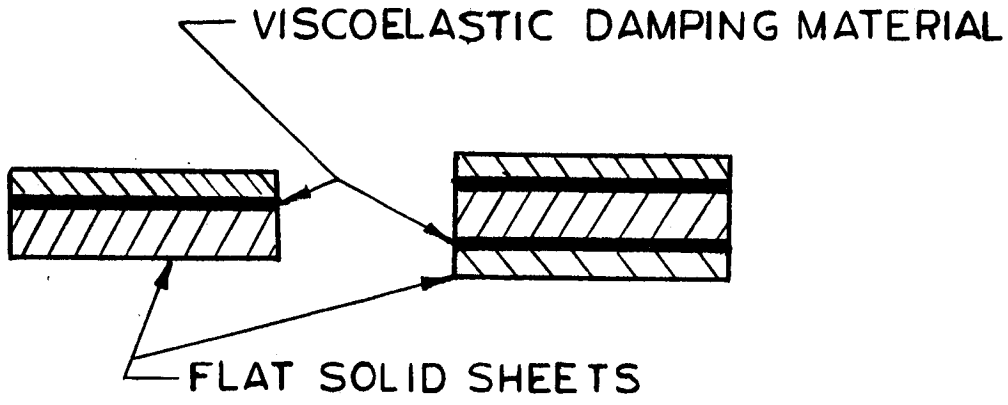

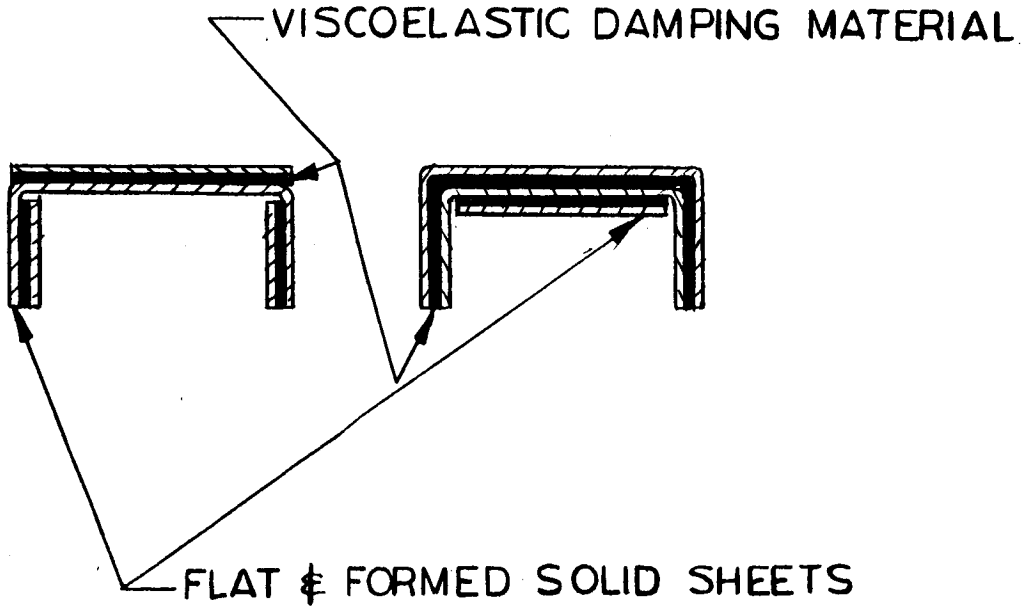

DAMPING WITH LAMINATED SHEETS

FIGURE 8

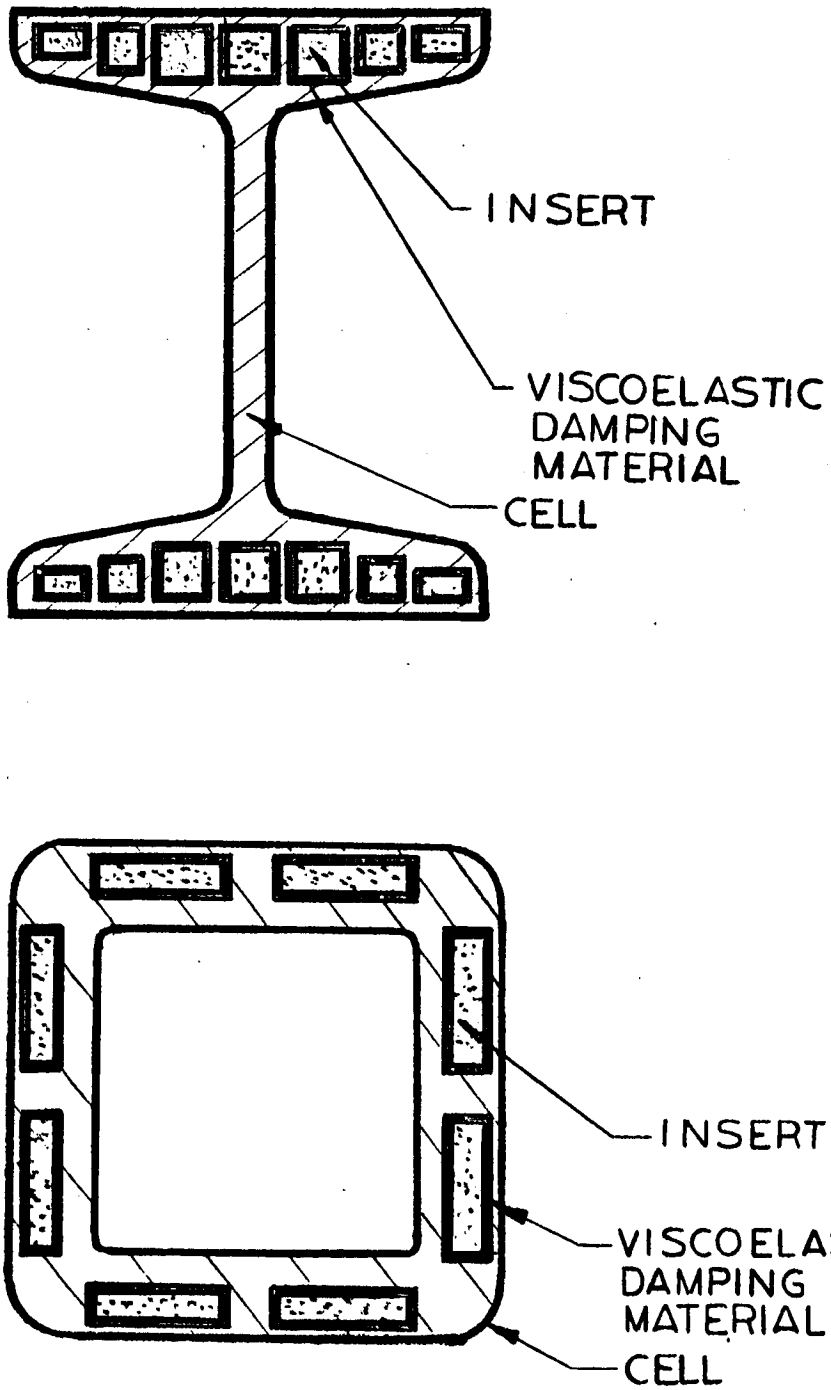

DAMPING WITH CELL INSERTS

FIGURE 9

Design criteria for most unconstrained viscoelastic-damped structural configurations have been established and are documented in the technical literature; however, the analysis of constrained viscoelastic-damped structural configurations is considerably more difficult to perform and design criteria are available only for relatively simple configurations. Even for simple structural configurations, general equations for the loss factor are extremely complicated and difficult to apply in practical design problems. In many practical applications which involve the use of thin layers of a viscoelastic material that is soft compared to the stiffness of structural materials employed in the structural composite, design equations may be simplified. The loss factor η of a constrained viscoelastic-damped structural member incorporating a soft viscoelastic damping material may be expressed in terms of three parameters as follows[14].

$$\eta = \eta\,(\eta_v,\ S,\ N)$$

where η_v is the loss factor of the viscoelastic damping material, S is a shear parameter, and N is a geometrical parameter. The loss factor η_v is given by

$$\eta_v = G''/G'$$

where G'' and G' are the loss modulus and the storage modulus of the viscoelastic damping material. The shear parameter S, which is a measure of the ability of the layers of viscoelastic material to couple the flexural motions of the elastic members of the structural composite, depends in a complicated way on the storage modulus G' and amount of the viscoelastic damping material used, the weight loading on the structural member, the

flexural rigidity of the structural member, the geometry of the cross-section, and the frequency of vibration. The geometrical parameter is a function only of the geometry of the cross-section and may be expressed mathematically as follows:[7,11,14]

$$N = \frac{(EI)_\infty}{(EI)_o} - 1$$

where $(EI)_o$ and $(EI)_\infty$ represent the flexural rigidity of the composite structure for zero and infinite shear stiffness of the viscoelastic damping material; that is, $(EI)_o$ is the flexural rigidity of the structural composite when its elastic members are uncoupled and $(EI)_\infty$ is the flexural rigidity of the structural composite when its elastic members are completely coupled.

Since the natural frequency of a structural beam or plate varies as the square root of its flexural rigidity EI, where E and I represent the modulus of elasticity of the structural material and the cross-sectional moment of inertia, respectively, the geometrical parameter N is also given by

$$N = \left(\frac{f_\infty}{f_o}\right)^2 - 1$$

where f_o and f_∞ are the resonant frequencies of the structural composite for zero and infinite shear stiffness of the viscoelastic damping material. The value of the damped resonant frequency f_r is bounded by f_o and f_∞ and is determined by the flexural rigidity of the structure, the shear stiffness of the viscoelastic damping material, and the degree of dynamic coupling which the damping material produces between the elastic members of the structural composite.

2.2.3 Design Considerations

Each individual structural sheet in a damped laminated structural plate or shape and both the cell and insert members of a cell-insert beam are load-carrying members; the number and size of individual sheets, cellular body, and inserts required for specific application are determined by considering weight, stiffness, space and damping as joint design criteria. The degree of damping exhibited by viscoelastic-damped structural composites is a function of the geometry of the cross-section configuration and the physical properties of the viscoelastic damping material, particularly as affected by vibration frequency and temperature.

A high structure loss factor is obtained for damped structural designs having large geometrical parameters; therefore, it is generally desirable to design viscoelastic-damped structural configurations having large geometrical parameters. However, for a specified weight of structure, the flexural rigidity $(EI)_o$, and therefore the static stiffness and the natural frequency of the structural element, is low for large values of the geometrical parameter. Hence, the geometrical parameter must be kept as small as is necessary to satisfy static stiffness or natural frequency design requirements.

To incorporate a high degree of damping in a structural composite, it appears desirable to employ a viscoelastic damping material having as high a loss modulus G" as possible. However, investigations have shown that an optimum degree of damping is required to maximize the loss factor. For a given cross-section geometry, there is an optimum value

of the viscoelastic damping material loss factor $(\eta_v)_{op}$ for which the loss factor η of the structural composite is maximized. The variation of the structure loss factor η with the geometrical parameter N and the viscoelastic damping material loss factor η_v is illustrated qualitatively in Figure 10. Large values of the damping material loss factor are required to provide maximum damping for structural composites having large geometrical parameters. If the damping material possesses a very low loss factor, the structure loss factor is relatively low and becomes less dependent upon the value of the geometrical parameter. There is a unique thickness of damping material layer which must be employed for a given value of the optimum loss factor $(\eta_v)_{op}$ and, therefore, both the loss factor η_v and the thickness h_v of the viscoelastic damping material may be varied to approach optimum damping conditions. However, a substantial degree of vibration control may generally be attained by use of viscoelastic damping material layers having only near-optimum damping properties inasmuch as the optimum damping phenomenon is of a noncritical nature[11,12].

For a viscoelastic damping material, the dynamic elastic coefficients G' and G'' are independent of spatial and time variables. However, these dynamic elastic coefficients vary with vibration frequency and temperature. Since it is expected that the space motion simulator will normally operate in environments approximating room temperature conditions, further discussion shall be presented only on the effect of vibration frequency.

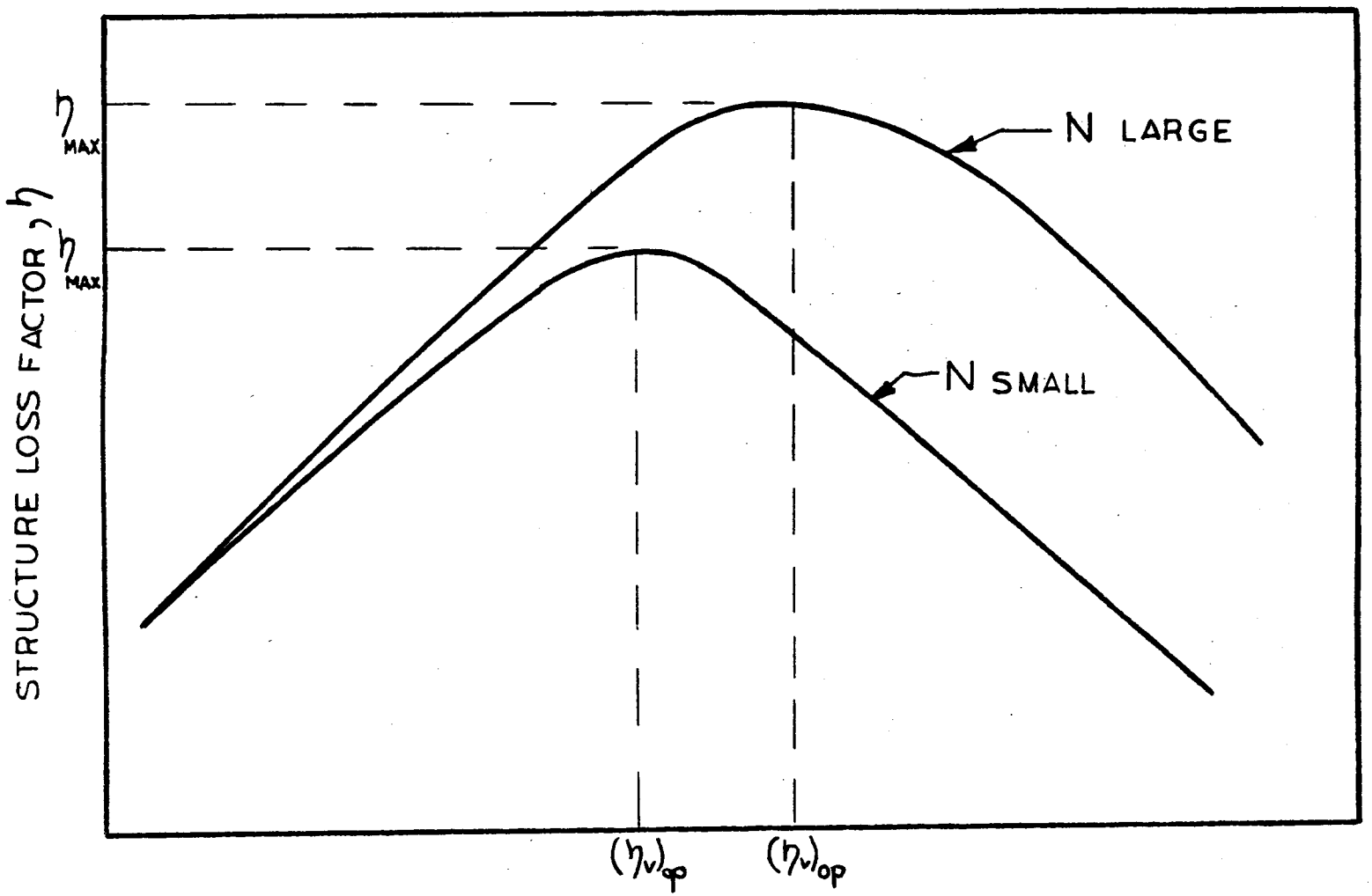
η_{MAX}
η_{MAX}
STRUCTURE LOSS FACTOR, η
N LARGE
N SMALL
$(\eta_v)_{op}$
$(\eta_v)_{op}$
DAMPING MATERIAL LOSS FACTOR, η_v (LOG SCALE)

FIGURE 10

2.2.4 Effect of Vibration Frequency

The frequency dependence of the shear modulii G, G', G" and the loss factor η is shown qualitatively in Figure 11 for a typical viscoelastic shear-damping material.[11] At low frequencies ("rubbery" region), the storage modulus G' and the loss modulus G" are both very small; hence, for a given amplitude of cyclic strain, the energy dissipation is also small. At high frequencies ("glassy" region), the storage modulus G' is large and the loss modulus G" is very small; hence, for a given amplitude of cyclic strain, the energy dissipation is also small. Therefore, very low and very high vibration frequencies represent conditions which are not generally conducive to a high degree of energy dissipation. The highest degree of energy dissipation occurs in an intermediate frequency range ("transition" region) in which the loss modulus G" is a maximum. The maximum value of the loss factor η is in this intermediate frequency range but at a lower frequency than that at which the maximum loss modulus G" occurs.

The frequency dependence characteristics of the dynamic elastic properties of viscoelastic shear-damping materials, as expressed qualitatively in Figure 12, may be employed to determine the effects of fundamental resonant frequency on the loss factor of a viscoelastic shear-damped structure. As indicated in Figure 12 for both a very low and a very high fundamental resonant frequency, G" is small and the structure loss factor is correspondingly small. In the transition region of the viscoelastic damping material, for intermediate values of fundamental

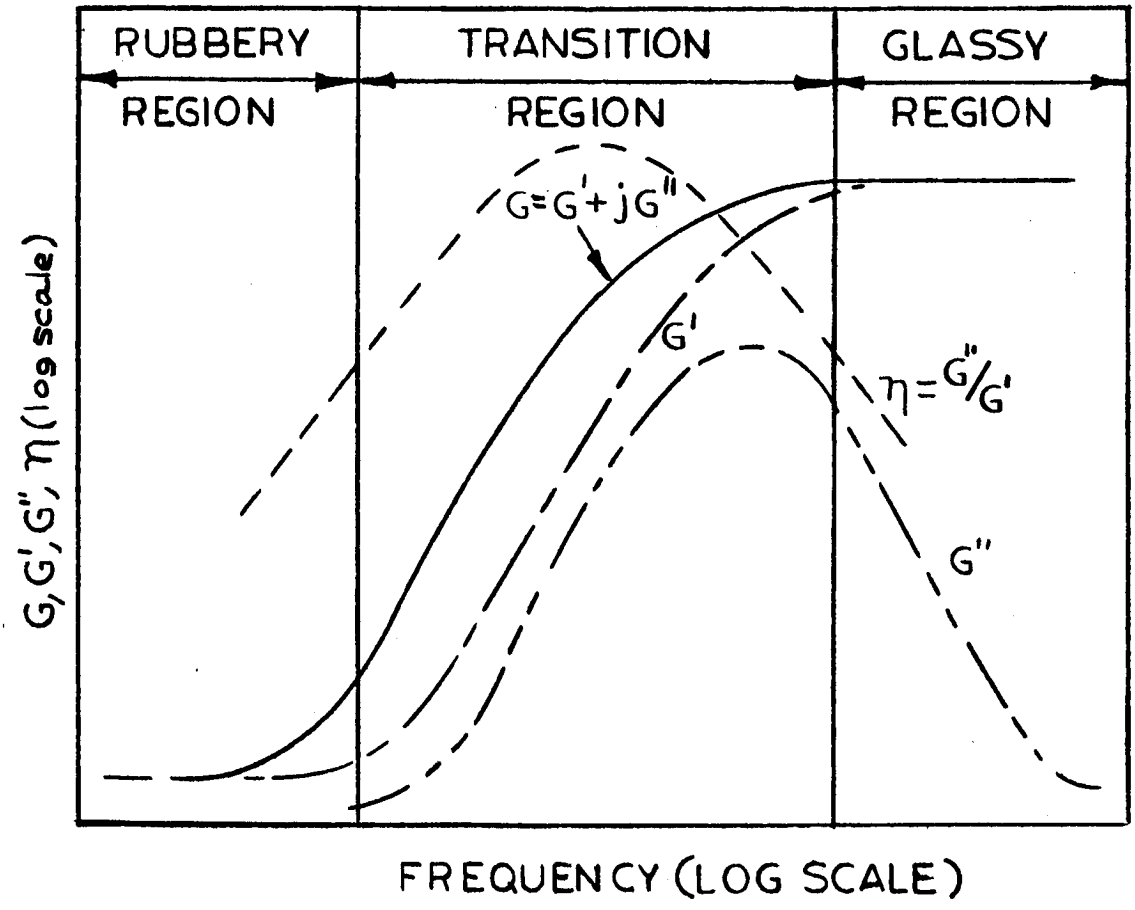

FREQUENCY DEPENDENCE OF VARIOUS
MODULI AND THE LOSS FACTOR

FIGURE 11

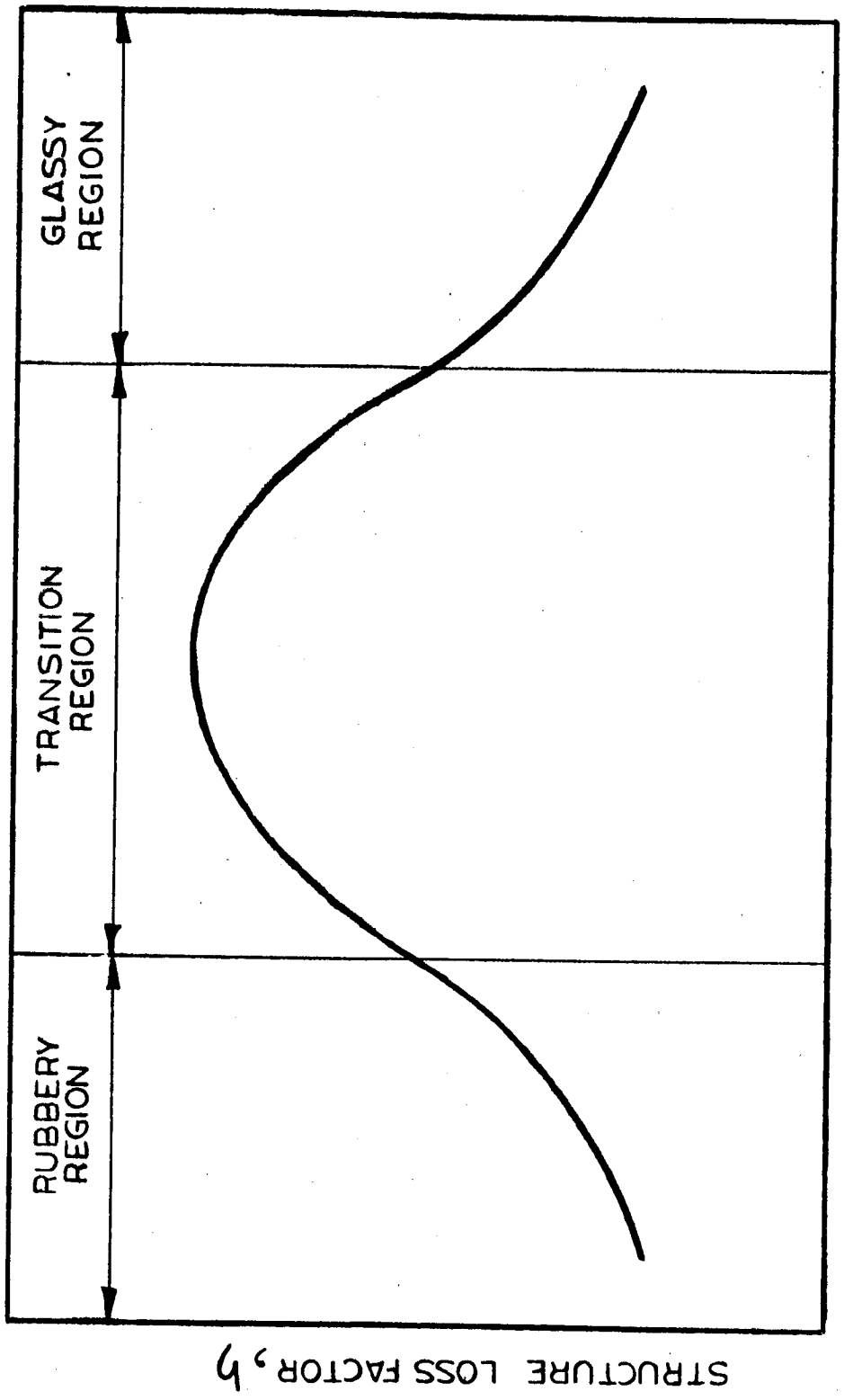
GLASSY REGION
TRANSITION REGION
RUBBERY REGION
FREQUENCY (LOG SCALE)
STRUCTURE LOSS FACTOR, η

FIGURE 12

resonant frequency, the viscoelastic-damped structural fabrication dissipates sufficient energy to provide good resonant vibration control and a high value of the structure loss factor is obtained.

The frequency dependence of the structure loss factor of a viscoelastic shear-damped structure is indicated in Figure 13 for a group of rectangular cross-section damped laminated cantilever beams having the same weight but designed to have different values of the geometric parameter N. The resonance amplification factor A_r, which is the reciprocal of the loss factor η.

$$A_r = 1/\eta$$

has been measured at the free end of the cantilever beam; test data are included for fundamental resonant frequencies ranging from approximately 15 to 300 cps.

The resonance amplification factor is only mildly dependent upon resonant frequencies ranging from approximately 50 to 300 cps for the particular viscoelastic damping material employed. However, this factor is strongly dependent upon beam resonant frequencies that are less than approximately 50 cps. It is apparent that the rubbery region of the viscoelastic material extends from very low frequencies to approximately 50 cps, whereas, the transition region of the viscoelastic material ranges from approximately 50 cps and extends beyond 300 cps; the glassy region of the viscoelastic material occurs for frequencies considerably greater than 300 cps.

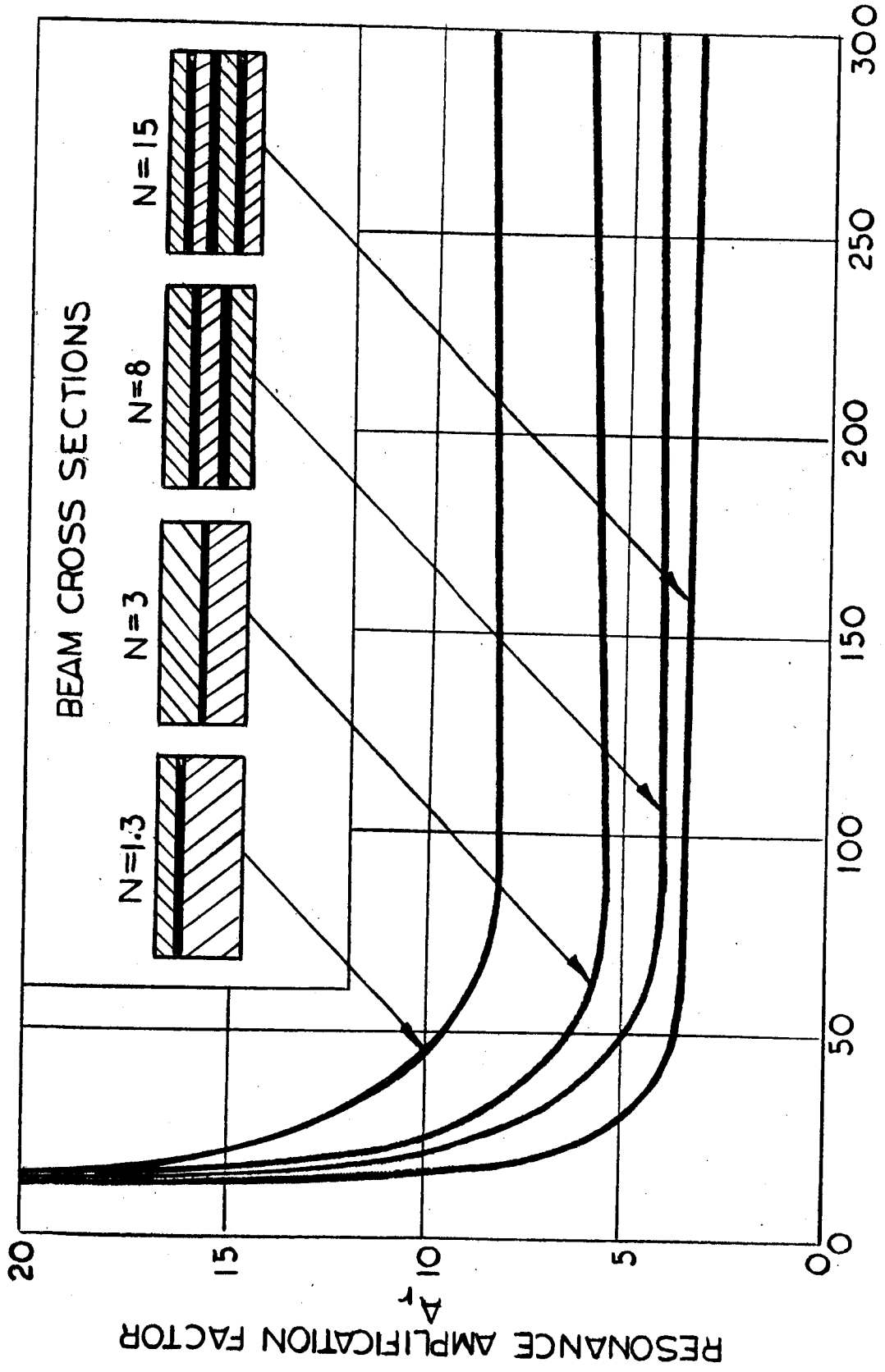

RESONANT AMPLIFICATION FOR DAMPED, LAMINATED BEAMS

FIGURE 13

In the transition region, substantial vibration control is provided by use of the viscoelastic damping technique and design configurations having geometric parameters ranging in value from 1.3 to 15 result in resonance amplification factors ranging from approximately 8.5 to 3.5. The effect of the geometrical parameter N on the resonance amplification factor for vibrations in the transition region is presented in Figure 14; these data are repeated in Figure 15 in terms of the structure loss factor. These curves indicate that, to obtain a highly-damped structural member, the geometrical parameter should be as high as possible. However, it is clear that, beyond a certain point, a substantial increase in the value of the geometrical parameter will provide only a slight increase in damping. Since the static stiffness and the resonant frequency (for a given weight) are inversely dependent upon the geometrical parameter, it is generally not desirable to design structures having geometrical parameters of extremely high value because of the significant loss in structural stiffness for a given weight. For the particular beams investigated, a considerable increase in damping was provided by increasing the value of the geometrical parameter from 1.3 to 3. By increasing the value of the geometrical parameter from 3 to 8, damping has been increased, but not in proportion to the increase in the value of the geometrical parameter or in proportion to the decrease in static stiffness of the beam. Increasing the value of the geometrical parameter to a value of 15, represents a clear case of diminishing returns inasmuch as the damping has been increased by only a small amount. These experimental

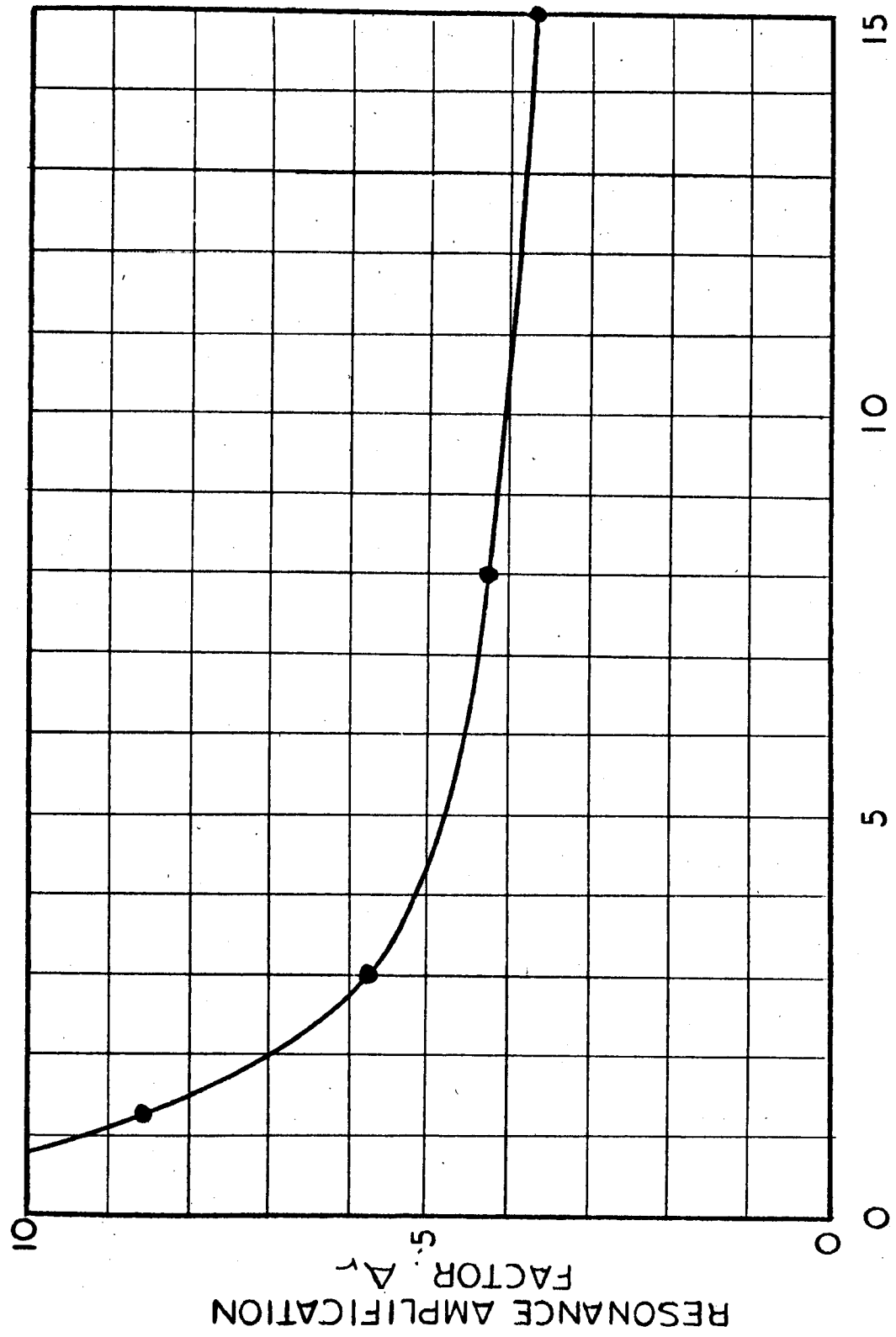

EFFECT OF GEOMETRICAL PARAMETER ON RESONANT AMPLIFICATION

FIGURE 14

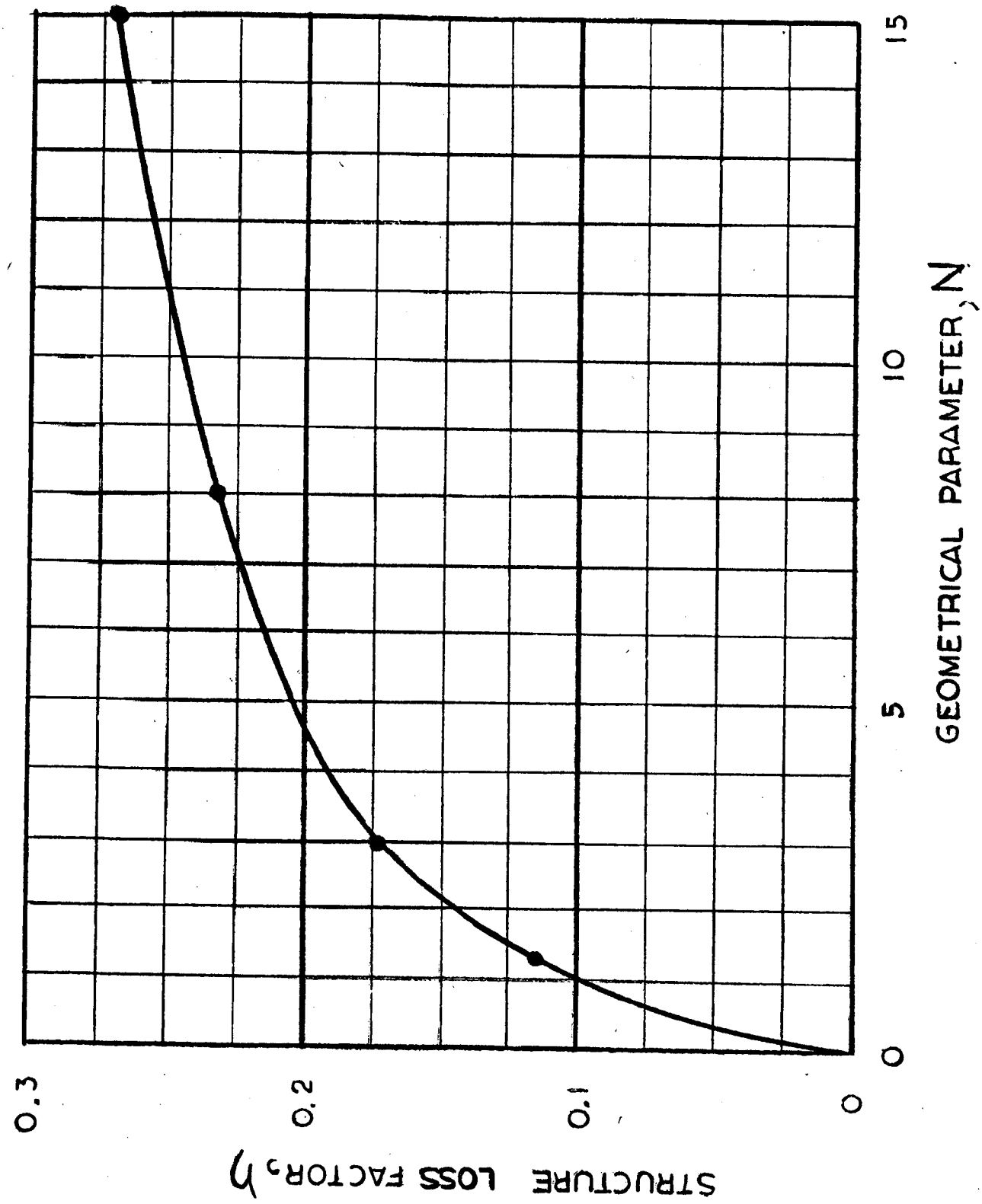
STRUCTURE LOSS FACTOR, η
0.3
0.2
0.1
0
0
5
10
15
GEOMETRICAL PARAMETER, N

FIGURE 15

data, coupled with other data obtained on viscoelastic-damped beams, indicate that the geometrical parameter having a value between 1 and 3 represents a reasonable compromise in designing the structural members when structural stiffness and resonant frequency are important design requirements.

2.2.5 Application to Space Motion Simulator

The general configuration of the proposed space motion simulator is illustrated in the frontispiece. A building houses a structural mechanism which is capable of transporting an astronaut through space as a body experiencing motions in six degrees of freedom. Translational motions along three mutually perpendicular axes are produced by a three-truss structural mechanism incorporating a dolly vehicle. The three-truss structural mechanism is illustrated in Figure 1; two vertical trusses are capable of moving in horizontal translation in tracks along the length of the building, one horizontal truss is capable of moving in vertical translation while guided in tracks incorporated in the two vertical trusses, and a dolly vehicle is capable of moving in horizontal translation along tracks incorporated in the horizontal truss. The three rotational motions are produced by a three-axis gimbal system, as illustrated in Figure 3; rotations about three mutually perpendicular axes are produced by the motion of the roll, pitch and yaw gimbal arms.

In Section 2.1, we have presented, for the truss members and the gimbal arms, conventional designs for fundamental structural resonant frequencies of 5, 10 and 15 cps. As discussed previously, we originally

considered using designs which exhibited fundamental resonant frequencies in the 10 to 15 cps range to minimize the effect of resonant structural vibrations on the performance of the servo-control system which actuates the motion of the truss members and the gimbal arms. This design criterion was based on the assumption that these structural members were lightly damped and it was necessary to have their fundamental flexural resonances substantially greater than the maximum servo-control excitation frequency of 2 cps. This report is concerned with the redesign of these structural members to incorporate a high degree of damping so that their fundamental resonant frequencies may be allowed to become as low as 5 cps. With such a redesign, it is desired to reduce the weight of the truss members and gimbal arms.

2.2.5.1 Gimbal Arms

The configuration and dimensional details of the gimbal arms are illustrated in Figure 16. The cross-section of each gimbal arm is a square tube with wall thickness dimensions that are thin compared to the side dimension of the square shapes. Table I gives the dimensions, weights, and moments of inertia of the conventional gimbal arm designs. A graphical presentation of the gimbal arm weights plotted as a function of the gimbal arm fundamental resonant frequency is shown in Figure 17. A considerable weight increase occurs when the design resonant frequency is varied from 5 to 15 cps.

Redesign for the purpose of incorporating viscoelastic shear-damping mechanisms in the gimbal arms shall be carried out while maintaining the basic square tube cross-sectional configuration. Since the thickness t of

ROLL ARM

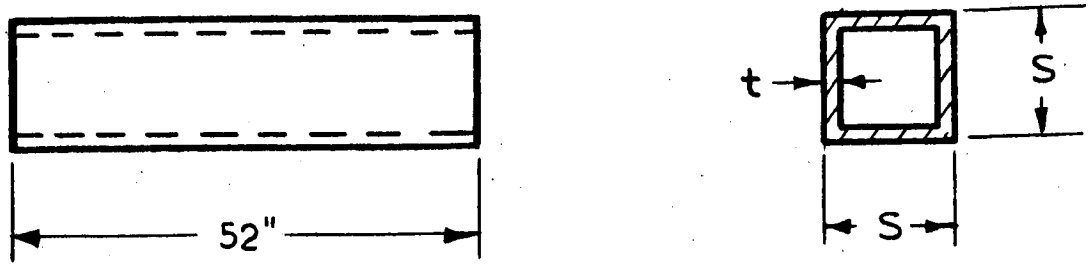

PITCH ARM

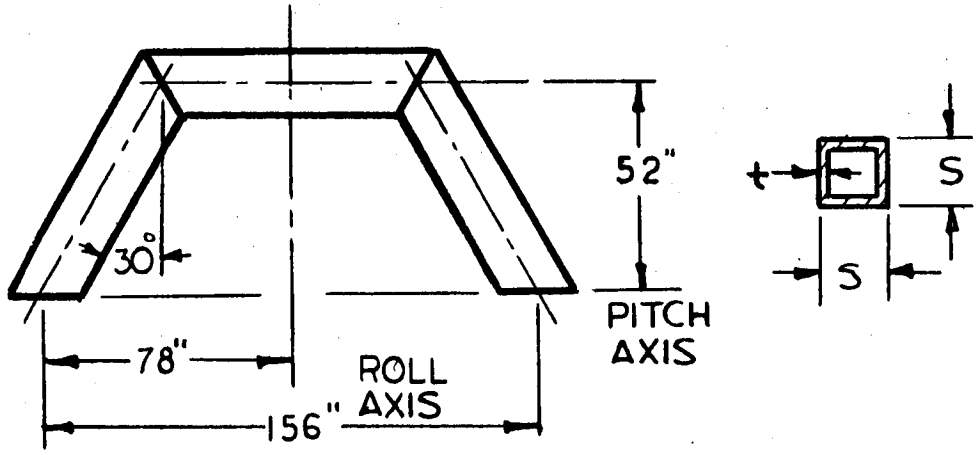

YAW ARM

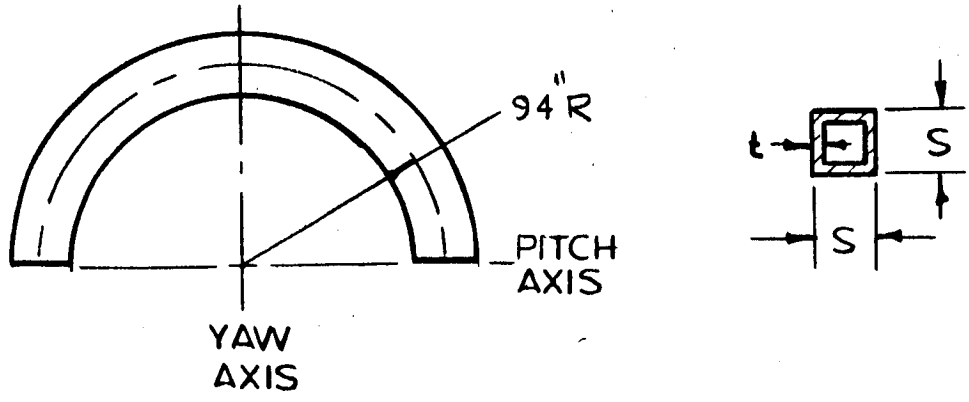

CONFIGURATION OF GIMBAL ARMS

FIGURE 16

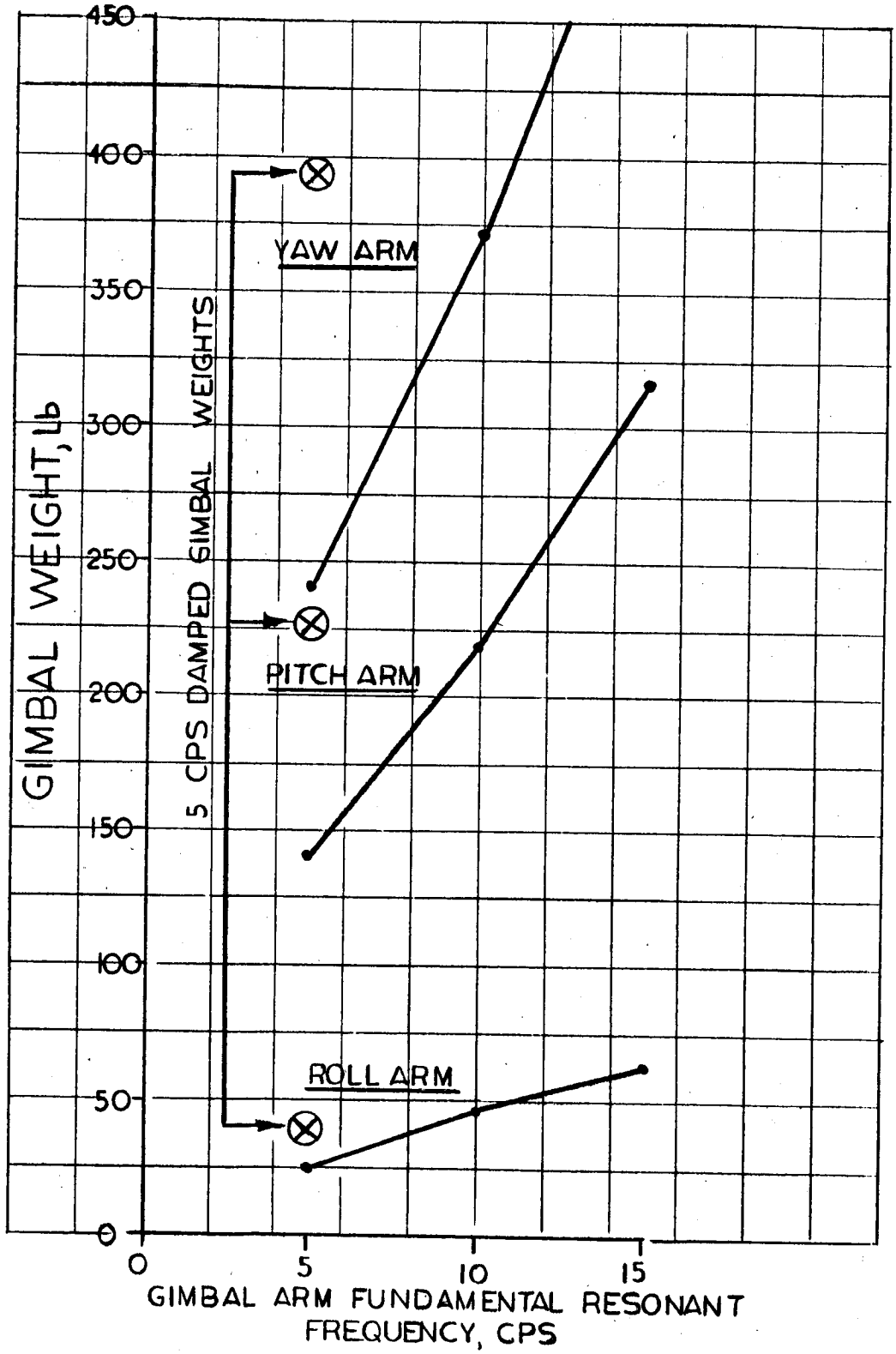

DEPENDENCE OF GIMBAL ARM WEIGHTS ON FREQUENCY

FIGURE 17

the tubes was determined on the basis of a buckling criterion, damped tubular designs shall be considered which involve only minor changes in the basic solid tubular section dimensions. Also, since the thickness t ranges from 0.111" to 0.184", damped-laminated techniques are more appropriate than cell-insert techniques. It has not been determined whether the basic tubular members would be fabricated from structural sheets, be extruded, or be a weldment; hence, only preliminary designs for viscoelastic-damped gimbal arms can be evolved at this time.

For the reasons discussed, the design of damped gimbal arms consists of constraining structural sheets laminated to the basic tubular member, as illustrated in Figure 18. The design shown in Figure 18 (a) involves laminating one constraining structural sheet to each of the four surfaces of the square tube; the design shown in Figure 18 (b) involves laminating a number of constraining structural strips to each of the four surfaces of the square tube. The major benefit derived from replacing a single constraining sheet by a number of constraining strips is that of obtaining a higher geometrical parameter N for the same added weight. The configurations illustrated in Figure 18 are only schematic representations of damped tubular members. For improved appearance and ease of maintenance, the constraining sheets or strips could be laminated to the inside surfaces, depending upon the final fabrication method chosen to manufacture the basic tubular members.

Based on the use of a relatively soft viscoelastic damping material (which is a realistic assumption), an approximate analysis of the viscoelastic-

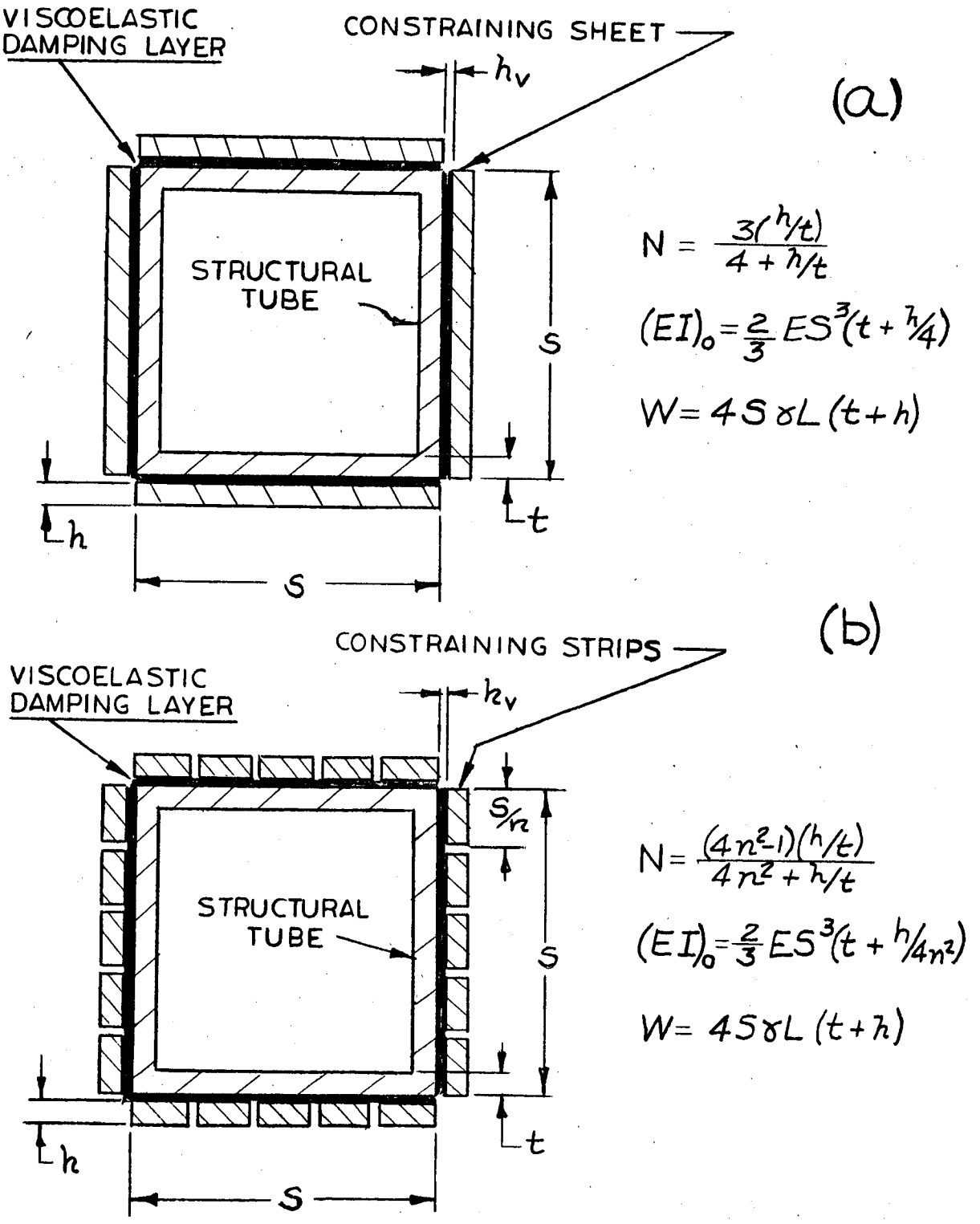

APPLICATION OF VISCOELASTIC DAMPING TO GIMBAL ARMS

FIGURE 18

damped tubular members illustrated in Figure 18 resulted in the relationships for the geometrical parameter N, the static flexural rigidity $(EI)_o$, and the weight W shown in the figure. In these equations, S is the side dimension of the square tube, t is the thickness of the basic square-tube section, h is the thickness of the constraining sheet or strip, n is the number of strips into which a constraining sheet is divided and E is the modulus of elasticity of the basic tube, constraining sheet, and strip structural materials. Assumptions made in performing the analysis include:

(1) $G_v << E$

(2) $h_v << t, h$

(3) $S >> t, h$

(4) $n << S/h$

where G_v' and h_v are the storage modulus and the thickness of the layers of viscoelastic damping material, respectively. The design problem is one of choosing the constraining sheet or strip thickness h to have a value (1) large enough to obtain a sufficiently high value of the geometrical parameter N, (2) satisfactory to obtain the required static flexural rigidity $(EI)_o$ or resonant frequency f_r, and (3) low enough to keep the weight W to a minimum. Hence, a compromise must be made regarding the requirements on damping, weight and stiffness.

The damped gimbal arms are designed as follows. A thickness ratio $h/t = 1.0$ and $n = 3$ is chosen to provide a geometrical parameter $N \approx 1.0$. Dynamic coupling between the basic tubular member and the constraining strips is assumed to be sufficient to produce a damped resonant

frequency 10 per cent higher than the structure undamped resonant frequency [11]. Hence, the static flexural rigidity $(EI)_o$ of the damped gimbal arms must satisfy the relation

$$(EI)_o = 0.83\ (EI)_{solid}$$

where $(EI)_{solid}$ is the flexural rigidity of the gimbal arms as determined in Section 2.1; that is, the static flexural rigidity of damped gimbal arms must equal the product of the modulus of elasticity E and the moment of inertia I listed in Table I for the various gimbal arms. By applying this relationship, a value of the tube wall thickness t and constraining strip thickness h is determined. With this information, the weight of the gimbal arm may be calculated.

The size and weight parameters determined in this manner are presented in Table III for the roll, pitch and yaw gimbal arms, each having a nominal damped fundamental resonant frequency of 5 cps. All weight calculations have been made in accordance with the method specified in Section 2.1; the calculated weights for the damped gimbal arms may therefore be directly compared with those for the conventional gimbal arms. The weight of the 5 cps damped roll gimbal arm could be used to produce a conventional 8.4 cps roll gimbal arm, the weight of the 5 cps damped pitch gimbal arm could be used to produce a conventional 10.4 cps pitch gimbal arm, and the weight of the 5 cps camped yaw gimbal arm could be used to produce a conventional 10.7 cps yaw gimbal arm.

TABLE III

5 cps Damped Gimbal Configuration (N = 1)

Gimbal Arm	Wt. (lb.)	S (in.)	t (in.)	h (in.)
Roll	41	10.4	0.094	0.094
Pitch	228	10.6	0.125	0.125
Yaw	388	11.84	0.139	0.139
Total Wt.	657			

2.2.5.2 Truss Members

The configuration and dimensional details of the horizontal and vertical truss members are illustrated in Figure 19. The cross-section of the conventional trusses is considered to consist of four rail sections of area $A/2$ positioned within a square outline having side dimensions d. While shear members are employed in the grillage, the moment of inertia of the cross-section is assumed to be determined solely by the four rail areas and the dimension d. A table of the dimensions, weights, moments of inertia, and flexural rigidities of the conventional truss members is presented in Table IV. A graphical presentation of the truss member weights plotted as a function of the truss member fundamental resonant frequency is shown in Figure 20. A considerable weight increase occurs when the design resonant frequency is varied from 5 to 15 cps.

With the information that is available, only preliminary designs for viscoelastic-damped truss members can be evolved at this time. Because of the geometrical configuration of the truss members, it appears that damped-

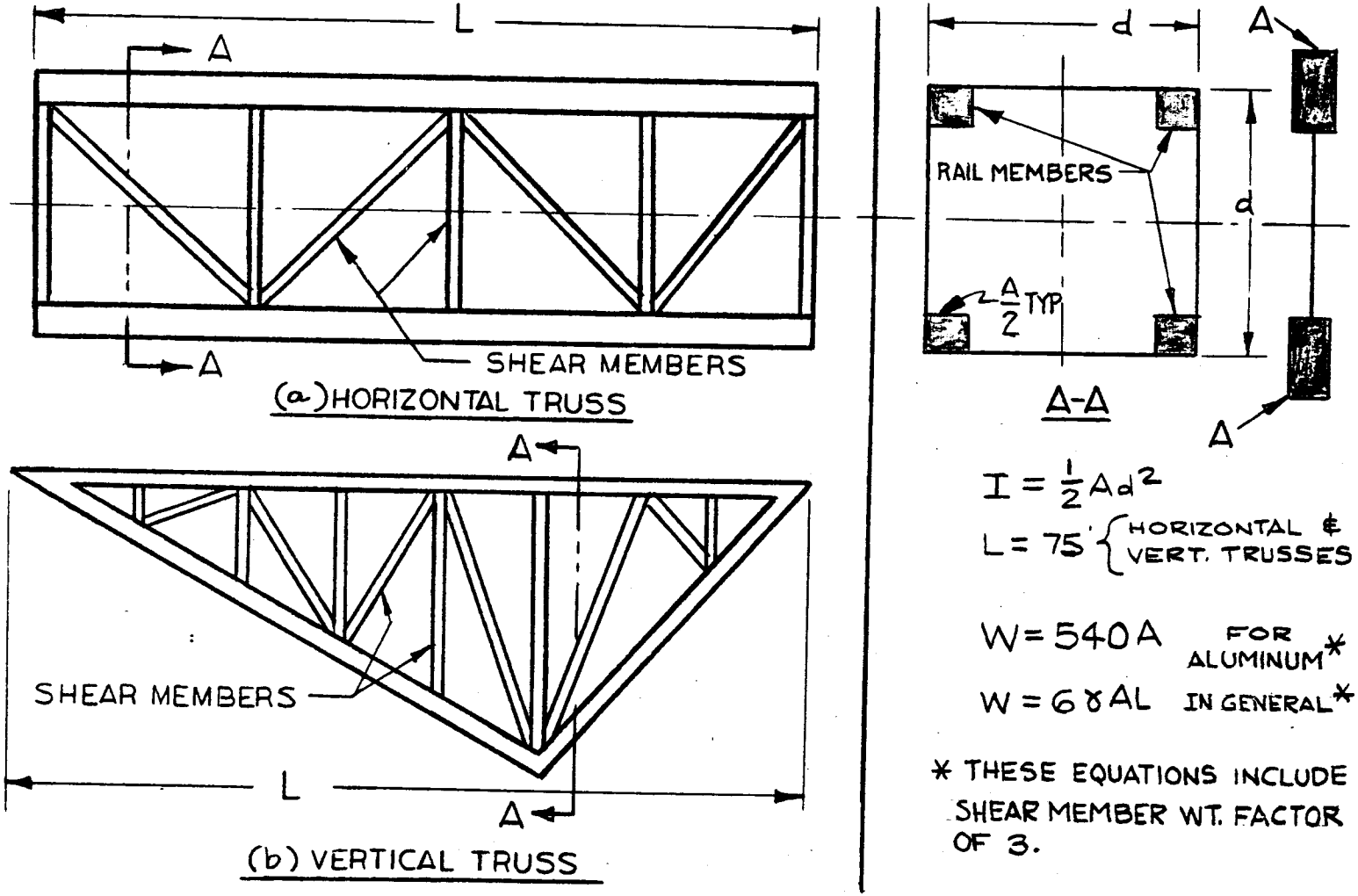

CONFIGURATION OF TRANSLATIONED TRUSSES

FIGURE 19

75-Ft. Cross Span & Vertical Truss Configuration: 5 cps Fundamental Frequency					
Truss	Wt. (lb.)	d(in.)	A($in.^2$)	1 x 10^{-4}($in.^4$)	EI x 10^{-10}(lb.-$in.^2$)
Horizontal	3,000	60	5.6	1.0	10
Vertical (each)	2,959	90	5.5	2.2	22.2
Total Wt.	8,918				

75-Ft. Cross Span & Vertical Truss Configuration: 10 cps Fundamental Frequency					
Truss	Wt. (lb.)	d(in.)	A($in.^2$)	1 x 10^{-4}($in.^4$)	EI x 10^{-10}(lb.-$in.^2$)
Horizontal	6,720	90	12.5	5.0	50
Vertical (each)	8,400	120	15.6	11.2	112
Total Wt.	23,520				

75-Ft. Cross Span & Vertical Truss Configuration: 15 cps Fundamental Frequency					
Truss	Wt. (lb.)	d(in.)	A($in.^2$)	1 x 10^{-4}($in.^4$)	EI x 10^{-10}(lb.-$in.^2$)
Horizontal	10,940	120	20.3	14.7	147
Vertical (each)	15,660	150	29.0	32.6	326
Total Wt.	42,260				

Total Wt. Equals weight of one horizontal and two vertical trusses.

$I = \frac{1}{2} A d^2$

W = 540A (aluminum)

TRUSS SIZES, WEIGHTS & PROPERTIES

TABLE IV

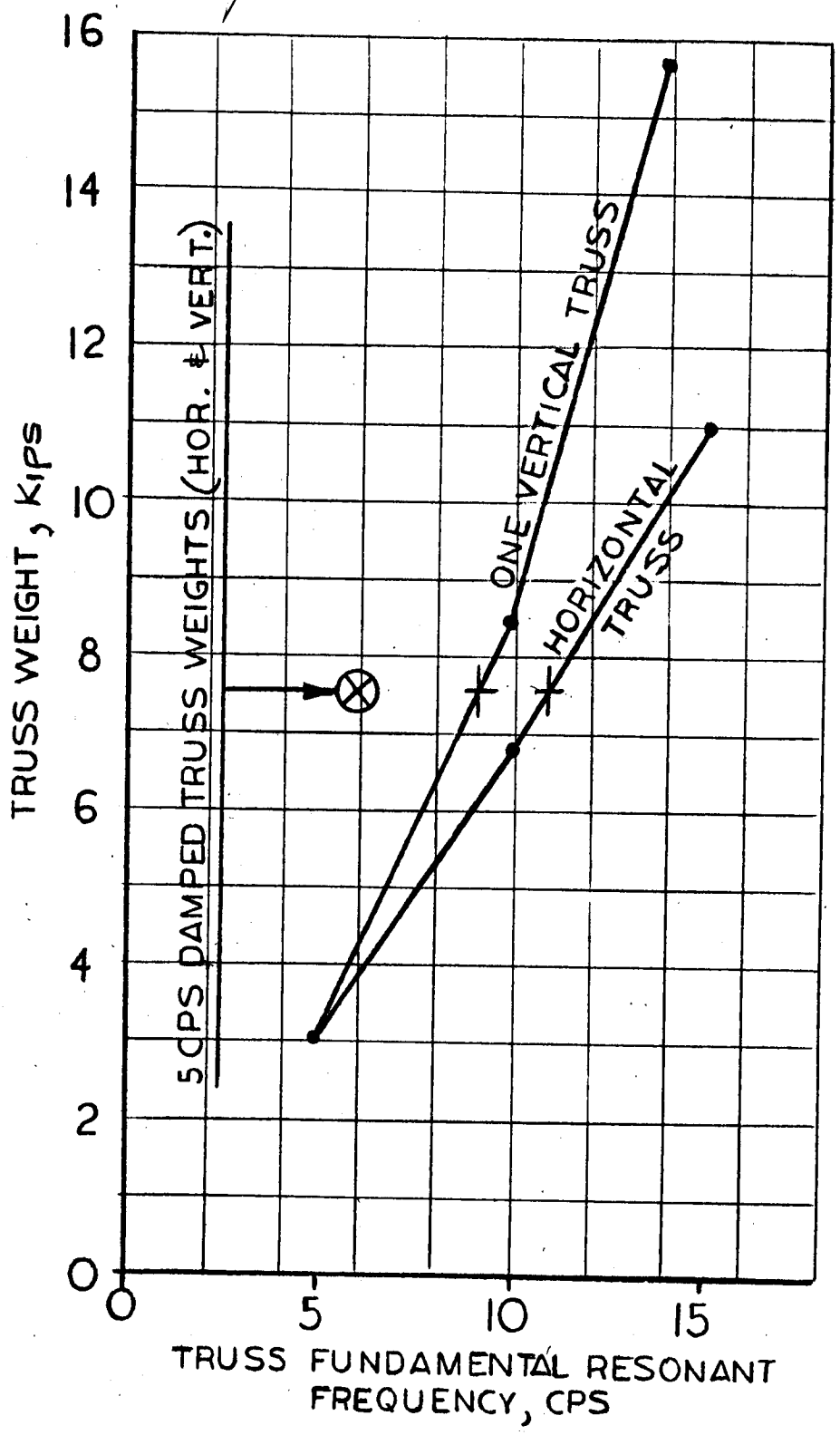

DEPENDENCE OF TRUSS WEIGHT ON FREQUENCY

FIGURE 20

laminated techniques are appropriate for the shear members of the truss, whereas either cell-insert or damped-laminated techniques are appropriate for incorporating damping in the four rail members. Both types of designs will be considered since the advantages and disadvantages of each can be investigated at a later date.

Viscoelastic-damped shear members can be designed and fabricated in the usual manner.[11,12] Since these members are usually loaded primarily in tension or compression, no problems are anticipated with regard to obtaining required stiffness and weight properties while still incorporating a high degree of damping in the members; therefore, no further discussion need be given with regard to the design of the viscoelastic-damped shear members.

Possible designs of the damped truss members are illustrated schematically in Figure 21 (cell-insert configuration) and Figure 22 (constrained-layer configuration). Each of these damped structure configurations may be analyzed by replacing the truss cross-sections by the dumbell model cross-sections illustrated in Figure 23. The dumbell model shown in Figure 23 (a) represents a cell-insert design whereas the dumbell model shown in Figure 23 (b) represents a constrained-layer design. These models are adequate for performing preliminary analyses but would have to be modified when full account is made of other practical requirements, such as the bearing strength necessary at the outer-most fibres to accommodate the wheel loads of the dolly vehicle or other translatory motion devices. Hence, while the four rail members ultimately may have to provide strength and

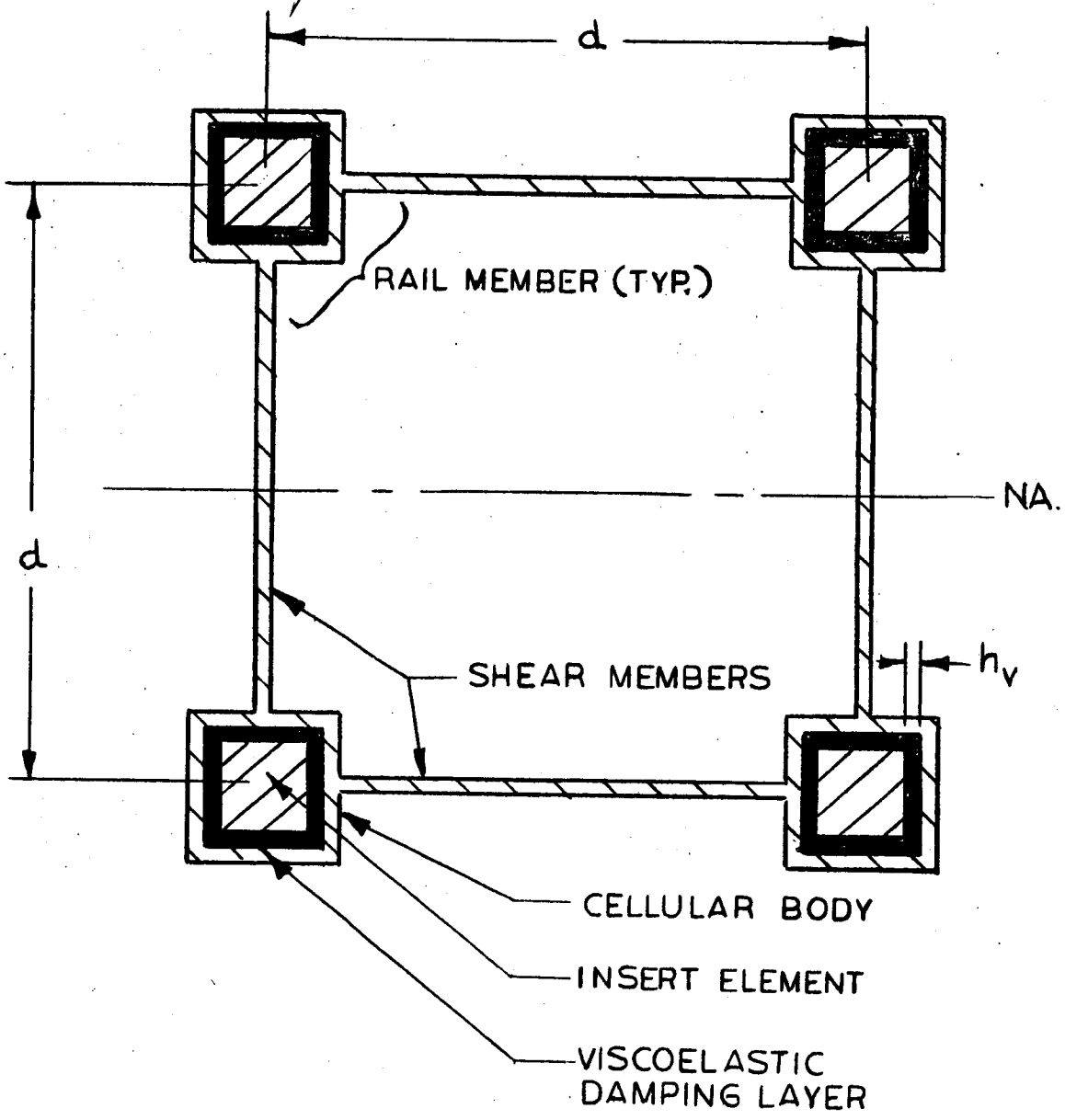

CELL-INSERT DAMPING FOR TRUSS MEMBERS

FIGURE 21

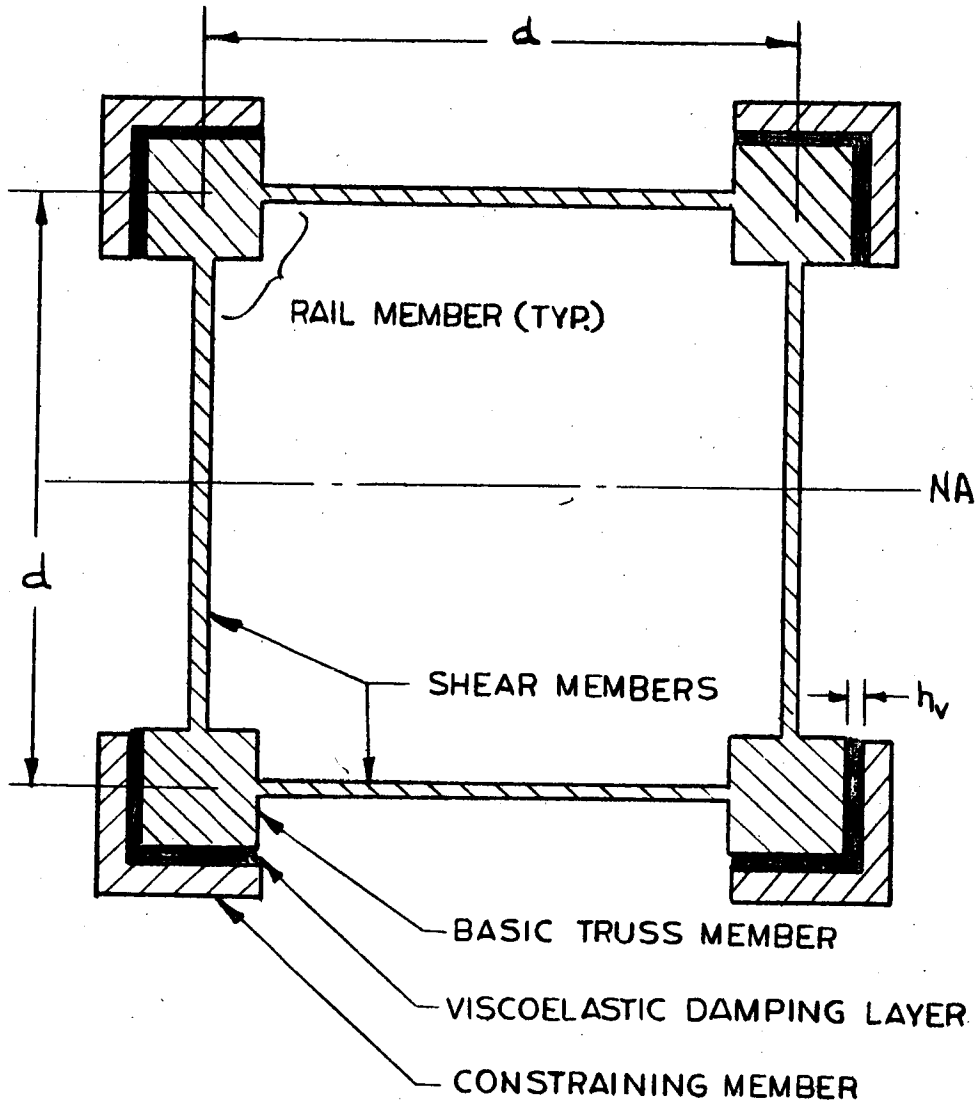

CONSTRAINED-LAYER DAMPING FOR TRUSS MEMBERS

FIGURE 22

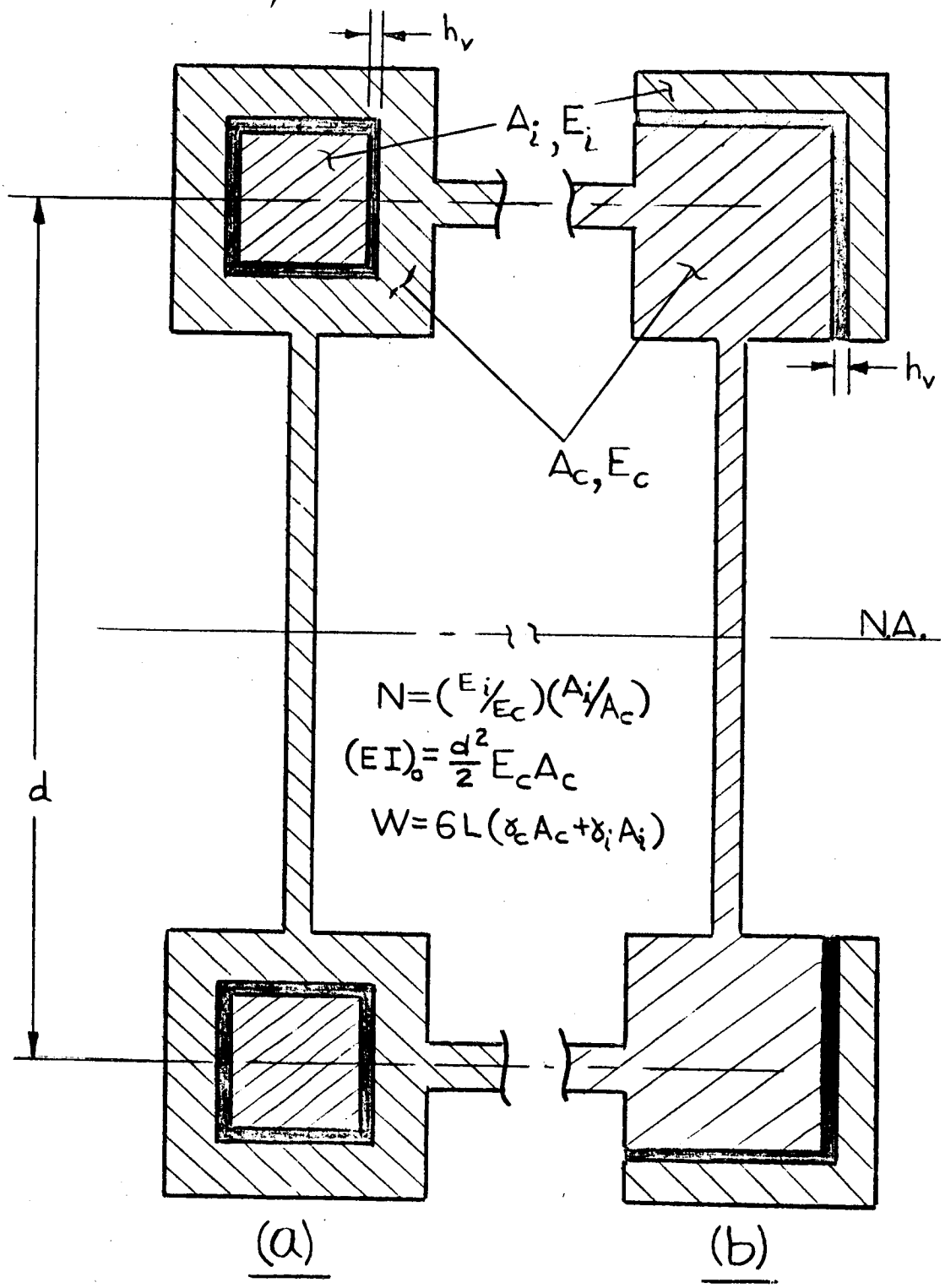

DUMBBELL MODEL FOR DAMPED TRUSS STRUCTURE

FIGURE 23

damping as well as act as a track on which wheels may travel, this report will consider only the damping, weight, and frequency properties of the damped truss-member dumbell models.

Based on the use of a relatively soft viscoelastic damping material, an approximate analysis of the viscoelastic-damped dumbell models illustrated in Figure 23 resulted in the relationship for the geometrical parameter N, the static flexural rigidity $(EI)_o$, and the weight W shown in the figure. In these equations, a c-subscript represents a cellular or basic structural element, an i-subscript represents an insert or constraining element, E is the modulus of elasticity, A is the element area, γ is the weight density, and L is the length of the truss member. Assumptions made in performing the analysis include:

(1) Cross-section is symmetrical about neutral axis of bending

(2) $G_v' << E$

(3) $h_v << \sqrt{A}$

(4) $d >> \sqrt{A}$

where G_v and h_v are the storage modulus and the thickness of the layers of viscoelastic damping material, respectively.

Based on the dumbell model configuration, the design problem is one of choosing the insert or constraining element area A_i and modulus E_i to have values (1) large enough to obtain a sufficiently high value of the geometrical parameter N, (2) satisfactory to obtain the required static flexural rigidity $(EI)_o$ or resonant frequency f_r, and (3) low enough to

keep the weight W to a minimum. Hence, a compromise must be made regarding the requirements on damping, weight and stiffness.

The damped truss members (using the dumbell model) are designed as follows. By selecting a value of the geometrical parameter N, the areas A_c and A_i are determined to ensure a 5 cps fundamental resonant frequency; the weight of the truss is then calculated. As discussed previously relative to the design of the gimbal arms, dynamic coupling between the cellular and insert elastic members is assumed to be sufficient to produce a damped resonant frequency 10 per cent higher than the structure undamped resonant frequency. Results of calculations that were performed indicated that for N = 1.0, W = 4,860 lbs., for N = 1.5, W = 6,200 lbs., and for N = 2.0, W = 7,550 lbs., where the weight W applies both for the horizontal and vertical truss members. It is important to have as high a value of the geometrical parameter as possible; therefore, the value N = 2.0 is chosen since the associated weight is reasonable compared to the weight for conventional 15 cps truss members. Steel is chosen as the insert or constraining element material since this allows a smaller area A_i to be used (making the truss members smaller) with no weight penalty incurred.

The size and weight parameters determined in this manner are presented in Table V for the horizontal and vertical truss members, each having a nominal damped fundamental resonant frequency of 5 cps. All weight calculations have been made in accordance with the method specified previously in Section 2.1; the calculated weights for the damped truss members may therefore be directly compared with those for the conventional truss

members. The total weight of 22,650 lbs. for one horizontal and two vertical 5 cps damped truss members is approximately equal to the weight of the corresponding three 10 cps conventional truss members.

TABLE V

5 cps Viscoelastic-Damped Truss Members: (N = 2)

Truss Member	Wt. (lb.)	d(in.)	$A_c(in.^2)$	$A_i(in.^2)$
Horizontal	7,550	60	4.6	3.1
Vertical (each)	7,550	90	4.6	3.1
Total Wt.	22,650			

Total Wt. equals weight of one horizontal and two vertical trusses.

c - subscript parameters represent aluminum elements.

i - subscript parameters represent steel elements.

More exactly, the weight of the 5 cps damped horizontal truss member could be used to produce a conventional 11 cps horizontal truss member, and the weight of the 5 cps damped vertical truss member could be used to produce a conventional 9.2 cps vertical truss member.

2.2.6 Damped Resonant Frequency

The nominal 5 cps resonant frequency of the damped gimbal arms and truss members was determined without regard for the increase in structure weight resulting from the application of the damping technique. An increase in the structure weight will tend to lower the resonant frequency. For the weight changes involved, the fundamental resonant frequencies of the gimbal arms and truss members could be as low as 4 cps. On the other hand, the dynamic coupling between the elastic elements of the structural

composites could be higher than has been assumed; this would tend to increase the resonant frequencies of the structural members. Therefore, a "nominal" 5 cps fundamental resonant frequency implies a resonant frequency in the 4 to 6 cps range.

2.2.7 Structure Loss Factors

Approximate values of the shear modulus G and loss factor for common metals and viscoelastic materials, as well as for structural fabrications employing these materials, are presented in Table VI. From these data, it is clear that the storage modulus of metals is always several orders of magnitude greater than its loss modulus, whereas the storage and loss modulii of viscoelastic materials may be approximately of the same order of magnitude.[15] The effect of fabrication devices and structural junctions on the damping of structural fabrications may be observed by comparing the loss factor of the metal with the loss factor of the structural fabrication employing the metal.

TABLE VI

	Metal	Viscoelastic Material
$G \times 10^{-6}$ psi	2 to 10	0 to 0.5
$\eta_{material}$	10^{-4} to 10^{-2}	10^{-3} to 10
$\eta_{structure}$	0.01 to 0.1	0.02 to 0.5

The range of loss factor values indicated for metals and metal fabricated structures is due primarily to (1) the variety of different structural metals available, (2) the nature of the structural fabrication, and

(3) the effect of stress level on the damping property. For metal structural fabrications, the loss factor increases as the induced stress level is increased. In general, unless the stress level induced in a metal fabricated structure is extremely high, the loss factor is likely to be quite low.

The range of loss factor values indicated for viscoelastic materials and viscoelastic-damped structures is primarily due to (1) the variety of different viscoelastic materials available, (2) the geometric parameter of the structural composite, (3) temperature, and (4) the effect of vibration frequency. Vibration frequency affects the loss factor of viscoelastic-damped structural fabrications in two ways; first, the loss factor of the viscoelastic damping material depends on frequency, as was previously discussed relative to Figure 11, and second, the shear parameter of the viscoelastic-damped structural configuration is inversely dependent upon frequency.

Having selected structural materials and established the geometry of the damped gimbal arms and truss members, the next step is to select a viscoelastic damping material having a high loss factor in the 4 to 6 cps frequency range. While some data of this nature are available[15], they are insufficient to make an immediate selection. Assuming that a suitable viscoelastic damping material is located, the shear parameter should then be made as close to optimum as possible by making appropriate changes in the geometry and in the thickness and amount of viscoelastic material used in the structural composite. This represents a trial-and-error solution inasmuch as different viscoelastic materials may have to be

employed if the optimum thickness of the viscoelastic damping layers is too small or too large from a practical point of view.

While a number of determinations remain to be made, experience indicates that, pending the development of appropriate shear parameter expressions and the selection of a suitable viscoelastic damping material, the loss factor of the damped gimbal arms and truss members (fabricated in an "optimized" configuration) will be in the range of 0.05 to 0.2. For purposes of comparison, the loss factor of the conventional gimbal arms and truss members is estimated to be in the range of 0.02 to 0.03.

2.3 Modifications to Drive and Control Systems

Since the time of the initial design study of this simulator under Contract NAS 9- 623, there have been significant developments in the state of the art of electric motors and power control. These developments can significantly improve the performance of the simulator, while at the same time reducing its cost. The performance improvements have been factored into the present study in the analysis of modifications to the drive and control systems, arising from the structural modifications.

2.3.1 Motor Control by Silicon-Controlled Rectifiers

In the previous study, it was determined that the best method of achieving power control for the D.C. drive motors was to use Amplidyne motor-generator sets to supply modulated power to each set of drive motors. Such a system is within the state of the art and has sufficiently fast response for desired simulator performance. Such a system, however, has the disadvantage of being quite heavy and requiring a large number of separate stationary generators, the total cost of which is quite high. Furthermore, this method requires a separate set of bus bars for each separate set of controlled motors, resulting in 21 separate sets on the simulator. From the viewpoint of dynamic response, an additional second-order lag is placed in the control loop, which would have a tendency to decrease dynamic stability.

The development of the silicon controlled rectifier (SCR) is not particularly new, since this device has existed for over ten years. Only within the last two years, however, has the SCR become a popular device for

the control of electric power. At the time of the initial design study, SCR's were not available in sufficiently high power ratings to handle the large currents required by the drive motors. In the last year the power ratings have increased greatly, and due to much larger production volumes, the price of these devices has been substantially reduced. It is now entirely feasible to use the SCR's as the primary power control element instead of the Amplidyne motor-generator sets.

The SCR would be used in this system as the basic component of a three-phase, full-wave rectifying bridge to convert public utility AC voltage to modulated DC voltage. These bridge rectifiers are all-electronic, static power amplifiers and light enough in weight so that they may be mounted on the simulator adjacent to the motors which they control. In such a configuration they receive power from a main AC bus, thus avoiding the problems of many sets of bus bars, as used in the rotating amplifier configuration. More important, however, is their speed of response, which is much faster than the Amplidyne units which they replace. Because this portion of the system has a much faster response than the remainder of the components of the drive and control loop, it can be treated dynamically as a pure gain with zero time lag. This somewhat reduces the stability problems which arise from the use of a rotating amplifier with its second order lag. Another major advantage of the SCR configuration is the ability to be operated directly off the AC power line, thus eliminating the costly requirement for two large diesel-driven DC generators previous recommended. Of course, this operation directly off the substation power line does not

provide the power demand isolation which was obtained by the use of diesel generators, but we believe this is a small price to pay for the increased performance and reduced cost of the SCR controllers. A block diagram of the control system is shown in Figure 24. This is basically the same system shown in Figure 60 on Page 7.33 of Ref. 1, the primary difference being the use of the SCR bridges to replace the Amplidyne generators.

2.3.2 Disc-Design Ironless Motors

In the initial study, the use of compensated high power DC motors was determined to be the best method of converting electrical power to mechanical power. These motors, although having excellent response characteristics compared to other electric motors of the same power rating, are nonetheless conventional motors. Recently, the Tapco Division of Thompson Ramo Wooldridge, Inc. has developed a very unconventional motor of proprietary design, and the characteristics of this motor make it ideally suited to application on this simulator. Because of the proprietary nature of this device, the full details of its design can not yet be released. However, the outstanding features of the motor are its aluminum construction, its high power-to-weight ratio, and its ability to deliver for short periods peak power up to 25 times its rated capability. These characteristics make the motor ideal because of the requirements for minimum weight and high peak power with considerably reduced RMS power.

The motor's ironless construction results in no saturable ferromagnetic material, thus providing linear operation in the overload region. The output capabilities of the motor are limited only by its temperature

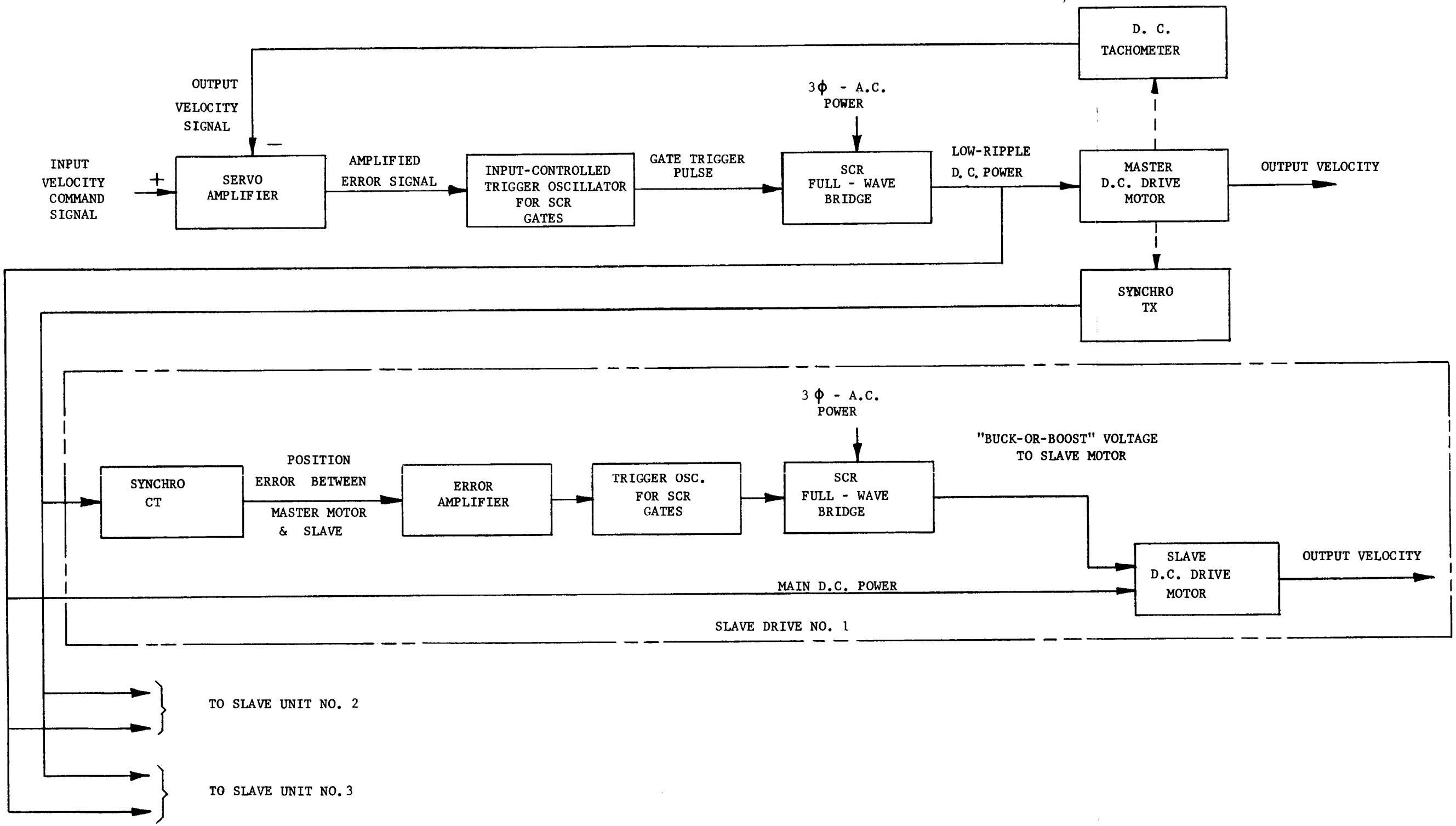

Figure 24
FUNCTIONAL BLOCK DIAGRAMS OF SCR - CONTROLLED DRIVE
SYSTEM FOR TRANSLATIONAL AXES OF SIMULATOR

rise and rim stress at the periphery of the rotor. Because of the disc design of the rotor and stator with almost all coil surfaces exposed to circulating cooling air, the motor can develop much higher torque than a conventional motor for the same temperature rise. In the previous design the weight of the drive motors was a significant portion of the total weight, and a large percentage of the motor power was consumed in driving its own weight. Now, by using the TRW motors, the motor weight can be made negligible compared to the structure weight, and thereby reduce the requirement for excess power to accelerate the mass of the drive motors themselves.

2.3.3 Drive System Based on Structural Modifications

Regardless of the availability of the raw developmental hardware discussed in the foregoing sections, a modification of the drive system for each degree-of-freedom would have been required because of the change in weights resulting from the modified structural analyses given in Section 2.1. We have considered both the changes in structural characteristics and the new drive and control equipment in the revised design of the drive systems. Drives were studied for the 10 cps lightly-damped structure and the 5 cps viscoelastic-damped structure. The masses and moments of inertia for each axis are so similar for the two configurations that the same drive system applies to both configurations for any particular axis. These drives are summarized in the following tables, Table VII being the gimbal drive, and Table VIII being the translational drive.

TABLE VII

GIMBAL DRIVE SYSTEM

Axis of Rotation	Drive Motor	Reduction Ratio	Max Load Speed (rad/sec)	Max Load Accel (rad/sec^2)	Peak Load Torque (lb in)	Peak Flow at 2000 psi Across Motors (gpm)	Peak Power to Hyd. Motor (hp)
X (Roll)	MF-3909-15	111:1	4.19	20.9	6660.	3.65	4.26
Y (Pitch)	(2) MF-3915-30	70:1	4.19	20.3	67,200.	36.4	42.4
Z (Yaw)	(2) See Note 2.	45:1	4.19	19.3	344,000.	180.	327.

Notes:
1. Motors for roll and pitch axes are Vickers Fixed Angle Airborne Axial Piston units.
2. Motors on yaw axis are Vickers new In-Line Axial Piston Units with 12.07 in^3 displacement. (No Model No. Assigned Yet).
3. Gear reduction units for the roll and pitch axes are Harmonic Drives and for the yaw axis are Spiroid gears.

TABLE VIII

TRANSLATIONAL DRIVE SYSTEM

Axis of Translation	No. of Drive Motors (1)	Reduction Ratio (2)	Max Load Speed (ft/sec)	Max Load Accel. (g)	Peak Load Torque (1b ft)	Peak Power To Load (hp)
X	4	5:1	15	2	37,000	2,020
Y	1	5:1	15	2	6,000	327
Z	2	5:1	15	2	16,000	871

NOTES:

1. Motors are TRW disc-type, nominally rated at 50 hp at 1400 rpm.
2. Gear reduction units are Philadelphia Gear modified Model 4109 hardened and ground helical gear reducers.

2.4 Analog Simulation of Structure, Drive and Control System

To compare the response to transient forces of our redesigned simulator structure in its damped and undamped configurations, we have prepared simplified mathematical analogs of the structure, drive and control system, and have obtained solutions on an analog computer. The simulation is limited to longitudinal response (x-axis motion) of the entire simulator to a force pulse applied along the x-axis.

The primary comparison is between the response of a lightly-damped simulator structure having a fundamental vibration frequency of 10 cps, and a heavily-damped structure having a fundamental frequency of 5 cps. For each structure, two types of feed-back control of motion are considered.

The basic drive system consists of a velocity servo. That is, a voltage proportional to the input velocity (ω_i) is compared to a voltage proportional to load velocity (ω_o) and the existing error is amplified to drive the servo-motor. A block diagram in Figure 25 shows this velocity servo system, K, in the first block at the left represents the composite gain of the amplifier, the motor, and the gear reduction. The S term in the denominator represents the servo-motor integral. Servo-motor time constants were neglected since they were considerably higher than the structural time constants. (A more exact determination would require inclusion of these time constants, but for a preliminary simulation, they can be safely ignored.) The next block to the right contains the transfer function of the structure, where K_L is the spring constant, B_L is the damping, and M_L is the mass. The last block contains the transfer function

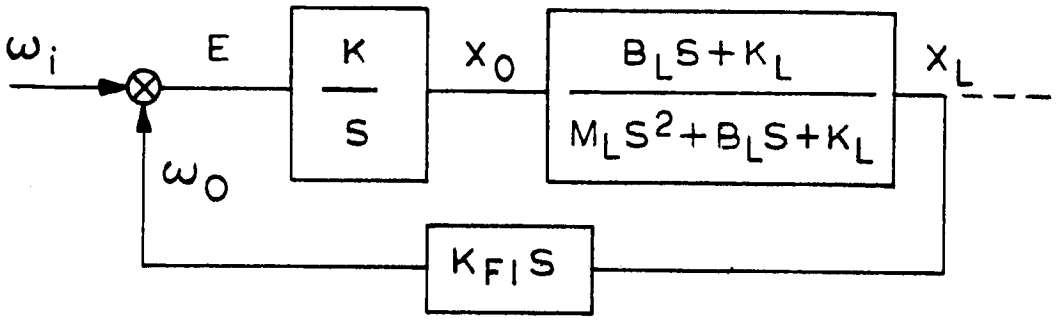

$$\frac{\omega_O}{\omega_i} = \frac{KK_{F1}(B_LS+K_L)}{M_LS^2+B_L(1+KK_{F1})S+K_L(1+KK_{F1})}$$

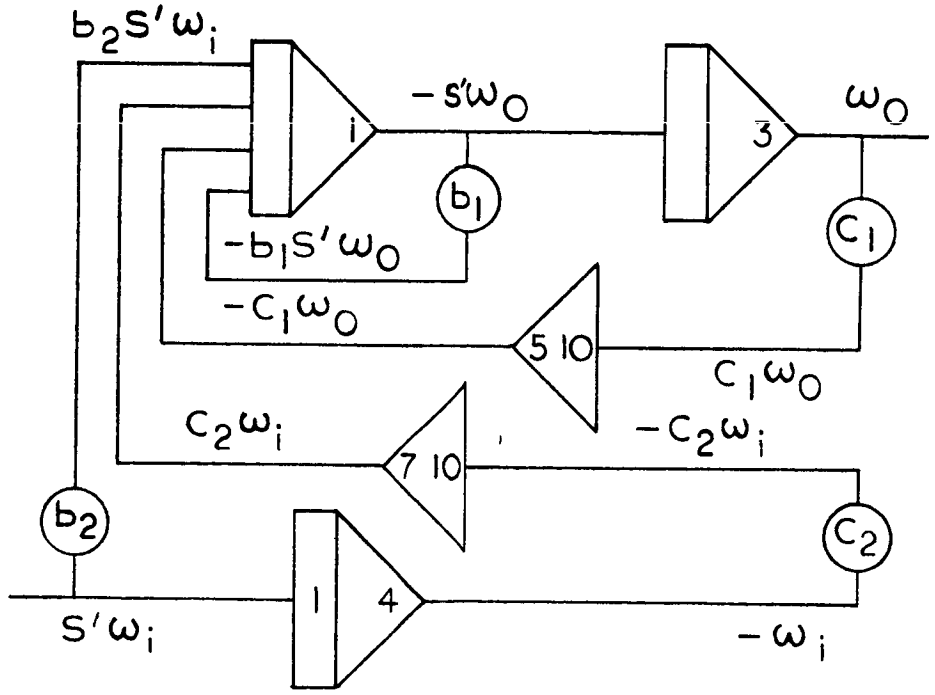

$$(S')^2\,\omega_O = 0.113S'\omega_i + 3.55\omega_i - 0.126S'\omega_O - 3.94\omega_O$$

Figure 25
COMPUTER SETUP FOR VELOCITY FOLLOW-UP

of the follow-up tachometer. The closed-loop transfer function ω_o/ω_i is shown directly below the system block diagram.

Using straightforward analog computer techniques, this transfer function is mechanized in the form shown at the bottom of Figure 25. Three integrator and two inverter amplifiers were required. A time division of 100/1 was used, and the resulting equation is shown at the very bottom.

By applying a pulse of acceleration, such as might be obtained by pushing oneself away from a wall, to the computer at $s'\omega_i$, an output such as shown in Figure 27(a) was obtained for the parameter ω_o. The various parameter values for this structure are given in Table IX. Structural mass is obtained from Table II, Section 2.2, with the addition of mass of drive system components. Spring constant is simply that for a single-degree-of-freedom structure with frequency of 10 cps, and mass M_L. Damping is obtained from Section 2.3.

TABLE IX

Characteristics of Structure, Drive and Control System for 10 cps, Lightly-Damped Configuration

Parameter	Magnitude	Dimensions
M_L	1.15×10^3	lb sec^2/ft.
B_L	1.45×10^3	lb sec/ft
K_L	4.54×10^6	lb/ft
$\zeta = \eta/2$	0.01	(dimensionless)
K	1.47	ft/sec/volt
K_{F1}	6.12	volt/ft/sec

With the proceeding set-up, that is a 10 cps, lightly damped structure, the velocity response is extremely oscillatory. However, by the addition of a single feedback term, the original block diagram is modified as shown in Figure 26. Note that a voltage proportional to load acceleration ($K_{F2}s^2$) is added for stabilization purposes. The new transfer function is shown directly below, as are the analog computer set-up and the 100/1 time-scaled equation.

Now, by inserting the same pulse of acceleration into the new system, the response of the system was obtained. This is shown in Figure 27(b). Note that the output velocity settles to its final value much more quickly. Apparently the effective damping coefficient was increased from 0.01 to about 0.3.

An examination of the output velocity response (ω_o) will show that it is actually oscillating at about 30 cps, even though the basic structure has an undamped natural frequency of 10 cps. This is a natural result of applying feedback from the load output-that is, enclosing the structure in the closed-loop system. Note that the characteristic equation of the structure is $M_L s^2 + B_L s + K_L$ and the undamped natural frequency is $(K_L/M_L)^{1/2}$. Also note that the characteristic equation of the closed loop system is $M_L s^2 + B_L\ (1 + KK_{F1})s + K_L\ (1 + KK_{F1})$ and its undamped natural frequency is now $\left[K_L\ (1 + KK_{F1})/M_L\right]^{1/2}$. The difference between the two is the addition of the term $(1 + KK_{F1})^{1/2}$, which is about 3, increasing the system frequency. Note also that the damping term B_L has been increased by the factor $(1 + KK_{F1})$, so that the effective damping of the servo-controlled system is greater than that of the structure alone.

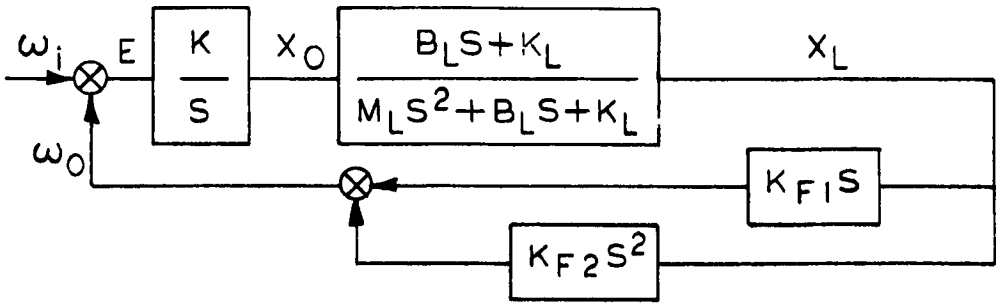

$$\frac{\omega_0}{\omega_i} = \frac{K(K_{F1}+K_{F2}S)(B_LS+K_L)}{(M_L+KK_{F2}B_L)S^2+(B_L+B_LK_{F1}K+KK_{F2}K_L)S+K_L(1+K_{F1}K)}$$

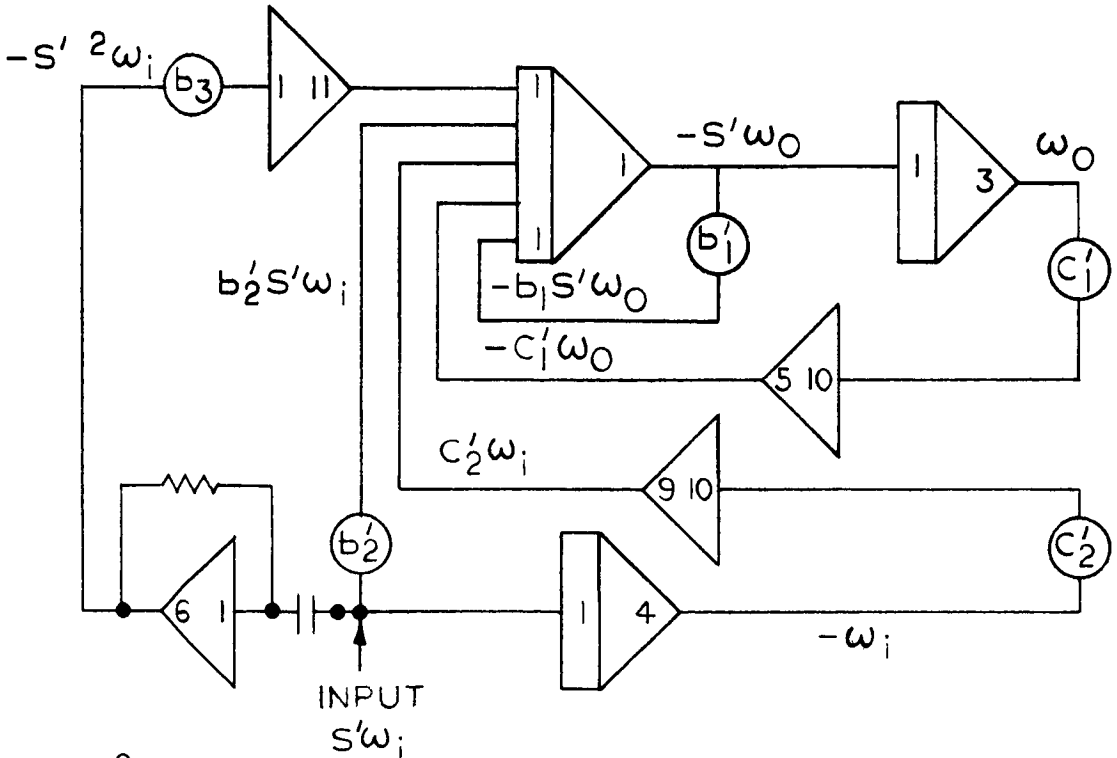

$$(S')^2\omega_0 = 0.028\,S'^2\omega_i + 0.99S'\omega_i + 3.54\omega_i - 1.05S'\omega_0 - 3.84\omega_0$$

Figure 26
COMPUTER SETUP FOR VELOCITY AND ACCELERATION FOLLOW-UP

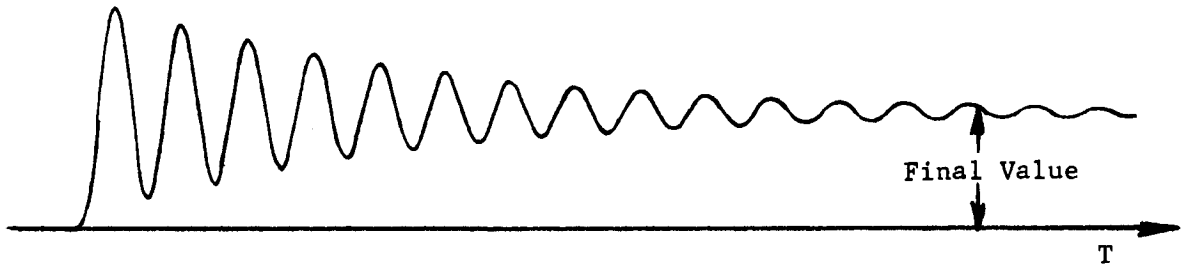

(a) Without Acceleration Feedback

Time Scale: 1 In = 10 Sec Real Time

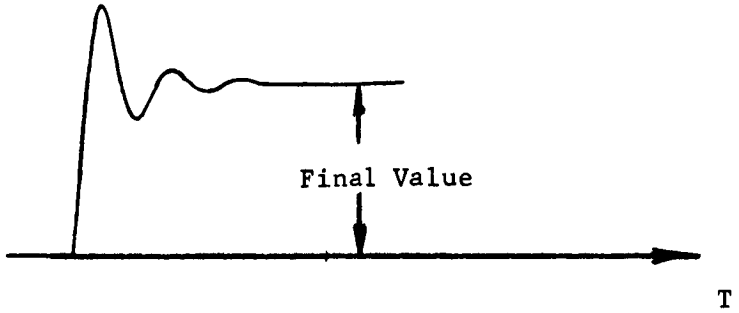

(b) With Acceleration Feedback

Figure 27
OUTPUT VELOCITY RESPONSES FOR ACCELERATION PULSE
INPUT: 10 CPS STRUCTURE

A further simulation was made using the 5 cps structure, with a damping coefficient of 0.1, and obtaining velocity responses with and without acceleration feedback such as was done for the 10 cps structure. The various parameter values for this structure are shown in Table X.

TABLE X

Characteristics of Structure, Drive and Control System for 5 cps, Heavily-Damped Configuration

Parameter	Magnitude	Dimensions
M_L	1.12×10^3	lb sec^2/ft
B_L	7.06×10^3	lb sec^2/ft
K_L	1.11×10^6	lb/ft
$\zeta = \eta/2$	0.1	(dimensionless)
K	1.47	ft/sec/volt
K_{F1}	6.12	volts/ft/sec

The same computer set ups were used as before, though the parameters were changed. Again acceleration pulses were inserted, and the velocity responses were obtained. These are shown in Figure 28(a) (no acceleration feedback) and 28(b) (with acceleration feedback).

The improvement obtained with acceleration feedback is not so dramatic this time, since the structure was much more highly damped to begin with. The overall damping coefficient apparently increased from $\zeta = 0.4$ to $\zeta = 0.5$ in this case.

An examination of the system responses of Figures 27 and 28 shows that the addition of acceleration feedback to the 10 cps lightly-damped

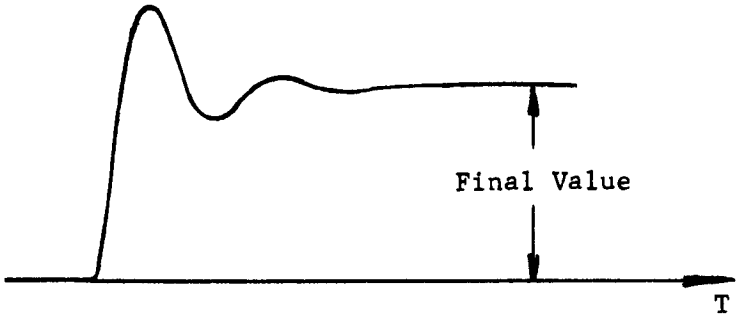

(a) Without Acceleration Feedback

Time Scale: 1 In = 10 Sec Real Time

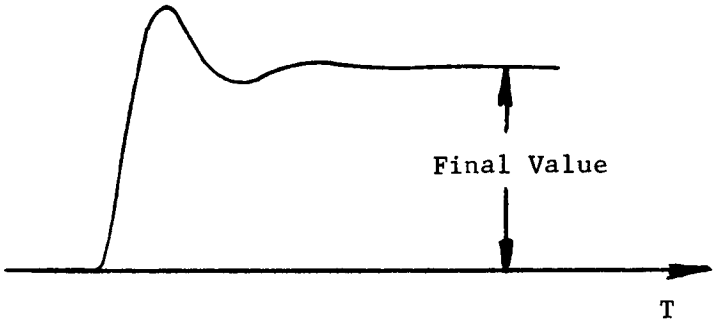

(b) With Acceleration Feedback

Figure 28
OUTPUT VELOCITY RESPONSES FOR ACCELERATION PULSE
INPUT: 5 CPS DAMPED STRUCTURE

system gives the greatest single improvement. Considering the fact that the 10 cps structure is probably less expensive and easier to fabricate than the moderately damped 5 cps structure, the obvious first choice is a 10 cps structure with acceleration feedback. Note that the cost of adding an acceleration feedback signal is very minor, so that the choice can be based almost solely on the structure cost and ease of fabrication.

2.5 Cost Analysis

In this section, we will present budgetary estimates of the cost of the simulator, for various sizes between 50' x 50' x 200' to 100' x 100' x 200'. These costs include costs of engineering and manufacturing labor and overhead, purchased equipment, materials, rigging and construction at MSC, power sub-station, etc. They specifically exclude the cost of a large digital computer which must be integrated into the simulator for control of motion. Table XI lists the budgetary estimates of costs for four specific sizes for the simulator. Estimates for other sizes can be obtained by interpolation between these figures.

TABLE XI

Budgetary Cost Estimates for Simulator

Simulator Size	Cost, 10^6 Dollars
50' x 50' x 200'	3.33
75' x 75' x 200'	3.66
85' x 85' x 200'	3.85
100' x 100' x 200'	4.11

2.6 Conclusions and Recommendations

2.6.1 Conclusions

A primary conclusion which we reached as a result of the more exact and detailed vibration analysis, reported in Section 2.2 and Appendix A, is that the structural weight can be considerably reduced below that estimated in Reference 1, for the same fundamental vibration frequency. Because this weight can be substantially reduced, we now feel that it is feasible to design a simulator structure larger than the 75' x 75' x 200' recommended in Reference 1. The size of 100' x 100' x 200' appears now to be quite feasible.

In evolving a minimum weight design for the gimbal structure, we concluded that there was little advantage in tapering the arms in either depth or width. Consequently, the recommended design for all gimbal arms employs elements with constant cross-sections.

The primary conclusions of our analysis of techniques for application of viscoelastic damping material to the simulator structure are that the weight of a 5 cps damped structure is approximately equal to the weight of a 10 cps undamped structure, and that the damping coefficient can probably be raised by no more than a factor of ten over the damping inherent in a conventional built-up structure. It was also concluded that considerable development work would be required before one could be assured of efficiently achieving high damping of our large, relatively low frequency structure by viscoelastic techniques.

From the further study of the drive and control systems, we concluded that we could achieve better control of motion and save considerable weight in translational drives by using new, lightweight DC motors, and controlling them by silicon-controlled rectifiers. Drive power requirements were also considerably reduced by reduction in structural weight.

As a result of our analog simulation of response of structure, drive and control systems to transient forces, we concluded that the 5 cps damped structure had considerably better transient response than the 10 cps undamped structure for a velocity feed-back control system, but that the addition of damping had very little effect for an acceleration feed-back control system.

2.6.2 Recommendations

From our analysis in this section, we make the following recommendations:

1. That the simulator structure be built in either the 75' x 75' x 200' size or the 100' x 100' x 200' size.

2. That the structure be of conventional construction (no viscoelastic damping) designed for 10 cps fundamental vibration frequency, and that the control system employ servo control based on feedback proportional to acceleration at the payload.

3. That additional development work be done, if viscoelastic damping of the structure is to be further considered.

4. That the drive system incorporate lightweight DC motors of new design, and control of these motors utilize silicon-controlled rectifiers.

3.0 MODIFICATION AND TEST OF MAN-SUPPORT HARNESS

In this section, we will present a discussion of our efforts on Phase II of the program, concerned with the development of a man support harness. The tasks in this phase include:

1. Modify the existing man support harness so that it comfortably supports a man in any static position or rotational mode while he is dressed in conventional clothing.
2. Make a harness for supporting the man in the simulator while he is encased in a pressurized space suit.
3. Devise a method for supporting a man in the simulator while he is wearing a back-pack propulsion unit.
4. Construct a test rig for evaluating the various harness designs, and test several subjects in "shirtsleeves" and pressure suit.

During our original feasibility study for the space motion simulator, an orthopedic appliance specialist was engaged to construct a support harness capable of holding a man safely in the simulator, while allowing him almost complete freedom of use of his limbs. This harness presented a good basic concept for a support harness, but it was recognized at that time that development, modification and testing remained to be done before we could be certain of having a safe useable harness for the simulator. We therefore proposed to test and modify the original support harness. A test rig design was formulated which could support a man in the harness in various attitudes and rotate him at low angular velocities about various axes.

Shortly after the initial testing of the modified harness began, it became apparent that more body surface contact would be essential to support the man adequately when he was in the upright position in the harness. A conceptual model of a two piece fiberglass harness was developed. These fiberglass parts were molded from a plaster cast that had been made to the exact contour of one of the subjects. These pants and vest were tested for feasibility at the end of the program.

3.1 Test Set-Up

3.1.1 Test Fixture

A harness test fixture (Figure 29) was constructed in the AAI Mechanical Laboratory. This fixture enabled the test conductor to position a subject (in harness) at various static positions or to slowly rotate the subject about his center-of-gravity in various axes.

Fundamentally, this fixture was a hand-powered one-degree of freedom half ring gimbal system supported by two end frames. The test subject was indexed about his Roll Axis (x) to allow him to be rotated continuously about his Pitch (y) or Yaw (z) axis. After the subject was placed in the test fixture, the system was balanced by positioning counterweights in the support arms of the gimbal.

To accommodate a subject in the Mercury Full Pressure Suit, a rotary joint was incorporated in one of the gimbal-end frame attachment points to supply breathable air to the harness area, and at the other attachment point an electrical slip-ring for the Mercury suit communications system was installed.

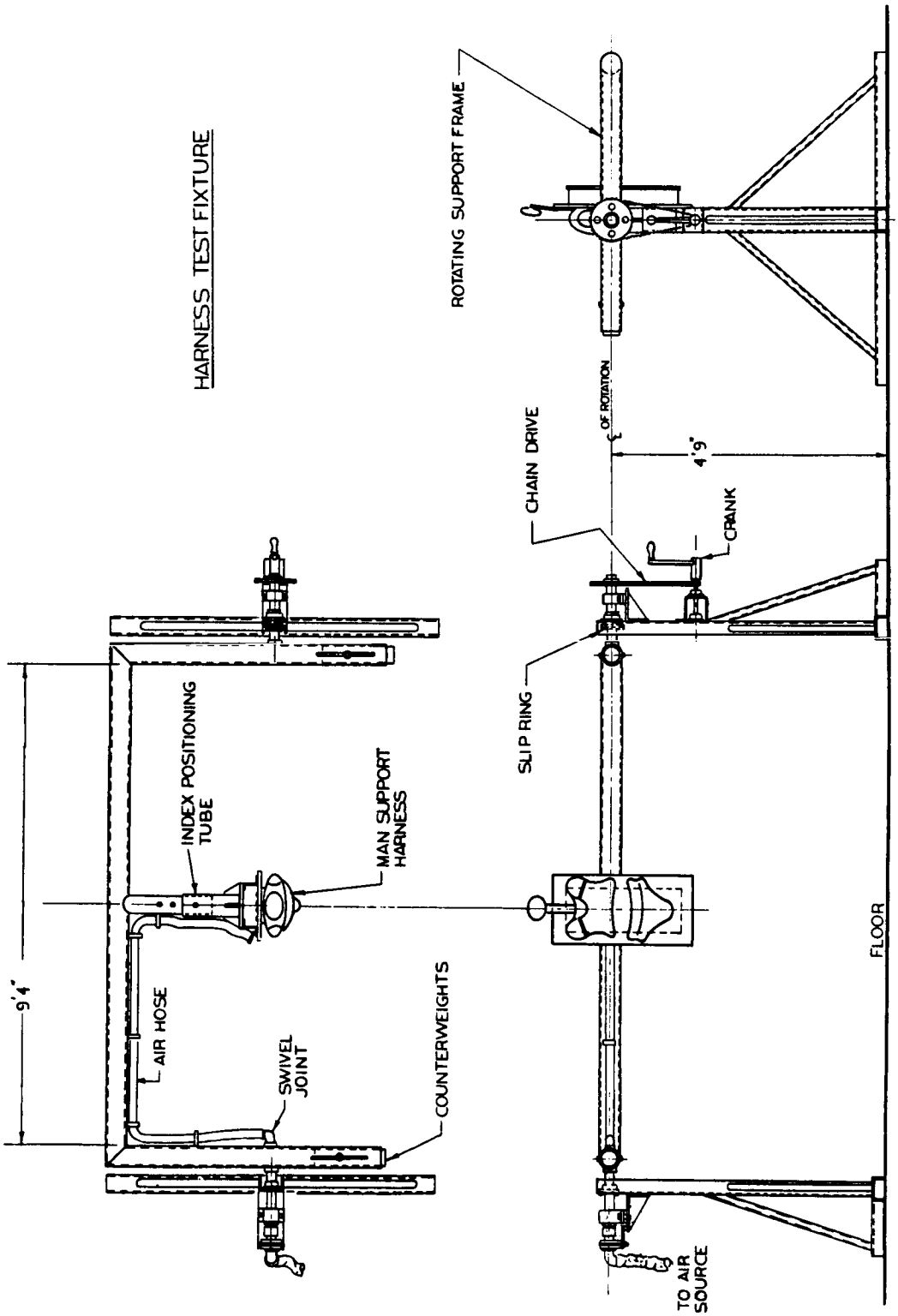

Figure 29
HARNESS TEST FIXTURE

3.1.2 Harness Ingress-Egress

As the purpose of the harness tests was to validate only the man-support capabilities of the harnesses, rapid, simplified ingress-egress features were not included in the prototypes. Nuts and bolts were used as attachment hardware in lieu of cam-lock type fasteners, etc. that would permit rapid installation or removal of the subject from the harness.

The procedure for test and removal of a subject in the modified harness was as follows: (1) the subject stood on a platform and rested against the harness back brace; (2) the corset was laced and the breast plate was attached to the back plate; (3) the swing seat was then placed under the subject's buttocks and adjusted to hold him firmly against the harness shoulder braces; (4) the platform was then removed and the subject was allowed to hang in the harness in an upright position for approximately 5 minutes; (5) the planned test was then run and the subject was returned to an upright position; (6) the subject was then asked his subjective opinion of the harness and examined for superficial evidence of pinching or welting.

The procedures for installation, test, and removal of a subject in the molded fiberglass harness were similar but simpler than that of the modified harness. The procedures were as follows: (1) the two-halves of the molded harness "pants and vest" were positioned on the subject and bolted in place; (2) the subject mounted the platform and backed the harness pickup attachment over the test fixture pickup shaft; (3) attachment was made by dropping a pin through four matching holes and securing

it; (4) the platform was then removed and the subject was allowed to hang, in an upright position for approximately 5 minutes; (5) the planned test was run and the subject was returned to an upright position; (6) the platform was emplaced and the securing pin holding the harness to the test fixture was removed; (7) as the two halves of the harness were removed from the subject, he was asked for comments on the harness "fit".

3.2 Harness Design

3.2.1 Modification of Initial Harness

The initial harness, (see Figure 30) designed under contract NAS 9-623, was adapted to the test rig, and several subjects were held in it in several attitudes. For all body positions except upright, the harness proved to be comfortable, for a number of test subjects of different size. However, with a subject in the upright position, he would gradually slip out feet first. To correct this defect, the harness was fitted with a canvas parachute-type seat attached to the breast-plate approximately at shoulder height. The harness back was shortened three inches at the bottom, and stronger aluminum straps were used to attach the breast plate to the harness back. The head support was stiffened and the lower safety belt was removed. A subject is shown in the modified harness in Figure 31 .

Preliminary tests of the modified harness pointed out another severe problem. With the subject's weight in the canvas seat, the breast plate was drawn down onto his sternum, interfering with normal breathing and inducing a nauseous condition. As the breast-plate portion of the harness does not have to form-fit, a 1/2 inch aluminum rod was attached to

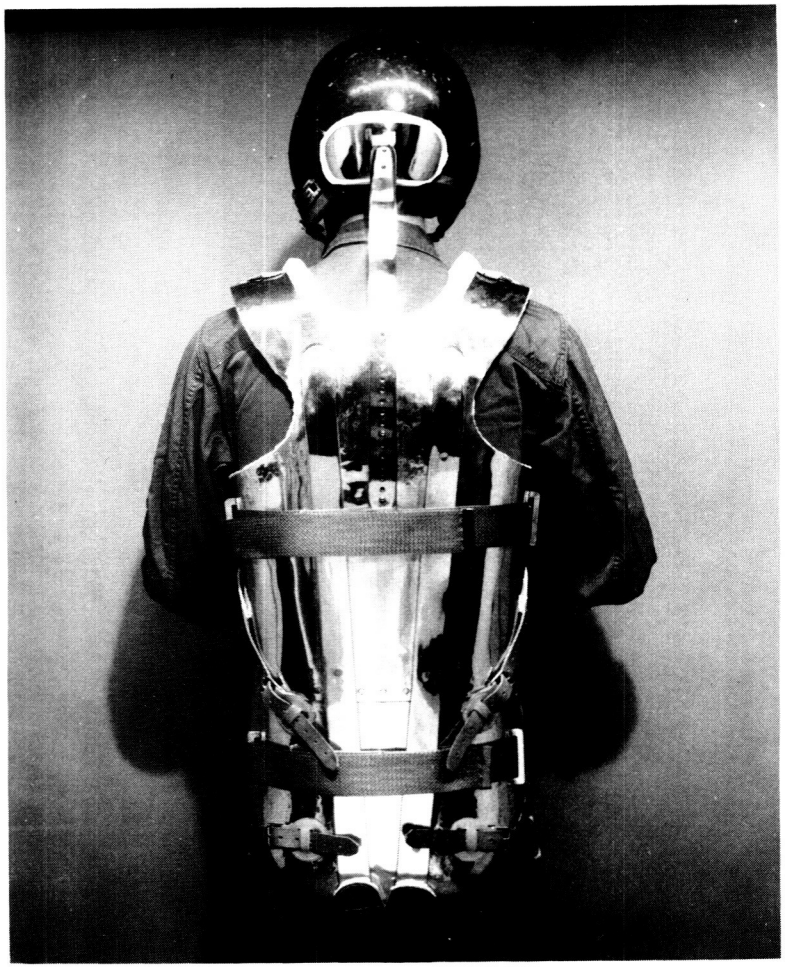

Figure 30
INITIAL HARNESS PRIOR TO MODIFICATION

Figure 31
TESTING OF THE INITIAL HARNESS AFTER MODIFICATION

the base of the breast-plate and curved to attach to the harness back plate, restricting the motion of the breast-plate when weight was added to the seat.

At this point, an experimental test program was defined and six subjects were selected on the basis of their general health, fit in the Mercury Full Pressure Suit, and interest in the biokinetics program. Simple medical monitoring procedures were established and pre-test familiarization runs were conducted for all subjects.

During these familiarization runs in the harness test fixture, radical blood pressure drops were noted on two subjects. All testing was stopped and medical advisors were consulted. Their analyses led to the conclusion that while involved in the rotational maneuvers, anxiety on the part of the subjects was causing nausea and blood pressure anomalies. Static time in the harness at various positions seemed to alleviate subjective anxiety.

The tests were conducted as follows:

1. Subject was placed in the harness and allowed to hang free for 5 minutes in an upright position.
2. Subject was rotated in pitch backward ($-\theta_y$) for 5 revolutions at approximately 20 rpm.
3. Subject rested one-minute on his back, face up.
4. Subject was rotated in pitch forward ($+\theta_y$) for 5 revolutions at approximately 20 rpm.
5. Subject rested one-minute in an upright position.
6. Subject was rotated in pitch backward ($-\theta_y$) for 5 revolutions at approximately 20 rpm.

7. Subject rested one-minute in a face-down position.
8. Subject was rotated in pitch forward ($+\theta_y$) for 5 revolutions at approximately 20 rpm and brought to an upright position.
9. Subject was removed from harness and inspected for welts, pressure marks, and superficial eruptions.
10. During inspection, the subject's answers to the question "How did it fit?" were recorded.

All six subjects were tested, and their comments and the results of their physical examinations were recorded.

It was apparent from the testing that the initial harness was inadequate in the lower trunk region, especially in the posterior area. The parachute seat slipped over the subject's buttocks and he was then supported by the leg straps alone. This condition was painful due to the constriction of the venal, arterial, and nerve trunks on the inner side of the upper thigh.

One attempted solution to this problem was to replace the parachute seat with a bicycle seat. Two subjects attempted to rotate in the test fixture with this fix, but could not tolerate the discomfort, even when the seat was amply padded with foam rubber.

To eliminate the seat swing problem, the seat support mounting was changed from the breast plate to the ends of aluminum bars located at approximate waist height. With a subject in the harness, the seat support straps were parallel to the harness back plate and much shorter than when attached to the breast-plate. It was determined that the seat leg

restraint straps were unnecessary and they were eliminated. This fix greatly reduced, but did not eliminate seat movement and the associated problems.

A wooden "swing-seat" was next tried. The wooden seat was supported by straps attached to the harness support bars. See Figure 32 . Six subjects were tested with this harness and all found it comfortable. Little or no pinching or welting was found in the pitch maneuver ($\pm \theta_y$) or when the subject was indexed 90^o about his roll axis and then rotated continuously about his yaw axis ($\pm \theta_z$). Following these tests, it was decided that this harness was fairly satisfactory and that no significant improvements were possible without a major redesign.

In the latter stages of testing, the corset portion of this harness became more and more of a problem. It is not adjustable in length and, in its present form, not entirely universal - although, with some problems in lacing, etc. we have tested subjects from 5' to 6'4" in height and 145 to 265 pounds in weight. The durability of the corset is also questionable.

It was thought that a more rigid, better fitting harness that could be donned by the subject and still permit freedom of movement, and rapid attachment/detachment from the simulator would be of more utility to the user. A fiberglass harness was therefore designed and fabricated.

3.2.2 Design and Test of a Molded Fiberglass Harness

Two female molds were made by taking plaster body casts of one of the test subjects: one from the waist to the upper thighs (pants) and one from the lower rib cage over the shoulders (vest). The subject was positioned in a semi-squat posture to produce a "saddle-effect" in the buttocks region of the "pants" mold.

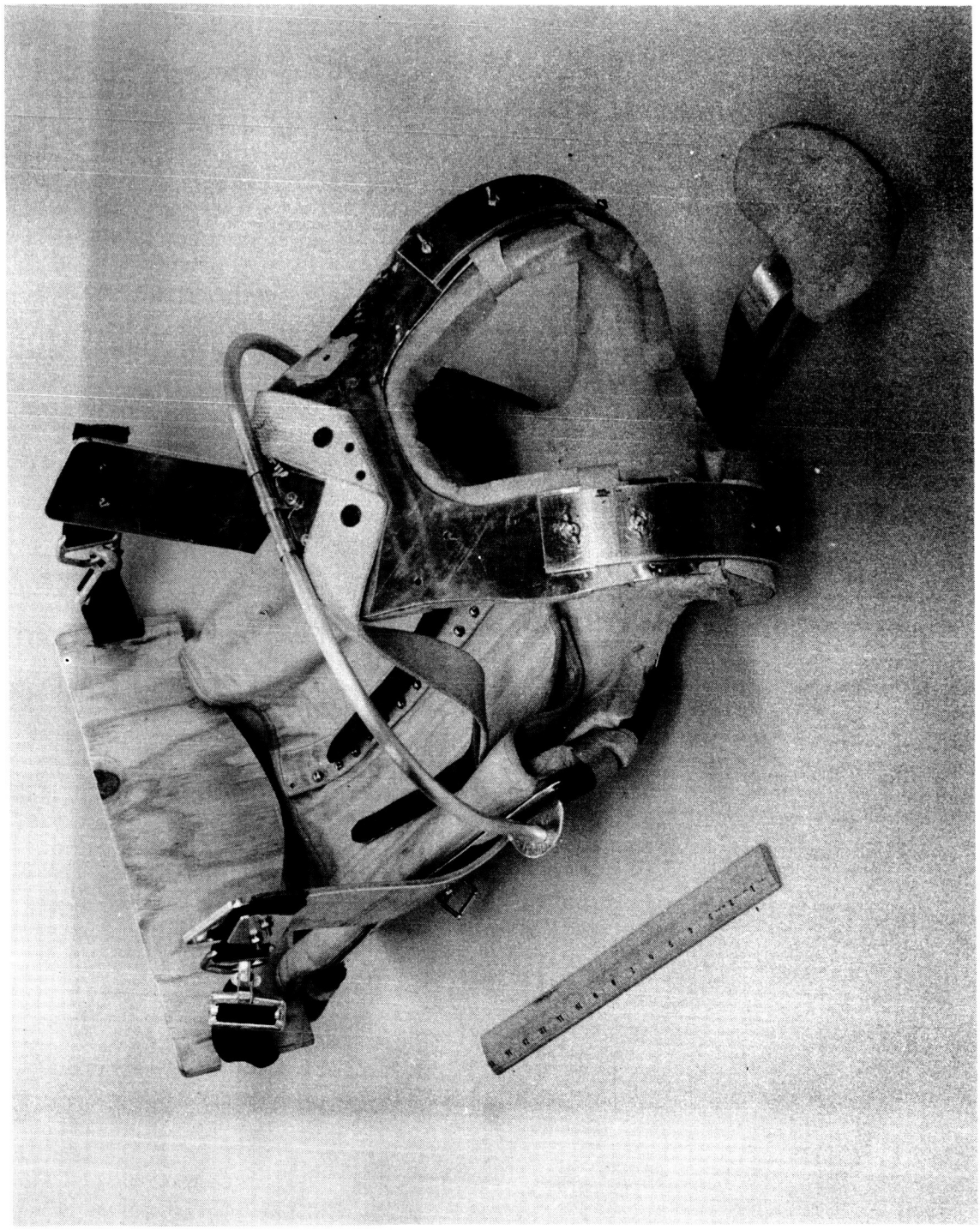

Figure 32

MODIFIED INITIAL HARNESS WITH WOODEN SEAT

The body casts were removed from the subject by parting them down the sides, then reassembled and used to produce plaster male molds. A hand layup of plaster in the crotch region of the "pants" male mold was done to improve the saddle-effect of harness. The male molds were then coated with a silicon-base parting compound to prepare for the fiberglass lay-up. The fiberglass polyester resin lay-up was applied to an approximate thickness of 1/4 inch. When cured, the fiberglass "pants and vest" were removed from the molds and trimmed and sanded. Reinforcing braces and attaching hardware were bolted to the fiberglass. All harness edges were covered with foam rubber as a safety feature and to increase the support surface area. See Figure 33 and 34 .

Initial tests of the fiberglass harness consisted of running a strap under the "pants" crotch and hanging in a vertical position to assure that the subject experienced no pressure points. Satisfactory results of this simplified test led to the fabrication of a fixture to adequately support both "pants and vest" portions of the harness and allow adjustment for height while affording the capability of donning the harness remote from the simulator. As can be seen in Figures 35 and 36 this harness allows the subject complete freedom of movement of his limbs.

Harness tests (θ_y and θ_z) were then conducted in the harness test fixture. Only two subjects were used in this testing as a given fiberglass harness will, by nature, fit only a small anthropometric range of the population. Figure 37 is a composite photograph of a subject rotating (θ_z) with his z-axis parallel to the floor.

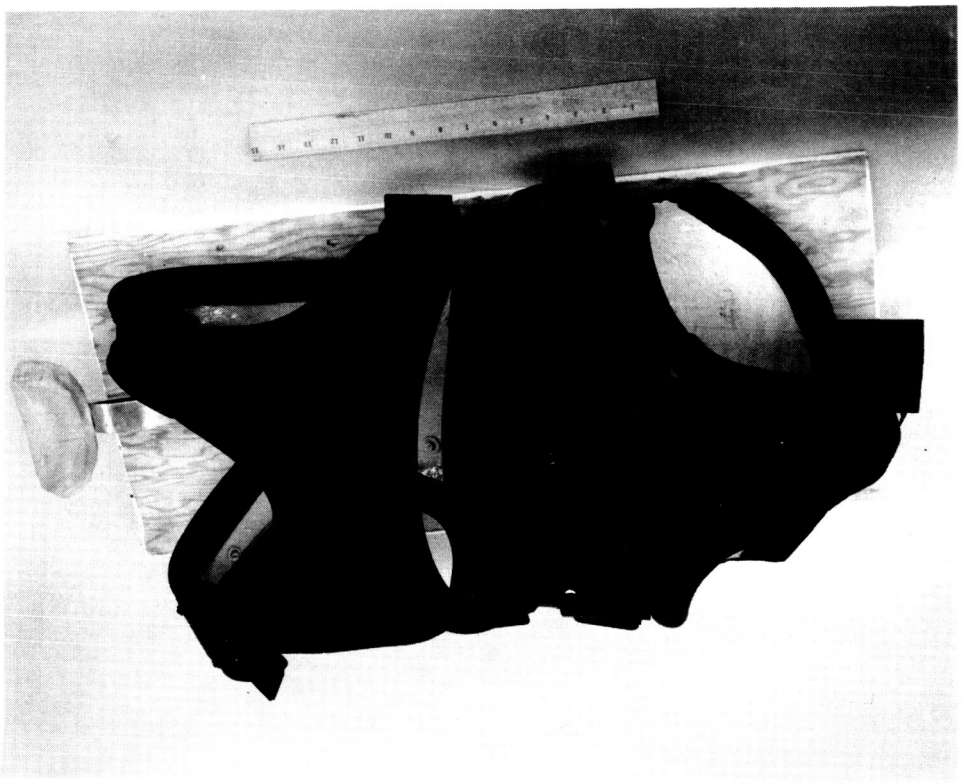

Figure 34
FIBER GLASS HARNESS ASSEMBLED

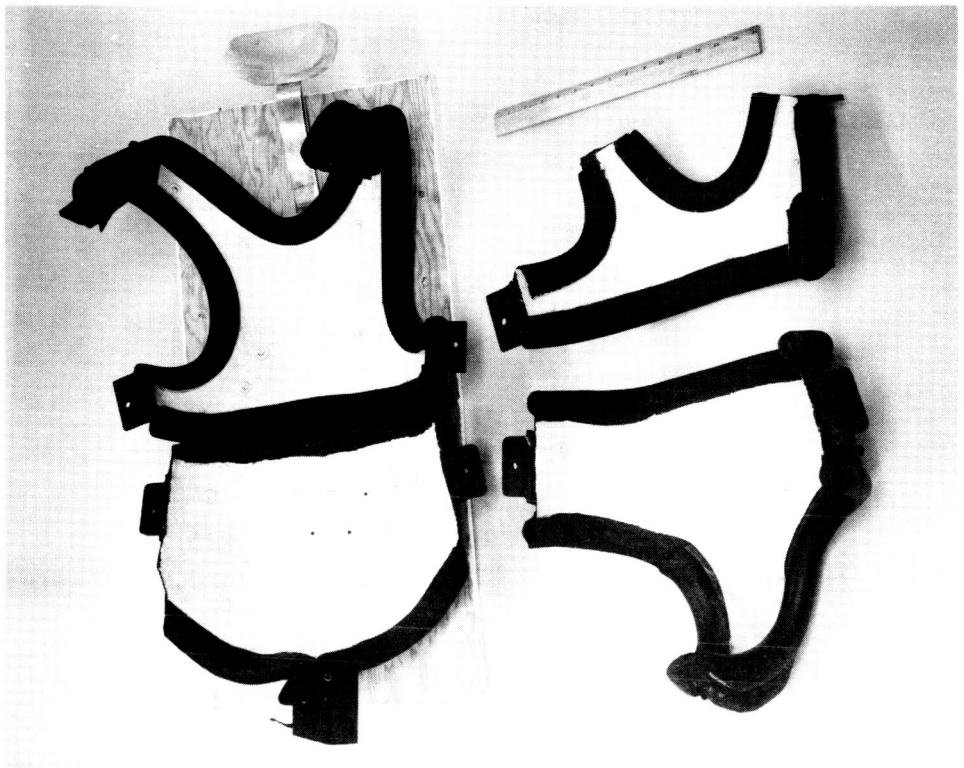

Figure 33
FIBER GLASS HARNESS WITH FRONT OPENED

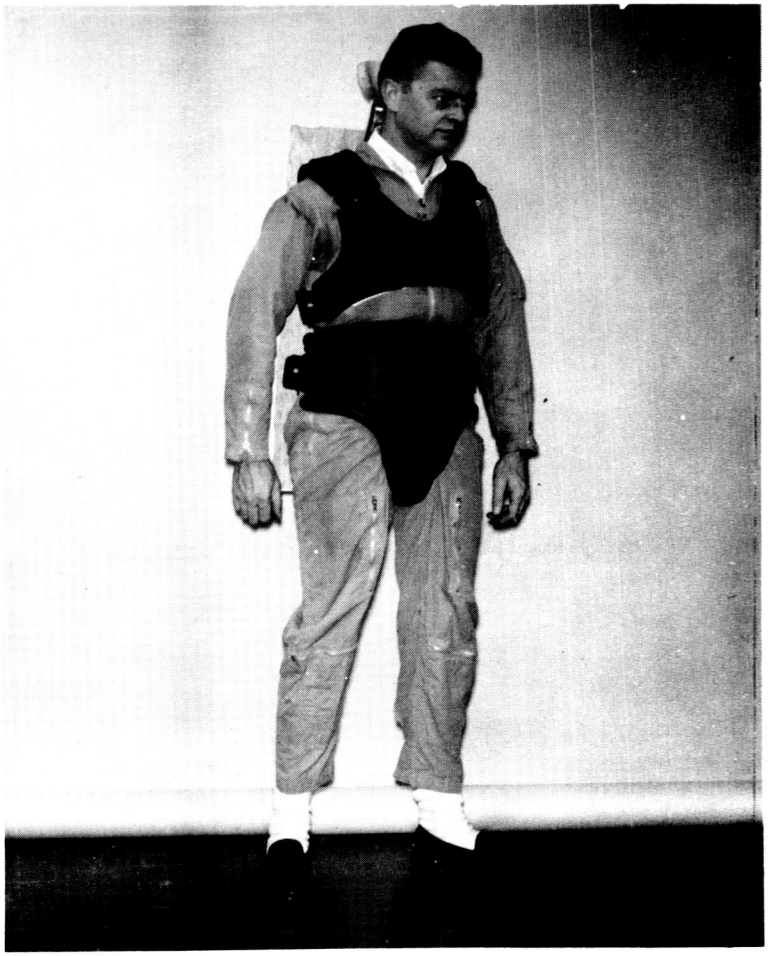

Figure 35
TEST SUBJECT IN FIBER GLASS HARNESS

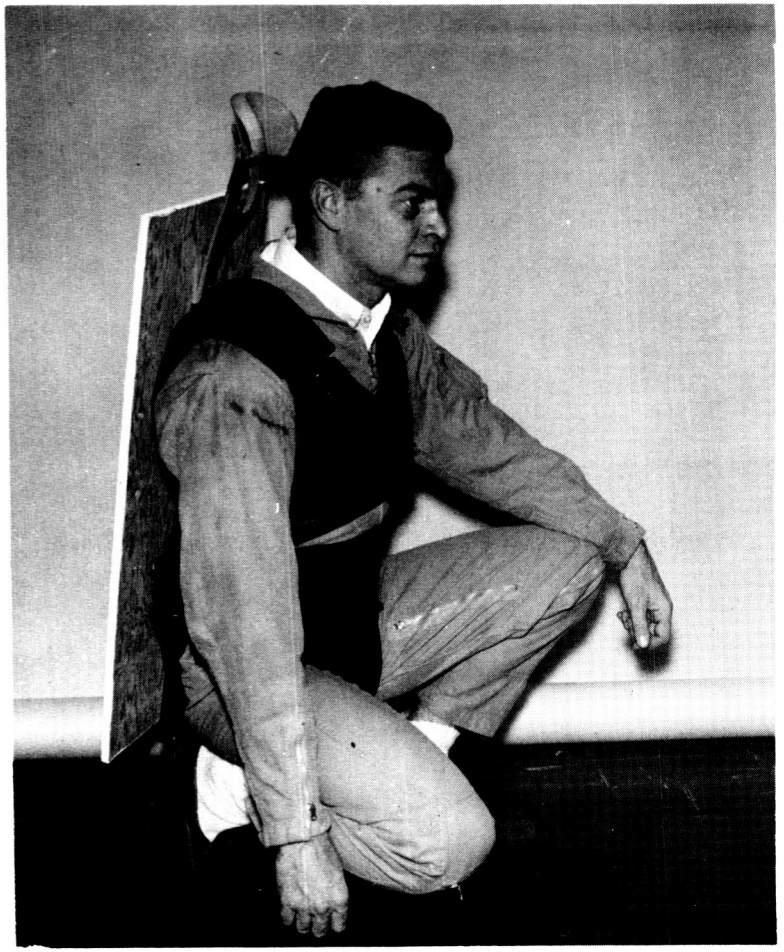

Figure 36
TEST SUBJECT DEMONSTRATING MOBILITY OF FIBER GLASS HARNESS

Figure 37
COMPOSITE PHOTO OF ROTATIONAL TEST

Both subjects were comfortable in the harness and showed no evidence of pressure points or pinching from the θ_y or θ_z maneuvers. Both subjects also expressed a preference for the fiberglass harness over the harness discussed under paragraph 3.1.1 of this report.

3.2.3 Harness For Pressure Suit Utilization

A harness for use when the subject is in the Mercury Full Pressure Suit under pressurized conditions, appears to be a fairly simple device. As long as the pressure suit was properly adjusted, i.e., the subject was more-or-less-standing in the suit leg stirrups, a simple lashing of the subject in the pressurized suit to a backboard provided adequate support. This lashing procedure was utilized to experimentally illustrate the concept that a subject was adequately protected from pressure points, etc. by the rigidity of the pressurized suit surrounding him and was not meant to be a final design.

The backboard was fitted with plastic-covered ropes - around the thighs, criss-crossed over the chest, and around the chest under the arms - and bolted to the test rig (see Figure 38). Three subjects were tested in static positions and low speed rotational maneuvers in this set-up, while maintained at 3.5 psi (10CFM) suit pressure, with no problems encountered.

3.2.4 Harness to be Used With the Back Pack Propulsion Unit

Figures 39 and 40 illustrate our design concept for supporting the man in the Space Motion Simulator while wearing an individual propulsion unit as a back pack. The most difficult situation from a support standpoint would be the situation where a subject must be positioned in the simulator with the propulsion unit while wearing street clothes or coveralls.

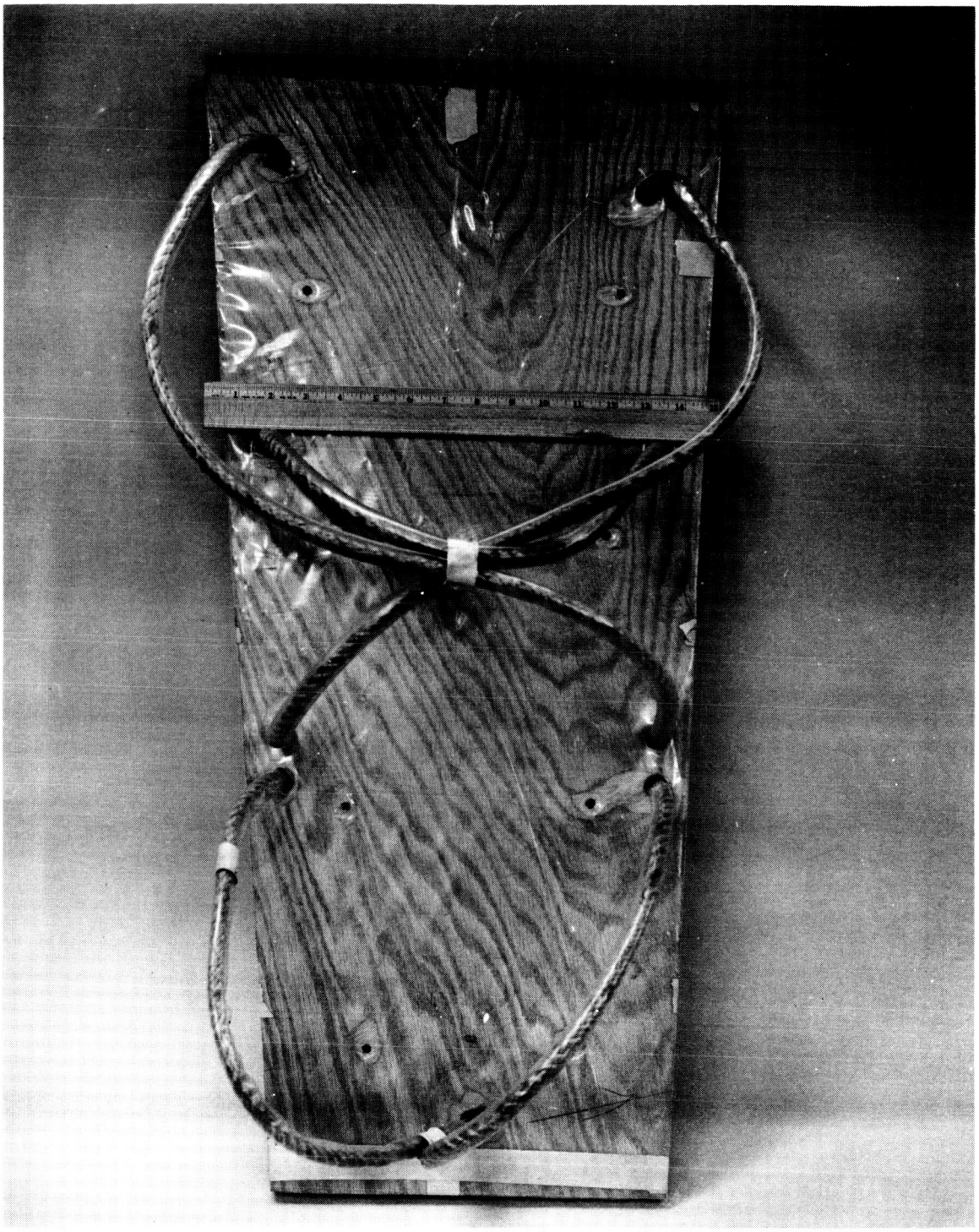

Figure 38
BACKBOARD AND STRAPS FOR SUPPORT OF SUBJECT IN A PRESSURIZED SUIT

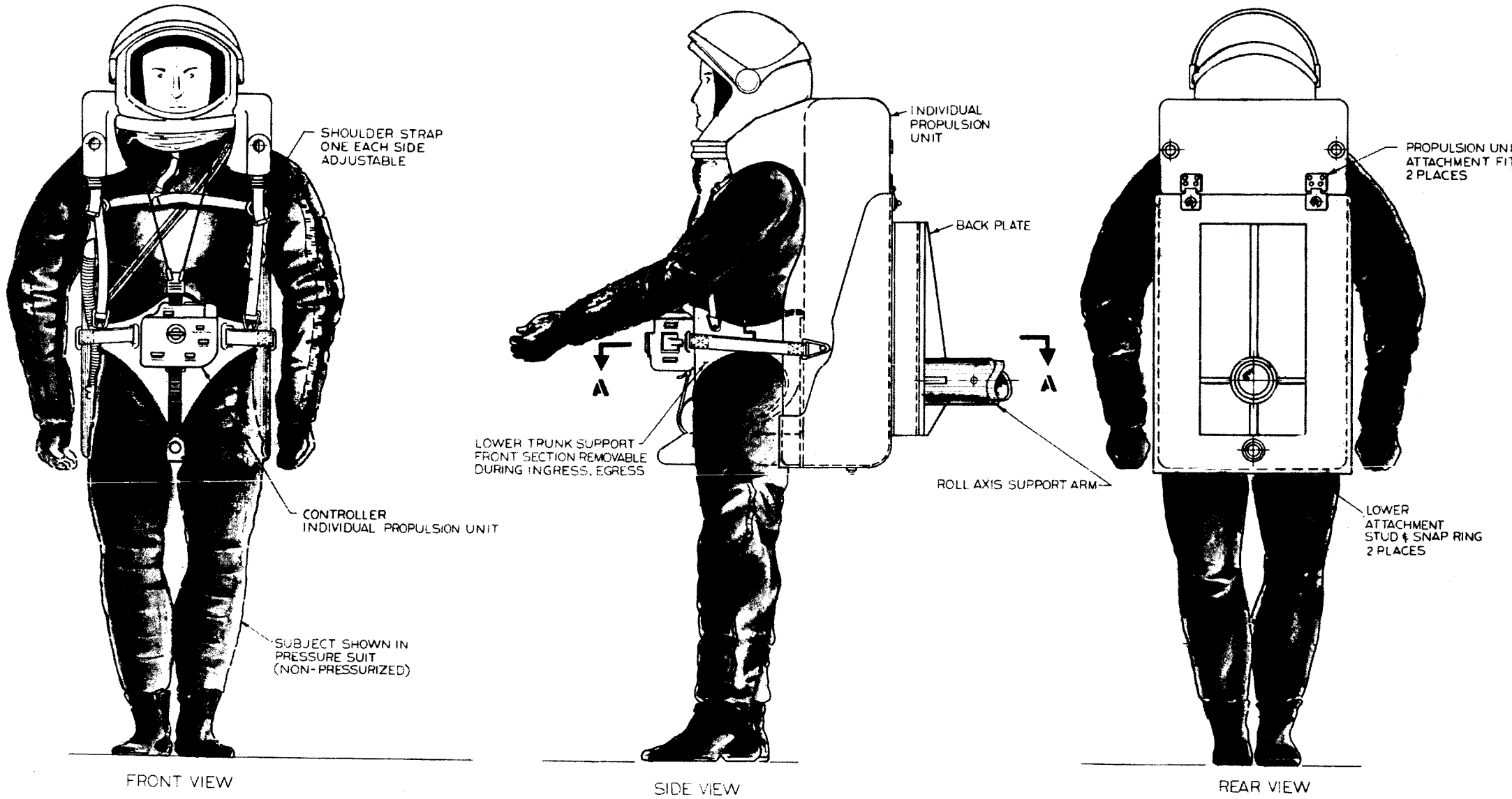

Figure 39
SIMULATOR SUPPORT HARNESS FOR USE WITH BACK PROPULSION UNIT

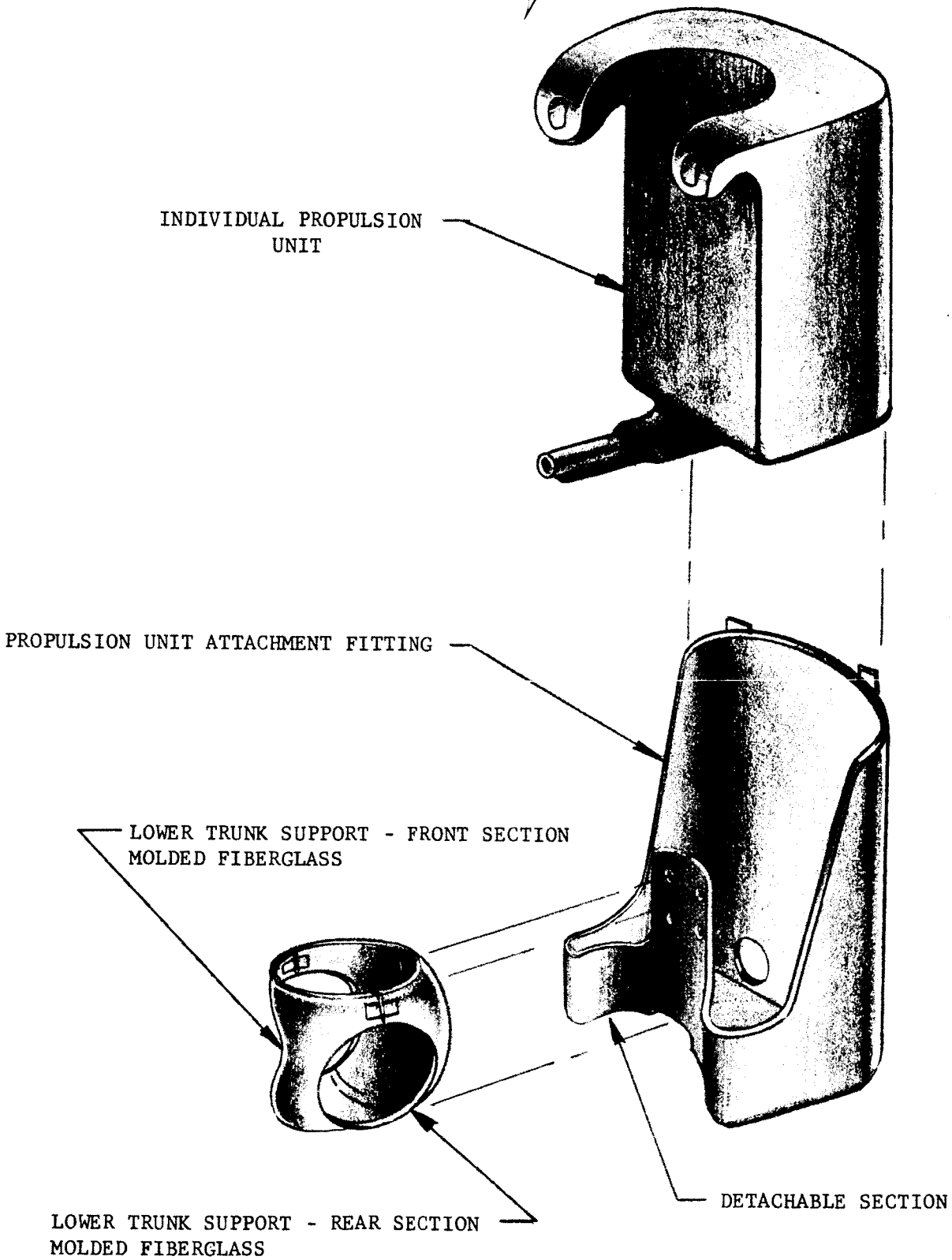

Figure 40

DETAILS OF SIMULATOR SUPPORT HARNESS FOR USE WITH BACK PROPULSION UNIT

Pickup of the propulsion unit can be accomplished by positioning it in a suitable attachment fitting (see Figure 40). This fitting is attached to a back plate (in the simulator this would be the front plate of the c.g. correction device on the end of the roll axis support arm).

The propulsion unit is mounted in the attachment fitting and fastened in four places. (See Figure 39 rear view). The subject is fitted with the front section of the lower portion of the fiberglass harness, the rear section of the harness being rigidly affixed to the propulsion unit attachment fitting (see Figure 40). The shoulder straps associated with the propulsion unit are tightened in place and the subject is adequately protected and supported for all attitudes. (See Figure 39 front and side views).

This design concept should be investigated, modified and proven by testing. Certain areas of restraint may need to be added. The upper portion of the trunk in contact with the propulsion unit will probably need to be padded in some manner.

3.3 Supplemental Testing

There were many tests run which can not be considered scientifically conclusive, but tend to validate our design and insure proper utilization in the proposed space motion simulator.

A summary of these tests and the conditions under which they were conducted are presented in the following subparagraphs:

3.3.1 Universality

The range of subject sizes 5'1" to 6'4", and subject weights, 145 to 265 pounds, demonstrated the universal nature of the modified harness.

The fiberglass harness is not completely universal although three sizes with three inserts affording nine combinations should accommodate the current range of the astronaut population. The harness used to demonstrate feasibility was so closely contoured to one subject that it would not fit other subjects closely resembling that subject. We believe that feasibility of the concept has been demonstrated, and that a polished finished product incorporating quick release devices, etc., can be easily developed during detail design.

3.3.2 Test of Back Articulation

This test was conducted by supporting the man in only the lower section of the fiberglass harness which was positioned in a parachute harness. After short periods of time, the subject's back became weary. He continually had to exert some muscular force to maintain his back in a vertical position. When he relaxed, he slumped radically and again, after some time, his back became weary.

3.3.3 Test For Balance and Unbalance Capability

With the subject mounted in the test rig in the molded fiberglass harness, two tests were conducted. In one test the subject's ability to position himself at various rotational attitudes was determined. In a second brief test series, the unbalance torque created by movement of the subject's extremities was measured.

The average subject demonstrated considerable ability in positioning himself at various attitudes by controlling the movement of his extremities to change the location of his c.g. with respect to his axis of rotation. Positioning accuracy within 15 degrees at any attitude was easily accomplished. Tests were conducted with the subject initially rotating and also initially at rest. Subjects were able to stop, start and maintain rotation in either direction at will. Continuous rotation at uniform velocities was not possible due to the constant movement required of the subject's arms and legs.

While the subject's orientation had some effect on the amount of unbalance torque created by movement of his arms and legs, it was determined that the average subject could, by movement of his extremities, create a torque unbalance of about 50 lb-ft in either direction, while in any attitude.

These two series of tests demonstrate the amount of freedom of movement that the subject has in a harness of this type. The legs and arms are, in fact, unrestricted. The only major restriction that the subject experiences in this harness is a lack of freedom to twist and bend at the waist. The subject's trunk is rigidly held in place. This is not unlike the restriction that the astronaut would experience while wearing an individual propulsion and life support, back-pack unit.

3.4 Conclusions

To adequately support the human body in any attitude while allowing him almost complete freedom of motion of his body presented a significant

design problem. To provide proper physiological support was a matter of covering enough body area to adequately distribute the weight of the subject. In all attitudes but one, this did not present a significant problem. While the subject is in an upright position,insufficient surface area is presented for comfortable support. The modified harness approached a solution by increasing surface contact area with a swing seat. It still has the defects that the subject must stay on the seat, and cannot stand in a bolt upright position or move his legs aft of the centerline of the harness. After a period of time, the seat tends to ride up the back of the subject's buttocks and causes pinching.

The laced corset would not be satisfactory for extended use. After many hours of usage during our testing, the corset elements started to deteriorate. The emplaced eyelets and hooks fatigued and began to rip free of the corset material.

The molded fiberglass harness affords increased surface contact while the subject is in an upright position by providing the maximum amount of bearing surface, in a contoured fashion, over the buttocks and lower abdomen. The molded lower section forms a "saddle" on which the subject is comfortably supported. The "saddle" is held in place by the rigid harness around the subject's hips and lower abdomen. The subject may swing his legs forward and backwards to almost their normal limits. He is somewhat constrained in moving his legs to the side; however, the value of this maneuver is doubtful. The upper molded section presents sufficient bearing surface over the shoulders to support the man comfortably in a head down

attitude. Since this section encompasses the upper trunk, sufficient support for front, back and side are afforded. Limited clearance avoids movement of the subject's body within the harness during rotation.

By supporting the hips and shoulders independently and fixing these sections with respect to each other, the total skeletal structure is supported. The arms, legs and head remain free to move in any normal direction. Of necessity while earth bound, the subject's limbs are affected by gravity and he must exert some force to support them while moving in rotation. The amount of effort required is not excessive for the arms and legs but the neck muscles become particularly tired after a period of time. Therefore, our design includes a head support against which the subject rests his head while rotating. It is interesting to note that in any stationary attitude (let us say face downward) the subject can relax his neck by pushing his head back against the head support.

From a comfort standpoint the molded fiberglass harness presents a close fitting support within which the subject can move slightly. He is not presented with any binding surfaces and only feels that surface upon which he is being supported at any given time. Some "slop" in the fit is desirable. Our prototype design did not include any padding inside the molded shell. Some rigid padding appears desirable.

The pressure suit appears to be a satisfactory support harness in itself when pressurized. The subject can be lifted and rotated into any attitude in the Mercury Full Pressure suit under 3.5 psi differential pressure. He is supported by the front, back, sides and shoulders of the

suit in attitudes of face down, face up, either side down or head down. When the subject is bolt upright, he is supported by standing in stirrups which are part of the suit. Picking up the suit can be accomplished with a strap and backboard fixture.

3.5 Recommendations

3.5.1 Modified Harness

Although the feasibility of this concept was verified during this program, the use of the modified harness in the space motion simulator is not recommended.

3.5.2 Molded Fiberglass Harness

During the current program a fiberglass harness was molded to one subject and the feasibility of its utilization was demonstrated. Conceptually, this harness appears to hold the most promise for a comfortable device allowing maximum freedom of movement of arms and legs. Further work is recommended in final design of the molded harness to determine requirements for sizing, more sophisticated attaching hardware, optimized saddle contour and internal cushioning. A finished product should be fabricated to demonstrate all these features.

3.5.3 Harness For Use With a Full Pressure Suit

During the current program, it was demonstrated that a simple back plate and straps would adequately support a man in the Mercury Full Pressure suit. It is recommended that a finished product be fabricated using fiberglass as the back plate and nylon straps with composition buckles

as restraining devices. This unit should be tested with the Gemini and Apollo Pressure suits to insure compatibility with suit perturberances.

3.5.4 Back Pack Utilization In The Simulator

A fixture to support the back pack, is shown in conceptual design in this study. Part of the pack can be used as a harness. However, the lower section of the fiberglass harness must be used when a subject is tested in the simulator in street clothes or in an unpressurized suit. It is recommended that a prototype be fabricated and tested with a back pack and either a Gemini or Apollo suit to insure compatibility.

3.5.5 Simulator Utilization

It is strongly recommended that a study of the utilization and training requirements of the proposed space motion simulator be conducted to determine what constraints should be imposed on motion characteristics to insure fidelity of simulation.

4.0 Biokinetic Experiments

4.1 Introduction

During the design study of a device to simulate the dynamic environment encountered under conditions of reduced or zero gravity, one of the initial tasks was that of defining the upper limits of motion of the device. The motion parameters of the simulator are to a great extent determined by the ability of the human subject to move himself about (by muscle power) in a zero gravity environment.

A thorough literature search revealed that information concerning the ability of subjects to maneuver in the zero gravity environment using muscle power was not available.

Under the initial study phase of this program, AAI conducted experiments to determine the linear motion capabilities of a number of subjects. In those experiments, the subject was supported on an air-bearing platform which allowed translation in one plane under nearly frictionless conditions. While standing on the air-bearing platform, the subject accelerated himself linearly across the test area by pushing against an instrumented platform mounted on the wall.

In order to obtain information concerning the subject's ability to produce angular motion about his center of gravity using muscle power, a series of angular motion tests have been conducted. These tests, with the subject applying torque to an instrumented torque handle while supported on an air-bearing platform capable of continuous rotary motion, are described in detail in this section. The results of these angular motion tests are given together with sample traces recorded during the tests.

4.2 Background

As the result of a literature search made to obtain information on the ability of human subjects to maneuver in the zero gravity environment, several reports of related experimental programs were obtained. Dezendolet and Rievely[16] have conducted experiments to determine the ability of subjects to apply torques with one hand while supported on a frictionless platform. Torque was exerted on a short bar mounted first overhead and then in front of the subject in two different experiments. The frictionless platform was supported by air-lubricated bearings to simulate in one plane the dynamic conditions of the zero gravity environment. While this report was informative concerning experimental technique, the tests conducted were not applicable to determining the upper limits of angular motion for the simulator.

Studies by J. T. Celentano et al[17] have been conducted to determine the maximum torque output capability for subjects using one hand in the performance of typical maintenance tasks. These tests were conducted with the subject seated on an air-bearing supported stool. Higher rotational rates and torques would have been obtained using two hands rather than one. For this reason these studies do not contain sufficient information to permit us to establish motion limits for the simulator.

Cording[18] reports similar studies using an air-bearing device having five degrees of freedom. These studies determined that under simulated zero gravity conditions, the subject's torque capability was

reduced to 70 to 90 percent of its normal value. In addition to this type of human capability information, time histories of torque application are required in order to specify design parameters.

To obtain the required angular motion information, a test program was established using a frictionless platform for supporting the subject and an instrumented torque handle rigidly attached to the laboratory ceiling, to measure the subjects' output. This test concept simulates the unrestrained astronaut exerting a torque on a tool handle or component which is fixed to the surface of a space vehicle. The instantaneous angular acceleration of the subject is a function of his torque output and his mass moment of inertia in the basic mechanics relationship[19]

$$\ddot{\theta} = \frac{T}{I} \tag{1}$$

where

$\ddot{\theta}$ = angular acceleration, radians per second^2

T = torque, lb. ft.

I = mass moment of inertia of subject, slug feet^2 (assumed to remain constant during the test)[20]

Integrating over a period of time (t) the relationship for angular velocity is obtained:

$$\int_o^t \ddot{\theta}\, dt = \frac{1}{I} \int_o^t T\, dt \tag{2}$$

which gives approximately, for slowly varying acceleration:

$$(\dot{\theta}_t - \dot{\theta}_o) = T\, t / I \tag{3}$$

where

$\dot{\theta}$ = angular velocity, radians per second

t = time, seconds

Now the torque integral is expressed as angular impulse:

$$T\,t = I_{imp} \tag{4}$$

where

I_{imp} = angular impulse, lb. ft. sec.

Then assuming that the subject's initial angular velocity is zero and substituting in equation (3):

$$\dot{\theta} = I_{imp} / I \tag{5}$$

The Law of Conservation of Angular Momentum, in the absence of external forces, governs the man-vehicle system as it travels through space. This law states that two bodies moving at the same initial angular velocity will, after a mutual reaction between them, have new angular velocities whose ratio is inversely proportional to the ratio of their inertias. Assuming that the bodies are initially at rest, the relationship following the action of one on the other is:

$$\frac{\dot{\theta}}{\dot{\theta}_v} = \frac{I_v}{I} \tag{6}$$

where Θ and I are the angular velocity and inertia respectively of the astronaut and:

$\dot{\theta}_v$ = angular velocity of the space vehicle, rad/sec.

I_v = inertia of the vehicle, slug feet^2.

The angular velocity of the vehicle resulting from a torque applied by the astronaut is expressed as :

$$\dot{\theta}_v = \frac{\dot{\theta} I}{I_v} \qquad (7)$$

Approximate moments of inertia for the Gemini type capsule are:

$I_{roll} = 750$ slug ft^2

$I_{pitch} = I_{yaw} = 1900$ slug ft^2

Assume an I = 10 slug ft^2 and $\dot{\theta}$ = 50 rpm = 5.24 radians per second as typical inertia and angular velocity values for an astronaut using muscle power to accelerate about his roll axis.

Then, from equation 7

$$\dot{\theta}_v = \frac{50 \times 10}{750} = .67 \text{ rpm}$$

This very low value of vehicular velocity validates the assumption that vehicular velocity is sufficiently small that it may be considered to be zero. For experimental purposes the vehicle was simulated as a fixed object without significantly degrading the test results.

To obtain data that would include the end points of the range of subject outputs for all possible body positions, it was decided to conduct tests with the subject in both standing and supine positions. The standing position (Yaw Axis rotation) offered the minimum subject inertia and hence maximum angular velocity. The supine position, (Roll Axis rotation) offered maximum subject inertia and minimum angular velocity.

Those two body positions bracketed the moment of inertia range for normal positions of the human subjects. Within this range, we hoped to obtain the end points of other relevant test parameters.

To approximate the moment of inertia about the vertical axis of the standing subject, we may represent the subject's body by a homogeneous right circular cylinder. The moment of inertia of the right circular cylinder about its longitudinal axis is

$$I = \frac{1}{2} MR^2 \qquad (8)$$

where M = mass of the subject, lb sec^2/ft

R = radius of the cylinder representing the subject, feet

The average subject varies from about 18" shoulder width to about 8" depth measured front to back at the stomach. For the cylindrical approximation, we will select an average value of R = 7 inches. Then the inertia approximation for a 170 lb subject in the standing position is:

$$I = \frac{1}{2} \times \frac{170}{32.2} \times \left(\frac{7}{12}\right)^2 = .90 \text{ slug ft}^2$$

For the subject in the supine position, a right circular cylinder rotated about a perpendicular axis through its center is used for an approximation. The moment of inertia of the cylinder is

$$I = \frac{1}{12} ML^2 \qquad (9)$$

where L = length of the cylinder (equivalent to the subject's body)

For the 170 lb subject with a height of 6 feet, his moment of inertia in the supine position is:

$$I = \frac{1}{12} ML^2 = \frac{1}{12} \times \frac{170}{32.2} \times (6)^2$$

$I = 15.85$ slug ft^2

For the average test subject, it is expected that Yaw Axis test inertias will be approximately 1.0 slug feet^2 while Roll Axis test inertias will be on the order of 15.0 slug feet^2.

4.3 Test Facility and Equipment

The rotary motion tests were conducted using air bearing support equipment to produce a simulated zero gravity condition. All tests were conducted in the AAI Mechanical Laboratory.

Six of the company personnel were selected to act as test subjects. All were well motivated volunteers in good physical condition. The subjects demonstrated high resistance to motion sickness and all completed the required tests satisfactorily. The pertinent anthropometric data and moments of inertia for each subject are given in Table XII.

The equipment and set-up for the yaw and roll axes tests are shown in Figures 41 and 42 respectively.

The principal items of test equipment are:

A. Work Surface - A smooth, flat floor of epoxy, poured in place, to provide a work surface for the air-bearing supported platform.

B. Air-Bearing Supported Platform - The platform had lower air pads for translation in a horizontal plane and upper pads which supported the circular platform in continuous rotation. The air supply hose was attached to the frame housing the air-bearing supports.

C. Tachometer - The tachometer was mounted on the frame beneath the rotating platform. A rubber wheel on the tachometer shaft contacted

TABLE XII

ANTHROPOMETRIC DATA

Subject	Age, Years	Weight, Pounds W	Height, Inches H	Ix,* Slug Ft^2 Roll Axis	Iz,** Slug Ft^2 Yaw Axis
AC	27	165	72	10.36	0.90
SD	28	146	69	8.57	0.77
HF	22	190	74	12.02	1.08
LM	31	173	70	10.04	0.98
MR	24	193	70	10.85	1.13
WT	27	180	70	10.34	1.03
Average	26.5	174.5	70.8	10.36	0.98

* Ix - Moment of Inertia of the test subject about his center of gravity[20] (Roll Axis) computed from the following relationship for the standing, arms at sides, position

$$Ix = \frac{1}{12}\left[- 232.0 + 3.77H + 0.512\ W\right] \qquad (4)$$

** Iz - Moment of Inertia of the test subject about his center of gravity, (Yaw Axis) computed from the following relationship for the standing, arms overhead, position.

$$Iz = \frac{1}{12}\left[1.4 - 0.085H + 0.094W \right] \qquad (4)$$

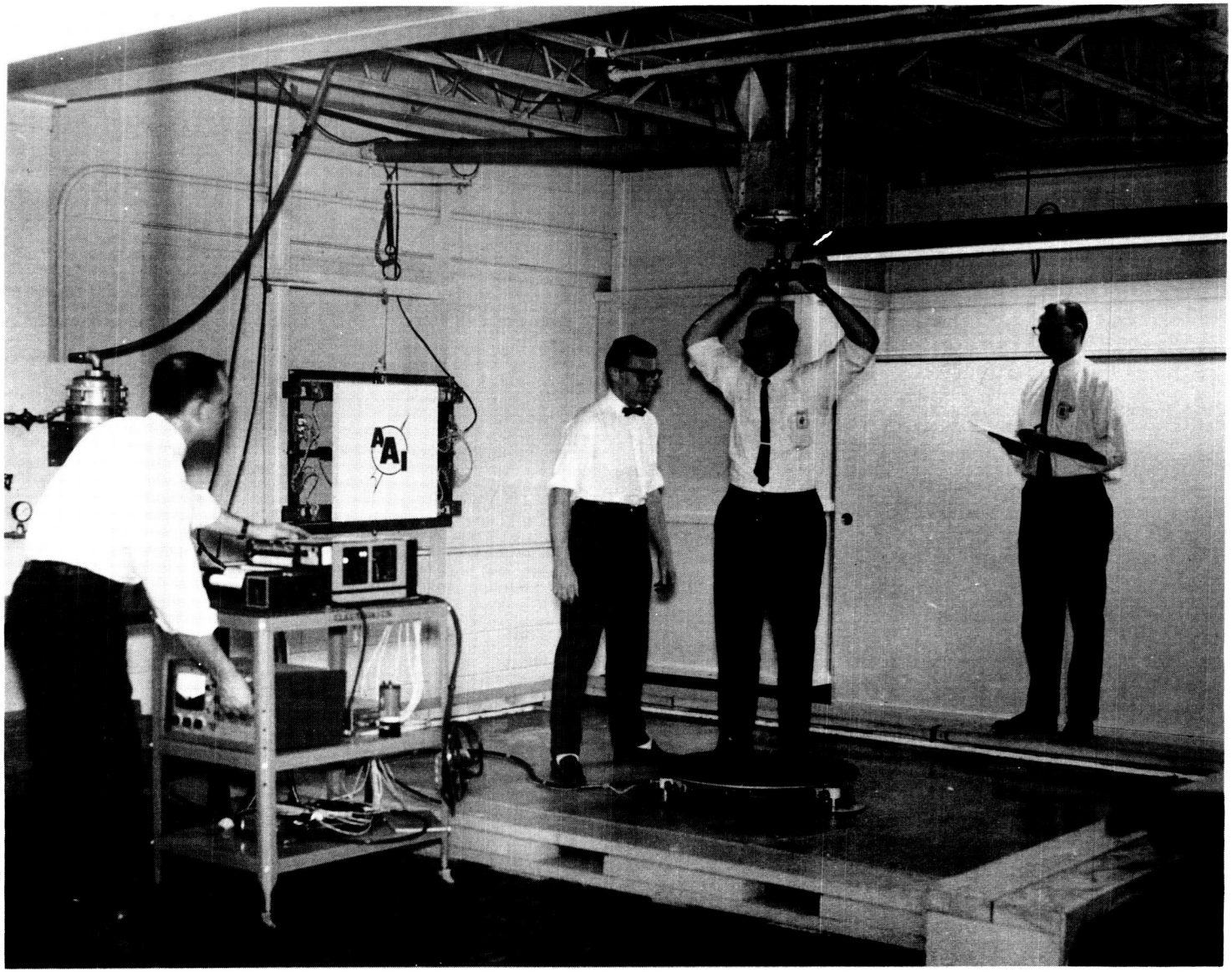

Figure 41
OVERALL VIEW OF TEST ARRANGEMENTS YAW AXIS TESTS -
STANDING POSITION

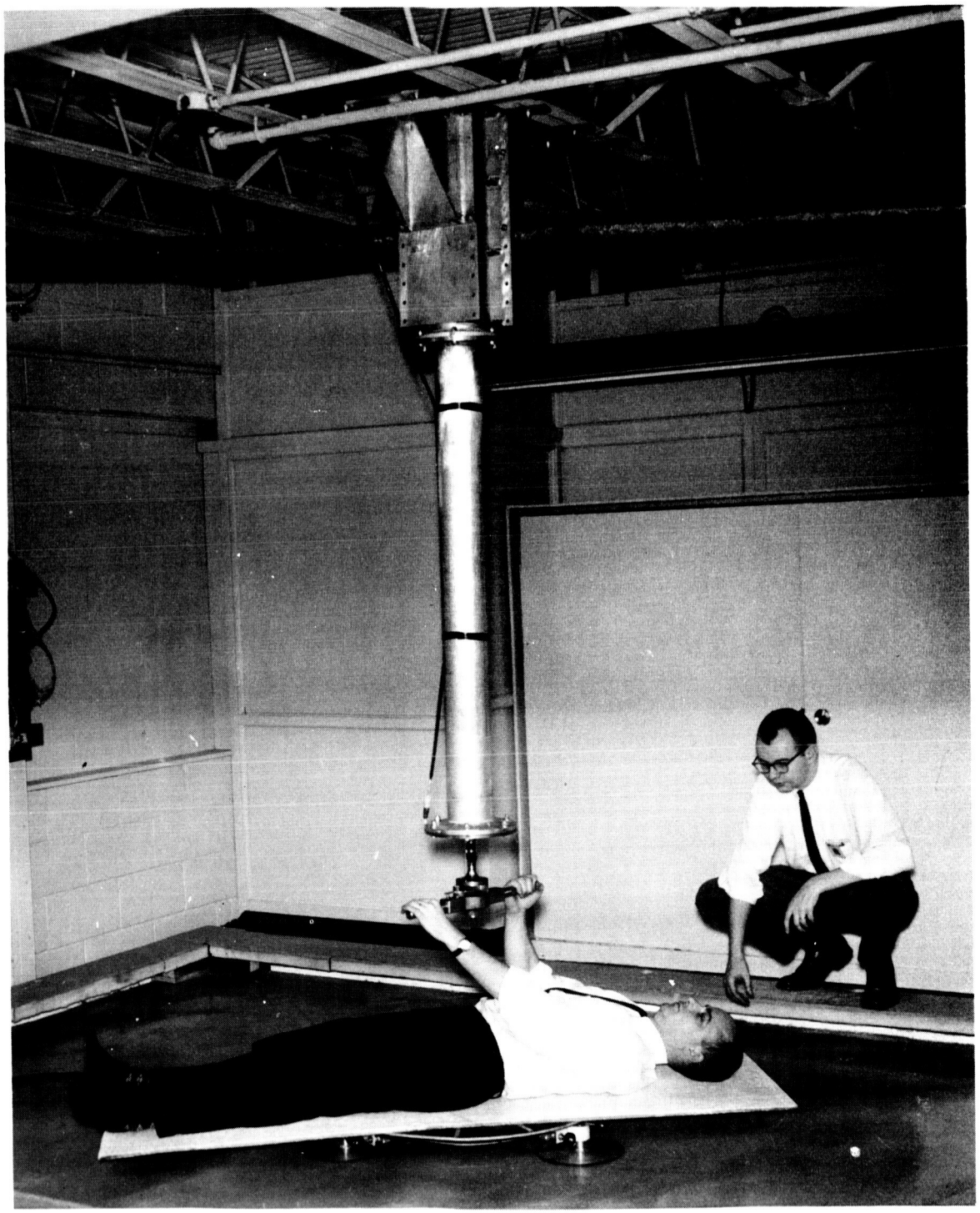

Figure 42
ROLL AXIS TESTS - SUPINE POSITION

the underside of the rotating platform to provide a voltage signal which was a linear function of the rotational velocity of both the platform and the test subject supported by the platform.

D. Torque Handle - The torque handle, through its supporting structure, was rigidly attached to the overhead ceiling support members. A torsion bridge on the vertical support shaft indicated the torsional strain in that shaft. This strain was proportional to the torque applied to the handle. The torque handle was 20 inches long and 1.0 inch in diameter.

E. Amplifier, Chart Recorder - The sensor signals were amplified by a CEC Type 1-127 amplifier and recorded on a CEC Type 5-124 recording oscillograph to provide signal output traces on a known time base.

F. Motion Picture Camera - A 16mm motion picture camera was used to record the test action at a framing rate of 64 frames/sec. These films were used for slow motion analyses and for frame by frame data verification.

G. Platform Scale - The height and weight of each subject was recorded at the time of testing.

H. Torque Support Extension - For the Roll Axis Tests the torque handle was lowered by 4.33 feet using the torque support extension.

I. Pallet - For the Roll Axis Tests, the subject was supported on a plywood pallet placed atop the air-bearing platform.

A more detailed description of the test equipment is included in Appendix B.

4.4 Experimental Procedure

With the exception of the subject's position on the platform, the same test procedures were used on both Roll Axis and Yaw Axis tests.

The supine tests (Roll Axis) were conducted with the subject lying on a 3 by 6 foot plywood platform that rested on top of the air-bearing supported platform as shown in Figure 42. The subject was positioned on the platform with the center line of the torque tube directly above his estimated center of gravity. The center line of the torque handle was 17 inches above the support platform.

From a series of preliminary tests, it was concluded that for the supine position tests the maximum rotational rates were obtained when the torque handle was initially positioned on a line 45 degrees from the subject's spinal axis. Thus, for tests in clockwise rotation his right hand was initially located above his right shoulder, and his left hand was extended to grasp the handle above his left hip. The torque handle was placed in this position to allow the subject the longest possible duration of the torque input. For counterclockwise rotation the left hand was initially above the left shoulder and the right hand was above the right hip.

During a clockwise rotational test, the subject pulled against the torque handle with his left hand and pushed with his right hand. This produced a counterclockwise torque on the bar and the resulting clockwise body rotation. The subject was able to continue to apply torque until his body had rotated approximately 135 degrees.

For the standing position (Yaw Axis) tests, the subject stood erect on the platform with his feet spread approximately 8 inches apart and his hands holding the torque handle, located 4 to 6 inches above his head.

It was determined that the maximum rotational rates were obtained for the standing tests, when the torque handle was initially aligned with the subject's mid-sagittal plane. For clockwise rotation, the subject initially grasped the torque handle in front of and above his forehead with his left hand. His right hand grasped the other end of the handle in back of his head. From this position he pulled on the handle with his left hand and pushed with his right to produce clockwise body rotation. He reversed this position for counterclockwise rotation.

In all tests in this series, the subjects were instructed to grasp the 20 inch long torque handle at its ends. In addition, the subjects were instructed not to change hand positions on the handle during the tests.

At the beginning of the test program, two different positions of the hands on the torque handle were considered. Subjects were about equally divided on the question of whether better results were obtained with the hands placed both overhand on the handle or one overhand and the other underhand. In the overhand position, the hand is placed on the handle with the thumb inside, palm downward and fingers pointing forward. In the underhand position, the thumb is outside, the palm is upward, and the fingers point toward the rear.

The question of which hand position would produce maximized results was not resolved during the test subject orientation phase of the

program. For this reason the Roll Axis test program was expanded from five tests in each rotational direction to 10 tests in each direction for all six subjects. The tests were equally divided between the overhand and the combined overhand-underhand positions, five in each mode.

The test results, discussed fully in Section 4.6, indicated no significant difference between the two hand positions. Consequently, the Yaw Axis tests were conducted, five repetitions in each rotational direction, with each subject selecting the hand position that seemed most natural and effective for himself.

At the onset of the test program, it was assumed that the best simulation of the zero gravity environment would be achieved using a support platform which was capable of both translation and continuous rotation. An air-bearing supported platform of this type is described in Appendix B. With all six air-bearings activated, this device permits both free translation in a horizontal plane and free rotation about a vertical axis. Preliminary tests in both supine and standing test positions failed to support the assumption that both translation and rotation were necessary for the subject's support platform. It was determined that with all six air-bearings activated there was a strong tendency for the subject and his supporting platform to orbit about the vertical axis through the center of the torque handle rather than undergo free body rotation about an axis through his center of gravity. As the objective of these tests was to obtain information concerning the ability of subjects to rotate about their centers of gravity, we could not tolerate appreciable separation of the axis of rotation and

vertical axis through the subject's center of gravity. As the support platform translates from beneath the torque handle, the tendency for the subject to orbit about a vertical axis through the handle increases while rotation about the subject's center of gravity decreases. The tachometer indicates only the rate of rotation of the platform and not its angular rate as it orbits a fixed axis.

Whether or not the subject could maintain sufficient control of the platform to keep it aligned under the torque handle throughout the test run was largely a function of his physical coordination ability. Undoubtedly this skill could be improved or acquired over the course of a lengthy training program. We found that all subjects could keep the platform reasonably well aligned if they limited their torque output to 25% to 50% of their maximum capability. As the torque output increased, the translation and hence orbiting of the platform increased and the subject became more preoccupied with keeping the platform in place than with the application of maximum torque. We found that identical recorded traces were obtained whether the platform was externally constrained in translation or maintained in alignment by a skillful test subject. On the basis of these findings, it was determined that either an extensive training program would be required for all test subjects or the lower air bearings would have to be deactivated to prevent translation and thereby maintain alignment of the rotational axes. Since the training program could not guarantee sufficient improvement in the subjects or free them from concentration on the alignment problem, it was decided to run all tests in the

rotational series with the lower air bearings deactivated. Satisfactory test results were obtained in this manner.

All tests were conducted in the same manner. The subject first placed himself comfortably on the platform. Then a test assistant checked to determine that the subject's estimated center of gravity (taken to be 3 inches below the navel for the supine position) was directly below the vertical axis of the torque handle. The subject placed his hands lightly on the torque handle, being careful not to exert torque until the signal was given by the test conductor. When the subject was in position, the test conductor commanded, "Ready", and at the same time started the chart recorder. Approximately two seconds later, the test conductor commanded, "Go" and the subject began to exert force on the torque handle. When the subject completed the torque application phase, he was rotating at his maximum angular rate. To assure that the event was not prematurely interrupted, the test conductor allowed the subject to rotate at the maximum rate for approximately two seconds and then he commanded "Stop". At that instant the tape feed of the recorder was stopped and the test assistant began decreasing the test subject's angular velocity.

The time between test runs was dependent upon the subject's state of angular motion anxiety. Test runs were not conducted when the subject felt that he could not produce maximum effort due to impending motion sickness. Generally, one to three minutes between test runs was sufficient to prevent motion sickness. Subjects were not scheduled for more than five test runs during any continuous series and not more than ten test runs during any one day.

At the completion of each test run, the test conductor entered the pertinent information concerning the subject and the instrumentation in the test program log book. The recorded traces were scanned to see that they were complete and; if so, assigned a test sequence number. A number of test events were selected at random to be photographed with the high-speed camera. This provided a means of data verification by a frame-by-frame analysis comparison with recorded traces.

4.5 Data Reduction

All traces recorded during the test program were evaluated using standardized data reduction techniques. Methods used for data analysis are described below:

A. Peak Torque, T, lb. ft.

The highest peak of the torque trace was scaled in inches. The torque tube calibration curve was used to convert the peak value in inches to pound-feet of torque.

B. Torque Duration, t, seconds

Elapsed time from torque application to termination measured in seconds using tenth-of-a-second timing lines on the recording paper.

C. Torque Onset, t_o, seconds

Elapsed time from initial torque application to first major torque peak. Although later peaks may have been higher, the first major peak was considered to end the onset phase of the torque pulse.

D. Torque Decay, t_d, seconds

Elapsed time from the last major torque peak to end of application of torque.

E. Angular Impulse, I_{imp}, lb. ft. sec.

The integral of the torque trace over torque duration, t. The area between the torque trace and the zero torque base line was measured using a Keuffel and Esser Company Compensating Polar Planimeter. This area in square inches was multiplied by a scale factor in units of lb. ft. sec. per square inch to obtain angular impulse in lb. ft. sec. The scale factor was based on the timing line frequency, the recording paper speed and the torque calibration curve.

F. Peak Angular Velocity, $\dot{\theta}_p$, Radians per Second

The height of the highest peak on the angular velocity trace above the zero velocity base line was measured in inches. From the tachometer calibration curve the peak angular velocity was obtained in radians per second.

G. Resultant Angular Velocity, $\dot{\theta}_R$, Radians per Second

The area under the angular velocity trace from the instant of torque termination to a point two seconds hence was measured using the planimeter. This area in square inches was divided by the length in inches corresponding to the two second time interval to obtain the average height of the curve in inches. The tachometer calibration curve was used to convert the average height in inches to resultant angular velocity in radians per second.

H. Peak Angular Acceleration, $\ddot{\theta}$, radians per second per second

First it was necessary to determine the limits of that sector of the angular velocity trace having the maximum slope. The height of the

sector in inches and the elapsed time in seconds included in the sector were measured. Using the tachometer calibration curve, this height in inches was converted to units of radians per second. To obtain the peak angular acceleration in radians per second per second, the sector height in radians per second was divided by the sector base length in seconds.

I. Actual Inertia of Test Subject, I, slug feet^2 [20].

The actual inertia of each subject, about his center of gravity, was computed initially, based on the subject's height (H) and weight (W) in the following manner:

For Roll Axis rotation

$$Ix = \frac{1}{12}\left[- 232.0 + 3.77H + .512\ W\right]$$

and for Yaw Axis rotation

$$Iz = \frac{1}{12}\left[1.4 - .085H + .094W\right]$$

J. Indicated Inertia of the Test Subject, I_{ind}, slug feet^2

The indicated inertia of the test subject equals the difference between the angular impulse, I_{imp}, divided by the resultant angular velocity, $\dot{\theta}_R$, and the mass moments of inertia of the rotating members of the subject's support equipment. For the Roll Axis tests this relationship is

$$I_{ind} = \frac{I_{imp}}{\dot{\theta}_R} - I_{plate} - I_{platform} - I_{handle} \qquad (10)$$

For the Yaw Axis tests, no platform was used, so $I_{platform}$ was omitted from eq. (10).

Three pieces of test equipment rotated with the subject at the same instantaneous angular velocity. The mass moments of inertia of these pieces of equipment were computed as follows:

A. Circular Plate

Radius (R) = 1.25 feet

Weight (W) = 26.00 pounds

Gravitational Constant (g) = 32.2 feet per second per second.

$$I_{plate} = \frac{1}{2} \times \frac{W}{g} \times R^2 \qquad (11)$$

$$I_{plate} = \frac{1}{2} \times \frac{26.00}{32.2} \times (1.25)^2$$

$$I_{plate} = .63 \text{ slug feet}^2$$

B. Plywood Platform

Width (a) = 2.0 feet

Length (b) = 6.0 feet

Weight (W) = 16.0 pounds

$$I_{platform} = \frac{1}{12} \times \frac{W}{g} \times (a^2 + b^2) \qquad (12)$$

$$I_{platform} = \frac{1}{12} \times \frac{16}{32.2} \times \left[(2)^2 + (6)^2\right]$$

$$= 1.66 \text{ slug feet}^2$$

C. Torque Handle

Length (L) = 1.83 feet

Weight (W) = 9.0 pounds

$$I_{handle} = \frac{1}{12} \times \frac{W}{g} \times (L)^2 \qquad (13)$$

$$I_{handle} = \frac{1}{12} \times \frac{9.0}{32.2} \times (1.83)^2$$

$$I_{handle} = .078 \text{ slug feet}^2$$

Using these mass moment of inertia values, the total equipment inertia is computed for both test positions.

Standing Position - Yaw Axis Tests

I_{plate} = 0.63

I_{handle} = 0.078

Equipment Inertia = 0.708 slug feet^2

Supine Position - Roll Axis Tests

I_{plate} = 0.63

$I_{platform}$ = 1.66

I_{handle} = 0.078

Equipment Inertia = 2.368 slug feet^2

4.6 Test Results

In this section, the results of the Roll Axis and Yaw Axis tests are presented in tabular form and discussed. Appendix C contains sample traces and a brief discussion of the significant trace characteristics.

4.6.1 Roll Axis Tests - Supine Position

The results of the Roll Axis tests are shown in Table XIII The high and low values given represent the end points of the range of recorded data. The mean values are the arithmetic averages of all data recorded or computed for each parameter. A total of 120 tests were made in the Roll Axis series. Half of these were in clockwise rotation and half were in counterclockwise rotation.

The Roll Axis test results indicated no significant difference between the two hand positions discussed in Section 4.4. The mean values in Table XIIIrepresent the average for all 120 tests in the supine position.

TABLE XIII

RESULTS OF ROLL AXIS TESTS ($\pm \theta_x$)

SUBJECT IN SUPINE POSITION

	High	Mean	Low
T, Peak Torque, lb. ft.	144.5	100.3	50.0
t Torque Duration, sec.	1.89	1.27	.65
t_o Torque Onset, sec.	.93	.44	.20
t_d Torque Decay, sec.	.67	.41	.20
I_{imp} Angular Impulse, lb. ft. sec.	87.9	67.4	45.6
I_{ind} Indicated Inertia of Test Subjects, slug ft.^{2}	14.9	11.4	7.3
$\dot{\theta}_R$ Resultant Angular Velocity, rad./sec. (revolutions per minute)	5.65 (54.0)	4.81 (46.3)	3.38 (32.3)
$\ddot{\theta}$ Angular Acceleration, rad. per sec^2	21.56	8.67	3.08

No. of Subjects - 6

No. of Tests - 60 Clockwise

- 60 Counterclockwise

Due to the high inertia of the subject in the Roll Axis tests, the results reflect long torque pulse durations (t) averaging 1.27 seconds while resultant angular velocity $\dot{\theta}_R$ averaged 4.81 radians per second. This high resistance to angular acceleration permitted the subjects to achieve high values of impulse (I_{imp}) and peak torque (T).

The indicated inertia of the subjects (I_{ind}) varied from 7.3 to 14.9 slug feet^2 with an average of 11.4 slug feet^2. These values compare favorably to the inertias (I) of the test subjects given in the Anthropometric Data Table XII . The theory does not support resultant inertias which are lower than the actual inertia given for the subject rotating about his center of gravity. For those few instances where the subjects' indicated inertia was lower than the actual inertia value the difference was attributed to the subject deviating slightly from the correct test position and to combined experimental tolerances.

Where the subject's indicated inertia was larger than the actual value, displacement of the subject's center of gravity from the true rotational axis was a major contributing factor. For the reason indicated inertias were, in almost all cases, higher than the actual inertias for each test subject.

4.6.2 Yaw Axis Tests - Standing Position

The results of the Yaw Axis tests are shown in Table XIV. The inertia of the subject in the Yaw Axis test position is about one tenth of his inertia in the Roll Axis test position. Thus, in the Yaw Axis tests

TABLE XIV

RESULTS OF YAW AXIS TESTS

SUBJECT IN STANDING POSITION

		High	Mean	Low
T	Peak Torque, lb ft.	77.5	52.5	29.0
t	Torque Duration, sec.	.84	.64	.50
t_o	Torque Onset, sec.	.46	.27	.12
t_d	Torque Decay, sec.	.33	.19	.08
I_{imp}	Angular Impulse, lb. ft. sec.	25.5	19.4	11.3
I_{ind}	Indicated Inertia, slug ft^2	3.02	1.70	.88
$\dot{\theta}_p$	Peak Velocity, rad. per sec.	14.10	11.01	8.01
	(Revolutions per Minute)	(135.0)	(105.2)	(77.5)
$\dot{\theta}_R$	Resultant Velocity, rad. per sec.	9.73	8.04	5.18
	(Revolutions per Minute)	(93.0)	(76.8)	(49.5)
$\ddot{\theta}$	Angular Acceleration, rad. per $sec.^2$	53.74	34.32	18.79

Number of Subjects - 6

Number of Tests - 30 Clockwise

30 Counterclockwise

the angular velocity is considerably higher while the peak torque and angular impulse are lower. The maximum value for peak angular velocity ($\dot{\theta}_p$) is 14.10 radians per second which is about 135.0 revolutions per minute. The angular acceleration, $\ddot{\theta}$, is much higher in the standing position due to the decreased inertial resistance to angular acceleration. The tachometer traces recorded during the standing tests revealed the simultaneous occurance of several types of body motion. A typical set of traces are illustrated in Figure 43.

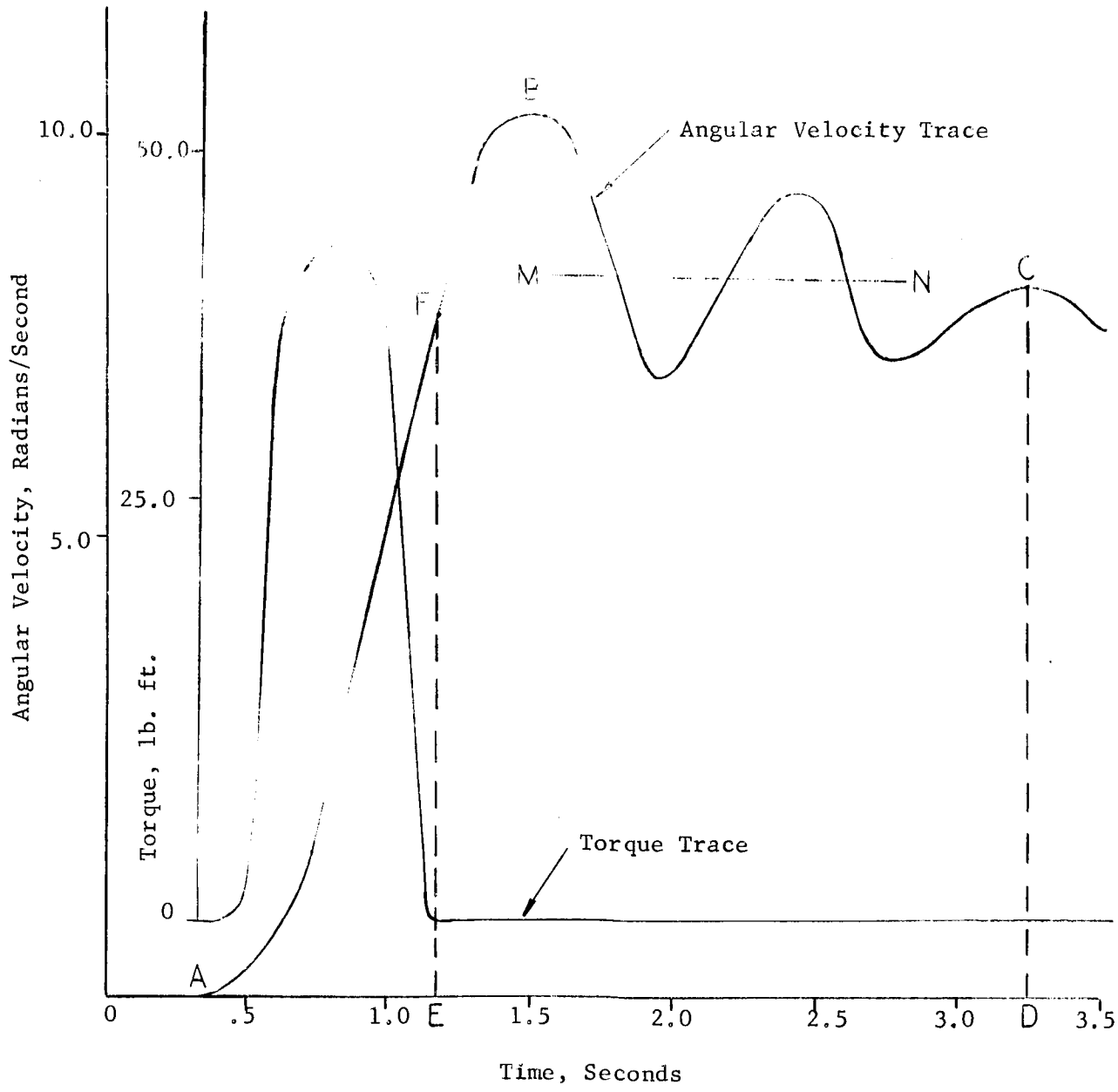

TYPICAL TRACES, YAW AXIS TEST

FIGURE 43

Angular velocity increased from zero to a maximum value over the duration of the torque pulse. See Figure 43 This velocity increase, covering sector A-B on the curve, was followed by several highly-damped oscillations about a median line M-N. This oscillation, in sector B-C, consisting of from one to three cycles is attributed to the torsional spring characteristics of the subject's body plus variations in the subject's position as he tried to maintain his center of gravity in alignment with the vertical axis of rotation.

In some instances the torque traces revealed small (.25 inch or less) trace deflections during the period following the torque termination. This was caused by forces applied by the subject through the torque handle. These forces were partly centrifugal as the result of center of gravity displacement from the rotational axis and partly due to corrective actions by the subject. Such forces caused bending strain in the torque tube. Small misalignment of the strain gages made the torque tube slightly sensitive to bending strains. While unimportant in the major data collection effort, the bending sensitivity provides additional information as to the subjects' position with respect to the axis of rotation.

The frame-by-frame analysis of the photographed tests revealed the torsional spring characteristics of the subject's body. This may be simply represented by a model consisting of two masses connected by a torsional spring, as in the figure on the following page.

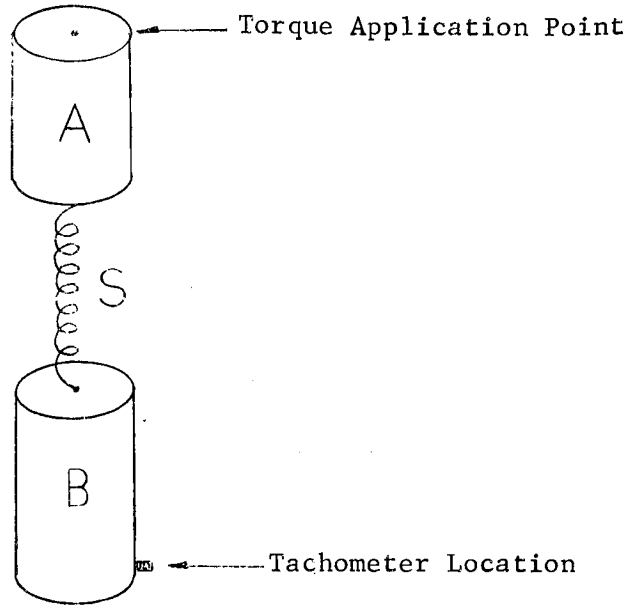

MASS-SPRING SYSTEM REPRESENTING THE TEST SUBJECT

Mass A represents the subject's head, shoulders and arms which move together as a unit while Mass B represents the subject's lower body and the rotary platform which supports him. The two masses are connected by a torsional spring S which represents the characteristics of the subject's midsection. When a torque is applied to Mass A of this system, Mass B will respond in an oscillatory manner at a frequency which is a function of the spring characteristics and the inertia of the two masses.

From the frame-by-frame analysis, the subject's upper body was clearly seen to rotate at a different instantaneous angular velocity than his lower body during and immediately following the angular acceleration phase of the test. The test instrumentation recorded the angular velocity

of the rotary platform corresponding to Mass B. This did not at all times reflect the true angular velocity of the subject due to the torsional spring influence.

In examining the sequence of motion in any single test, the subject was initially at rest. At the initial torque onset the upper part of the subject's body (Mass A) moved rapidly in the direction of angular rotation while the lower body (Mass B) moved in the same direction at a much slower rate. As the torque pulse decreased, the lower body accelerated more rapidly while the upper body moved noticeably slower. At the end of the torque pulse, the lower body was moving at its maximum rate while the upper body was moving at a lesser rate.

The exchange of energy and hence angular velocity between masses A and B was noticeable for one or more additional cycles. At the same time, the subject was observed to move his trunk either forward or backward in an effort to maintain alignment between his center of gravity and the vertical axis of rotation. Depending primarily on the balancing of centrifugal force sensations to maintain alignment, overcorrections were noticeable as the subject attempted to center himself immediately following the torque application. This change of center of gravity position changed the subject's mass moment of inertia about the rotational axis and produced a corresponding change in angular velocity. The oscillation in the angular velocity trace varied from test to test for each subject.

The oscillations in the angular velocity traces of the Yaw Axis tests made it necessary to revise the method used for determining the true angular velocity attained by the subject. The highest peak of the angular

velocity trace reflected not only the subject's angular velocity but also the momentary velocity increase in Mass B as the result of energy transferred through the torsional spring from Mass A.

In order to determine accurately the angular velocity attained by the subject, several alternatives were considered. First we considered discarding those traces with prominent oscillatory patterns. This thought was discarded because the results would not represent a true sample of the subject's capability. We considered extending the test duration until sufficient damping and stabilization were present to produce a non-oscillating trace. This greatly increased subject fatigue due to the increased number of revolutions necessary, and it did not guarantee positive results.

It was decided that an average, obtained by integrating the area (FCDE in Figure 43) under the angular velocity trace and dividing this area by the length of the baseline (DE) would provide the most accurate indication of the subject's resultant angular velocity. This integral was taken over a two-second period beginning at the instant of torque termination. Using this method, the resultant angular velocity ($\dot{\theta}_R$) averaged about 70 percent of the peak angular velocity ($\dot{\theta}_p$).

4.7 Conclusions

By using the recorded outputs of two independent sensing devices, we were able to obtain accurate motion data, and to compute a value for the indicated mass moment of inertia of the test subject. By comparing this inertia value to that of the actual inertia of each subject given in Table XII , we were able to validate both the experimental method

and the instrumentation calibration. The air-bearing support platform provided adequate simulation of the true zero gravity environment. Although limited to translation in one plane and rotation about one axis, this method lends itself to laboratory experimentation techniques. Much useful data can be accurately obtained and verified. Replications can be performed under duplicated experimental conditions.

The values of resultant angular velocity reflect the capability of the subjects in the production of angular motion using muscle power. This does not imply that these rotational rates could be tolerated by human subjects on a continuous basis. All tests in this series were terminated by a test assistant in from three to five seconds after torque onset. Human tolerance to continuous rotation must be based on safety considerations and not on the subject's ability to achieve certain rotational rates using muscle power.

5.0 Program Summary

5.1 Phase I

This phase of the program was concerned with redesign of the simulator structure to incorporate more exact analysis of structural vibrations, to consider incorporation of artificial damping in the structure, to consider modifications to the drive and control systems, and to make budgetary estimates of cost of the simulator for several sizes.

The results of our efforts on this phase can be largely summarized in Table XV, which compares the previous estimates of weights of structure and associated equipment (from Reference 1) with the results of the current study. We can see that a drastic reduction in weight has been accomplished, both by refinement of the structural analysis and modifications to the drive system.

TABLE XV

Estimates of Weights of Simulator Structure and Drive Equipment
75' x 75' x 200' Size

	Old Est., Ref. 1	New Est., 10 cps Undamped Structure	New Est., 5 cps Damped Structure
Weight of Gimbal Structure, lb.	1,730	635	657
Total Weight of Structure, lb.	68,500	24,400	22,700
Weight of Structure plus Drive Equipment, lb.	103,000	37,000	36,000

From our analog simulation of the response to transient force of the two structures whose weights are given in the last two columns of Table XV, we were able to demonstrate that the damped 5 cps structure

possesses little advantage over the undamped 10 cps structure, provided we utilize a servo control system employing acceleration feed-back.

The estimated cost of the simulator, exclusive of the associated computer, ranges from 3.33 million dollars for the 50' x 50' x 200' structure to 4.11 million dollars for the 100' x 100' x 200' structure.

5.2 Phase II

In this phase of the program, we were concerned with further design and experimentation on the support harness for holding a test subject in the simulator, while allowing him nearly complete freedom of motion of his extremeties. Testing of harnesses for support of a man in shirtsleeves and in a full-pressure suit was accomplished, plus a conceptual design for a harness for a man in back-pack propulsion unit.

We built a test rig which allowed us to support a subject in any position, and to rotate him at speeds up to 20 rpm about one axis. Prototype designs were evolved, and proven by test, for subjects in both shirtsleeves and a Mercury full-pressure suit. The final harnesses could support test subjects for periods of thirty minutes or longer with little discomfort, and allowed essentially complete freedom of use of arms and legs, while immobilizing the torso.

5.3 Phase III

For this phase, we were required to build a rotational air-bearing platform which would allow continuous freedom of rotation, plus translation on a level floor; to acquire data on the capabilities of humans to apply

torque and rotate themselves about various axes; and to deliver the air-bearing platform to MSC after completion of testing. Tests were conducted with six subjects, in standing (yaw axis) and supine (roll axis) positions. Time histories were measured for impulsive torques which these subjects could apply, and for the angular velocity of the rotating table beneath the subject. For rotation about the yaw axis, peak torques ranged from a low of 29.0 lb-ft to a high of 77.5 lb-ft; resultant angular velocities from 49.5 rpm to 93.0 rpm; and peak angular accelerations from 18.8 rad/sec^2 to 53.7 rad/sec^2. For rotation about the roll axis, peak torques ranged from 50.0 to 144 lb-ft; resultant angular velocity from 32.3 to 54.0 rpm; and peak angular acceleration from 3.08 to 21.6 rad/sec^2. The upper limits from these tests can be used to establish upper limits of rotational motion for the space motion simulator.

5.4 General Conclusions and Recommendations

As a result of the work performed under this contract, AAI personnel have strengthened their conviction that the simulator is indeed feasible, and can probably be built to the full size (100' x 100' x 200') desired by MSC. Suitable support harnesses can be made to support test subjects in the simulator in shirtsleeves or full pressure suit, with or without a pack-pack propulsion unit, while allowing nearly complete freedom of use of arms and legs.

We feel that there remains one critical portion of the simulator which requires further study prior to detail design of the simulator. The system for correction of center of gravity of the test subject as he moves

about, and some method of estimating mass moments of inertia of the subject are both essential to accurate simulation of motion. Several techniques for accomplishing these measurements and correcting motion of the test subject were discussed in Reference 1, but one must decide which of these techniques can actually be applied in the final design of the simulator.

We also recommend that, either prior to final design or during the first stages of such design, a dynamic structural model of the simulator be constructed and subjected to vibration tests to verify the complex vibration analysis which we have included in this report.

6.0 References

1. W. E. Baker, A. W. Criswell, H. E. Fineman and W. S. Thayer, Jr., "Design Study of a Device to Simulate the Dynamic Environment Encountered under Conditions of Reduced or Zero Gravity", AAI ER-2938, January 1963.

2. W. E. Baker (Editor), Use of Models and Scaling in Shock and Vibration, ASME, New York, N. Y., 1963.

3. J. P. Den Hartog, Mechanical Vibrations, Fourth Edition, McGraw-Hill Book Co., Inc., New York, 1956, p. 81.

4. S. Timoshenko and D. H. Young, Vibration Problems in Engineering, Third Edition, D. Van Nostrand Co., Inc., New York, 1955, p. 26.

5. (No author) Alcoa Structural Handbook, Aluminum Co. of America, Pittsburgh, Pa., 1960, p. 160.

6. J. E. Ruzicka, (Editor), Structural Damping, ASME, New York, 1959.

7. J. E. Ruzicka, "Increased Reliability of Aviation and Missile Electronics by Use of Damped Structures", SAE Paper No. 100Y, October 1959.

8. E. M. Kerwin, Jr., "Damping of Flexural Waves by a Constrained Visco-Elastic Layer", Journal of Acoustical Society of America, Vol. 31, No. 7, July 1959, p. 952.

9. E. E. Ungar, and D. Ross, "Damping Flexural Vibrations by Alternate Viscoelastic and Elastic Layers", Proceedings of Fourth Midwestern Conference on Solid Mechanics, Univ. of Texas, 1959, p. 468.

10. E. E. Ungar and E. M. Kerwin, Jr., "Damping of Composite Structures by Viscoelastic Interlayers", Journal of Acoustical Society of America, Vol. 32, July, 1960, p. 912 (A).

11. J. E. Ruzicka, "Damping Structural Resonances Using Viscoelastic Shear-Damping Mechanisms", Trans. ASME, Series B, Journal of Engineering for Industry, Vol. 83, No. 4, 1961, p. 403.

12. J. E. Ruzicka, "Vibration Control", Electro-Technology, Vol. 72, No. 2, August 1963, p. 63.

13. E. M. Kerwin, Jr. and D. Ross, "A Comparison of the Effectiveness of Homogeneous Layers and Constrained Layers of Viscoelastic Material in Damping Flexural Waves in Plates", Transactions of Third International Congress on Acoustics, Elsevier Publishing Co., Amsterdam, 1961, p. 410.

14. E. E. Ungar, "Loss Factors of Viscoelastically Damped Beam Structures", Journal of Acoustical Society of America, Vol. 34, No. 8, August 1962, p. 1082.

15. E. E. Ungar and D. K. Hatch, "High Damping Materials", Product Engineering, April 17, 1961, p. 44.

16. Ernest Dzendolet and John F. Rievley, "Man's Ability to Apply Certain Torques While Weightless", WADC Technical Report 59-94, Wright Air Development Center, Wright Patterson A.F. Base, Ohio, April 1959.

17. J. T. Celentano, H. S. Alexander, R. A. Baer, D. P. Balkin, S. P. Johnson, J. B. Reyonlds,"Bioengineering for the Zero G Environment", Physical and Biological Phenomena in a Weightless State, Page 350, Advances in the Astronautical Sciences, Volume 14, Western Periodicals Co., North Hollywood, California, 1963.

18. Carl R. Cording, "Extra Vehicular Maintenance and Techniques" 2nd Manned Space Flight Meeting, American Institute of Aeronautics and Astronautics, 500 Fifth Avenue, New York 36, N. Y., 1963.

19. Ferdinand L. Singer, Engineering Mechanics, Harper & Brothers, Publishers, New York, N. Y., 1954

20. "Moments of Inertia and Centers of Gravity of the Living Human Body," Technical Documentary Report No. AMRL-TDR-63-36, May 1963, Behavioral Sciences Laboratory, 6570th Aerospace Medical Research Laboratories, Aerospace Medical Division, Air Force Systems Command, Wright-Patterson Air Force Base, Ohio.

APPENDIX A: Structural Vibration Analysis of Simulator

I. Gimbal System

Considering the gimbal system as a single degree of freedom spring network vibrating in the fore and aft mode, determine the arm sizes, weights and mass moments of inertia for a gimbal system design frequency of 5 cps.

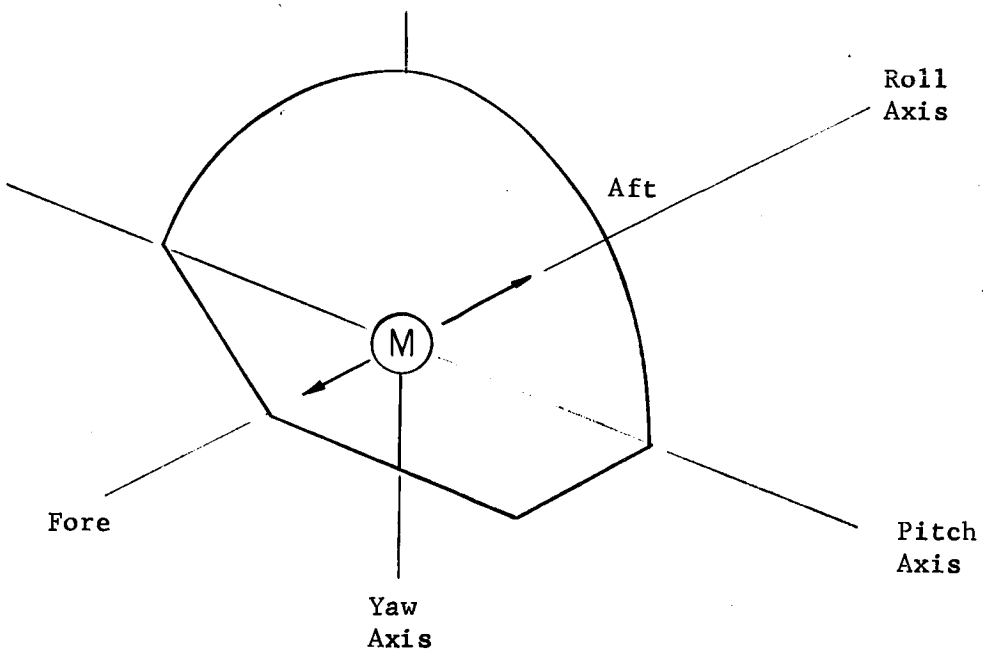

Schematically the gimbal system can be shown as follows:

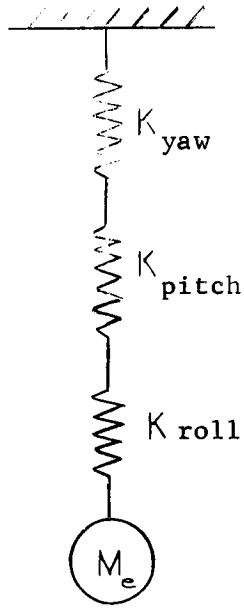

$$K_T = \frac{1}{\frac{1}{K_r} + \frac{1}{K_p} + \frac{1}{K_y}}$$

$$M_e = \frac{1}{g}\left[W_{payload} + \frac{W_{gimbal\ system}}{3} \right]$$

If we look at the gimbal system structure from the side, the deflected shape would appear similar to that shown in the following sketch.

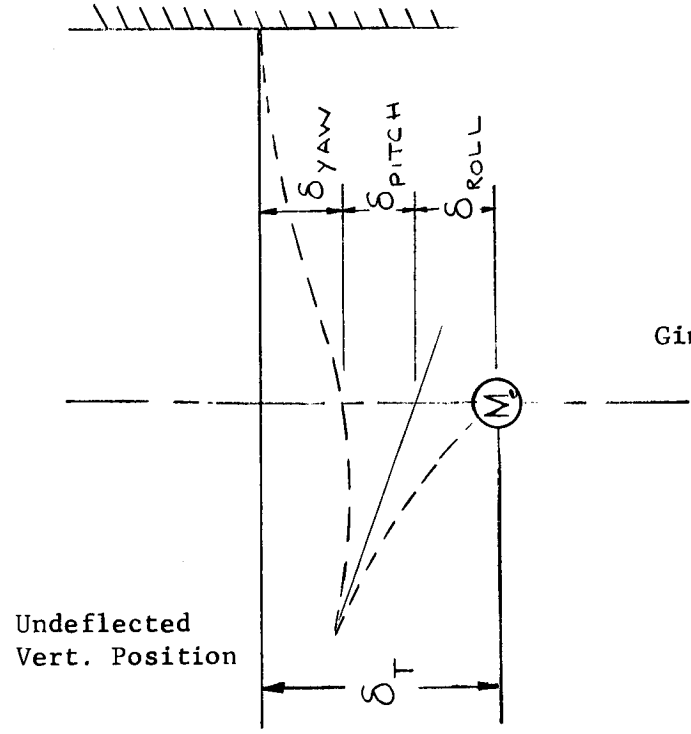

From this sketch we can write the total deflection equation for the gimbal system.

$$\delta_T = \delta_{roll} + \delta_{pitch} + \delta_{yaw}$$

These individual deflections can be obtained by considering each arm as a separate cantilever beam and neglecting the secondary rotation effects.

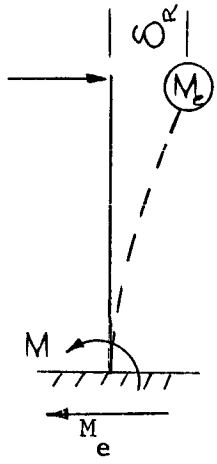

Roll Arm

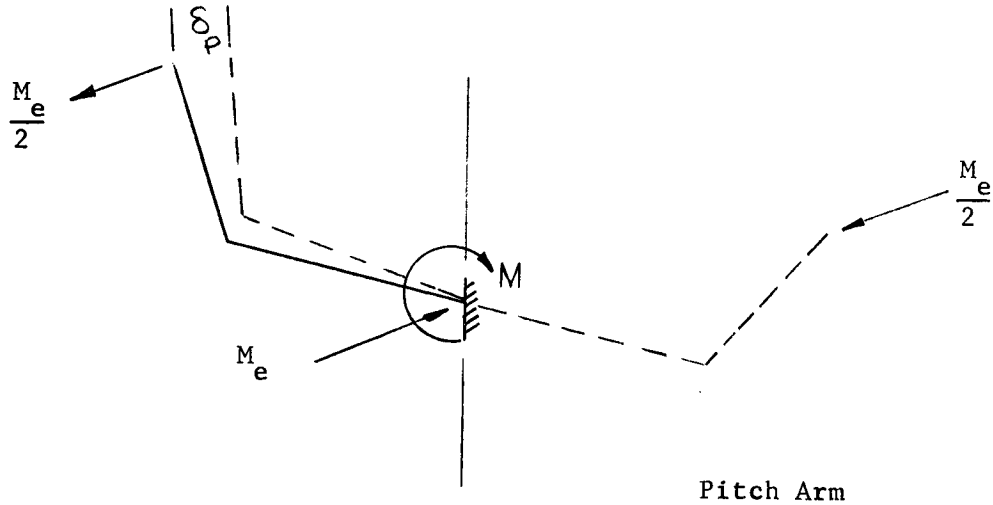

Pitch Arm

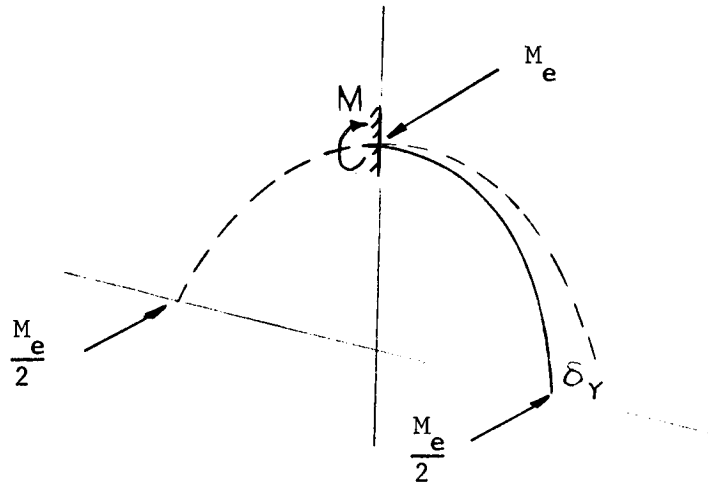

Yaw Arm

By using the gimbal system geomtry established by the clearance envelope and the method of unit loads we can now obtain a deflection expression for each arm.

Roll Arm Deflection

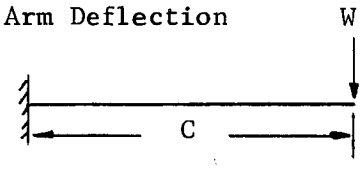

For W = 1 lb

$$\delta_R = \frac{C^3}{3EI_R}$$

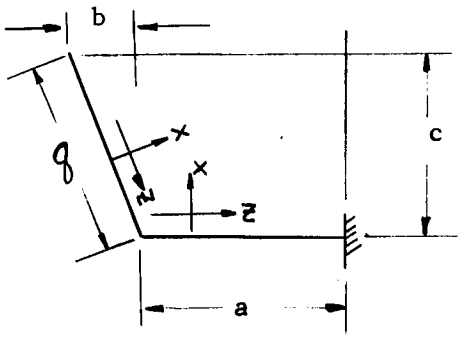

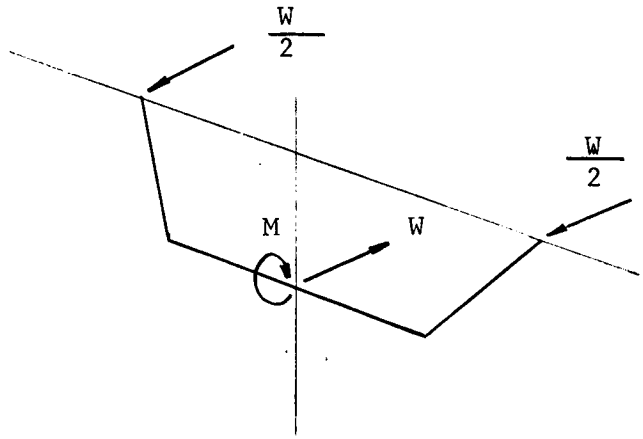

$$\delta_P = \int_o^L \frac{Mmds}{EI_p} + \int_o^L \frac{Mmds}{GK_p}$$

$$M_x = W\frac{X}{2}\Big|_o^q + \frac{W(b+x)}{2}\Big|_o^a$$

$$M_z = 0\Big|_o^q + W\frac{c}{2}\Big|_o^a$$

moments due to load $\frac{W}{2}$

$$m_x = X\Big|_o^q + (b+x)\Big|_o^a$$

$$m_z = 0\Big|_o^q + C\Big|_o^a$$

moments due to dummy unit load.

$$\delta_P = \frac{1}{EI_p}\int_o^q \left(\frac{Wx}{2}\right) x\,dx + \frac{1}{GK_p}\int_o^q 0\,dx + \frac{1}{EI_p}\int_o^a \frac{W}{2}(b+x)(b+x)\,dx + \frac{1}{GK_p}\int_o^a \left(\frac{Wc}{2}\right) c\,dx$$

$$\delta_P = \frac{1}{EI_p}\left[\frac{Wx^3}{6}\right]\Big|_o^q + 0 + \frac{1}{EI_p}\left[\frac{Wb^2x}{2} + \frac{2Wbx^2}{4} + \frac{Wx^3}{6}\right]\Big|_o^a + \frac{1}{GK_p}\left[\frac{Wc^2x}{2}\right]\Big|_o^a$$

$$\delta_p = \frac{1}{EI_p}\left[\frac{q^3}{6} + \frac{b^2 a}{2} + \frac{ba^2}{2} + \frac{a^3}{6}\right] + \frac{1}{GK_p}\left[\frac{c^2 a}{2}\right]$$

for W = 1 lb.

Yaw Arm Deflection:

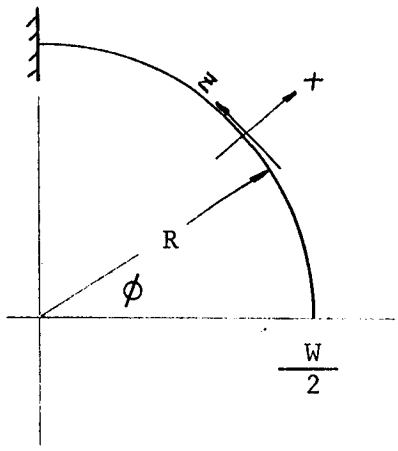

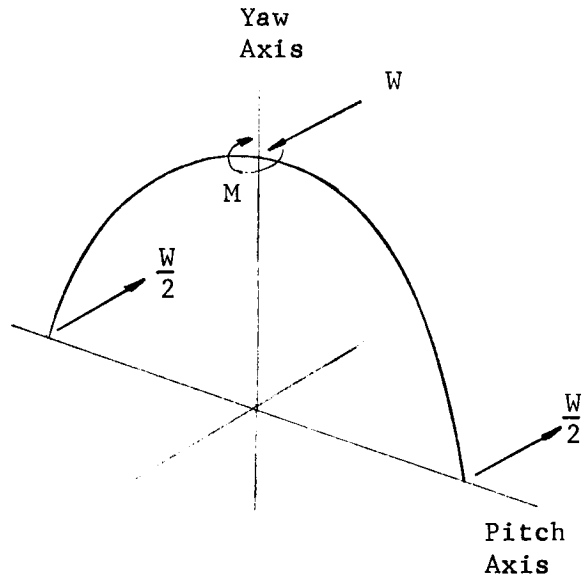

$$\delta_Y = \int_0^L \frac{m_x M_x \, dx}{EI_y} + \int_0^L \frac{m_z M_z \, dx}{G K_Y}$$

$$M_x = \frac{W}{2} R \sin \phi$$

$$M_z = \frac{W}{2} R (1 - \cos \phi)$$

Moments due to load $\frac{W}{2}$

$m_x = R \sin \phi$

$m_z = R (1-\cos \phi)$

Moments due to dummy unit load

$$\delta_Y = \frac{1}{EI_y} \int_o^{\frac{\pi}{2}} \frac{W}{2} R \sin \phi \, (R \sin \phi) \, R d\phi + \frac{1}{GK_y} \int_o^{\frac{\pi}{2}} \frac{W}{2} R (1-\cos \phi) \, R$$

$$(1-\cos \phi) \, R dy$$

$$\delta_y = \frac{WR^3}{2EI_y} \int_o^{\frac{\pi}{2}} \sin \phi^2 d\phi + \frac{WR^3}{2GK_y} \int_o^{\frac{\pi}{2}} (1-2 \cos \phi + \cos^2 \phi) d\phi$$

$$\delta_y = \frac{WR^3}{2EI_y} \left[\frac{\phi}{2} - \frac{1}{4} \sin 2\phi \right] \Bigg|_o^{\frac{\pi}{2}} + \frac{WR^3}{2GK_y} \left[\phi - 2 \sin \phi + \right.$$

$$\left. \frac{\phi}{2} + \frac{1}{4} \sin 2 \phi \right] \Bigg|_o^{\frac{\pi}{2}}$$

$$\delta_y = \frac{R^3}{2EI_y} \left[\frac{\pi}{4} \right] + \frac{R^3}{2GK_y} \left[\frac{3\pi}{4} - 2 \right]$$

for W = 1 lb.

The expression for the total deflection (δ_T) of the gimbal system due to the dummy unit load (W = 1) becomes:

$$\delta_T = \frac{C^3}{3EI_r} + \frac{1}{EI_p}\left[\frac{q^3}{6} + \frac{b^2a}{2} + \frac{ba^2}{2} + \frac{a^3}{6}\right] + \frac{1}{GK_p}\left[\frac{c^2a}{2}\right] +$$

$$\frac{R^3}{2EI_y}\left[\frac{\pi}{4}\right] + \frac{R^3}{2GK_y}\left[\frac{3\pi}{4} - 2\right]$$

Substituting the values of the gimbal geometry shown below and a square hollow box section for each arm we get a final deflection equation for a unit dummy load in terms of arm properties.

a = 47.5 inches

b = 30.0 inches

c = 52.0 inches

q = 60.0 inches

R = 94.0 inches

E = 10×10^6 psi. (Aluminum)

G = 3.8×10^6 psi. (Aluminum)

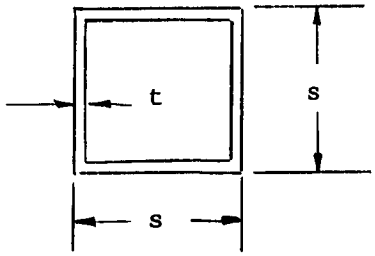

$$I \approx \frac{2}{3} s^3 t, \text{ inches}^4$$

$$K \approx \frac{3}{2} I = s^3 t, \text{ inches}^4$$

$$A \approx 4\,st, \text{ inches}^2.$$

$$\delta_T = \frac{47 \times 10^{-4}}{I_r} + \frac{222 \times 10^{-4}}{I_p} + \frac{587 \times 10^{-4}}{I_y} \quad \text{(inches)}$$

Since we wish to minimize the gimbal system weight and design for a specific δ_T or frequency the total deflection equation and the weight equation must be combined to give a minimum weight for the specified frequency. This can be done in the following manner.

$$\delta_T = \frac{A''}{I_r} + \frac{B''}{I_p} + \frac{C''}{I_y}$$

where $A'' = 47 \times 10^{-4}$

$B'' = 222 \times 10^{-4}$

$C'' = 587 \times 10^{-4}$

$$W_{\text{gimbal system}} = W_{\text{roll}_{\text{arm}}} = W_{\text{pitch}_{\text{arm}}} + W_{\text{yaw}_{\text{arm}}}$$

Since weight of any arm (i) is $W_i = 4 S_i t_i L_i \rho$ and the section inertia $I_i = \frac{2}{3} S_i^3 t_i$ the I_i of any arm in terms of its weight, W_i becomes

$$\frac{I_i}{W_i} = \frac{\frac{2}{3} S_i^3 t_i}{4 S_i t_i L_i \rho} = \frac{S_i^2}{6 L_i \rho} W_i$$

Since $6 L_i \rho$ is a constant for each arm we can now write the total deflection equation in terms of W_i's and S_i's.

$$\delta_T = \frac{A'}{S_r^2 W_r} + \frac{B'}{S_p^2 W_p} + \frac{C'}{S_y^2 W_y}$$

where

$A' = A'' 6 L_r \rho$

$B' = B'' 6 L_p \rho$

$C' = C'' 6 L_y \rho$

To further obtain structurally realistic arms we will establish an $S/_t = R$ ratio based on buckling of the sides of each arm. Letting $S_i/t_i = R_i$ for any arm we can now write the weight of the arm as

$$W_i = 4S_i t_i L_i \rho$$

$$= \frac{4S_i^2 L_i \rho}{R_i}$$

Since $\frac{4L_i\rho}{R_i}$ is constant for each arm we can now write the total deflection as follows:

$$\delta_T = \frac{A'}{(aS_r^2)(S_r^2)} + \frac{B'}{(bS_p^2)(S_p^2)} + \frac{C'}{(cS_y^2)(S_y)^2}$$

where $a = \frac{4L_r\rho}{R_r} = \frac{20.8}{R_r}$

$b = \frac{4L_p\rho}{R_p} = \frac{86.0}{R_p}$

$c = \frac{4L_y\rho}{R_y} = \frac{118.0}{R_y}$

Rewriting the equation so that

$A'a = A \qquad B'b = B \qquad C'c = C$

we get

$$\delta_T = \frac{A}{(aS_r^2)^2} + \frac{B}{(bS_p^2)^2} + \frac{C}{(cS_y^2)^2}$$

or

$$\delta_T = \frac{A}{W_r^2} + \frac{B}{W_p^2} + \frac{C}{W_y^2}$$

Now using the total deflection equation

$$\delta_T = \frac{A}{W_r^2} + \frac{B}{W_p^2} + \frac{C}{W_y^2}$$

and the gimbal system weight equation $W_g = W_r + W_p + W_y$ we can obtain expressions for the minimum weight of each arm in terms of the required deflection. For W_g to be a minimum value the following mathematical conditions must be satisfied.

$$\frac{\partial W_g}{\partial W_r} = 0 \qquad \frac{\partial W_g}{\partial W_p} = 0 \qquad \frac{\partial W_g}{\partial W_y} = 0$$

By solving the total deflection equation for the weight of one arm in terms of δ_T, W_g and the other two arms and combining it with the gimbal system weight equation we can obtain the minimum arm weight expressions. For example*

$$\delta_T = \frac{A}{W_r^2} + \frac{B}{W_p^2} + \frac{C}{W_y^2}$$

Solving for W_r we get

$$W_r = \pm \sqrt{\frac{AW_p^2 W_y^2}{\delta_T W_p^2 W_y^2 - BW_y^2 - CW_p^2}}$$

Substituting this into

$$W_g = W_r + W_p + W_y$$

we get

$$W_g = \sqrt{\frac{AW_p^2 W_y^2}{S_t W_p^2 W_y^2 - BW_y^2 - CW_p^2}} + W_p + W_y$$

* The complete analysis will not be presented here since it is lengthy and involved in nature.

Solving for $\frac{\partial W_g}{\partial W_p}$ and $\frac{\partial W_g}{\partial W_y}$ we get

$$\frac{\partial W_g}{\partial W_p} = 1 - \frac{B\sqrt{A}\ W_y^3}{(\delta_T W_p^2 W_y^2 - BW_y^3 - CW_p^2)^{3/2}} = 0$$

$$\frac{\partial W_g}{\partial W_y} = 1 - \frac{C\sqrt{A}\ W_p^3}{(\delta_T W_p^2 W_y^2 - BW_y^2 - CW_p^2)^{3/2}} = 0$$

Combining these equations we get

$$W_y = W_p \sqrt[3]{\frac{C}{B}}$$

Then returning to the equation for $\frac{\partial W_g}{\partial W_y}$ we can solve for the expression for W_p. In doing this we get the following result.

$$W_p = \sqrt{\frac{B + \sqrt[3]{AB^2} + \sqrt[3]{CB^2}}{\delta_T}}$$

In a similar manner we can obtain

$$W_r = \sqrt{\frac{A + \sqrt[3]{BA^2} + \sqrt[3]{CA^2}}{\delta_T}}$$

$$W_y = \sqrt{\frac{C + \sqrt[3]{AC^2} + \sqrt[3]{BC^2}}{\delta_T}}$$

Combining these individual arm weights we get the gimbal system weight.

$$W_g = \sqrt{\frac{A + \sqrt[3]{BA^2} + \sqrt[3]{CA^2}}{\delta_T}} + \sqrt{\frac{B + \sqrt[3]{CB^2} + \sqrt[3]{AB^2}}{\delta_T}} + \sqrt{\frac{C + \sqrt[3]{AC^2} + \sqrt[3]{BC^2}}{\delta_T}}$$

Letting $Q^{\frac{1}{2}} = \sqrt{A + \sqrt[3]{BA^2} + \sqrt[3]{CA^2}} + \sqrt{B + \sqrt[3]{CB^2} + \sqrt[3]{AB^2}} + \sqrt{C + \sqrt[3]{AC^2} + \sqrt[3]{BC^2}}$

the expression now becomes

$$W_g \frac{Q^{\frac{1}{2}}}{\delta_T^{\frac{1}{2}}} \quad \text{or} \quad \delta_T = \frac{Q}{W_g^2}$$

Since the frequency of the system can be calculated by the expression

$$f = \frac{1}{2\pi}\sqrt{\frac{K_T}{m_e}} \quad \text{and} \quad K_T = \frac{1}{\delta_T}$$ we can write the following

expression for the total deflection of the system.

$$4\pi^2 f^2 m_e = K_T \quad \frac{1}{\delta_T}$$

Since $m_e = \frac{W_e}{g}$, where $W_e = W_{pL}$ (pay load) $+ \frac{W_g}{3}$

$$\delta_T = \frac{g}{4\pi^2 f^2 W_e}$$

Equating this deflection expression to the one obtain for the minimum gimbal system weight we get

$$\frac{g}{4\pi^2 f^2 W_e} = \frac{Q}{W_g^2}$$

letting $G = \frac{g}{4\pi^2}$

$$\frac{G}{f^2 W_e} = \frac{Q}{W_g^2}$$

$$Q^2 f^2 W_e = G W_g^2$$

$$Q f^2 \left(W_{pL} + \frac{W_g}{3}\right) = G W_g^2$$

$$W_g^2 - \frac{Q f^2 W_g}{3G} - \frac{W_{pL} f^2 Q}{G} = 0$$

Solving

$$W_g = \frac{Qf^2}{6G} \pm \frac{f}{6G}\sqrt{Q^2f^2 + 36\,QGW_{PL}} \qquad \text{(lbs)}$$

Now once the gimbal system payload, arm configuration, and frequency or stiffness are established we can determine the size and weight of each arm. The following is an example of this procedure.

5 cps Gimbal System:

$$\delta_T = \frac{A''}{I_r} + \frac{B''}{I_p} + \frac{C''}{I_y}$$

$$\delta_T = \frac{47 \times 10^{-4}}{I_r} + \frac{222 \times 10^{-4}}{I_p} + \frac{587 \times 10^{-4}}{I_y}$$

$$\frac{I_r}{W_r} = \frac{S_r^2}{6L_r\zeta} = \frac{S_r^2}{6 \times 52 \times .1} = \frac{S_r^2}{31.2}$$

$$I_r = \frac{W_r S_r^2}{31.2}$$

$$\frac{I_p}{W_p} = \frac{S_p^2}{6L_p\rho} = \frac{S_p^2}{6 \times 215 \times .1} = \frac{S_p^2}{129}$$

$$I_p = \frac{W_p S_p^2}{129}$$

$$\frac{I_y}{W_y} = \frac{S_y^2}{6L_y\rho} = \frac{S_y^2}{6 \times 295 \times .1} = \frac{S_y^2}{177.3}$$

Therefore

$$\delta_T = \frac{47 \times 10^{-4}}{\frac{S_r^2 W_r}{31.2}} + \frac{222 \times 10^{-4}}{\frac{S_p^2 W_p}{129}} + \frac{587 \times 10^{-4}}{\frac{S_y^2 W_y}{177.3}}$$

$$= \frac{.147}{S_r^2 W_r} + \frac{2.865}{S_p^2 W_p} + \frac{10.41}{S_y^2 W_y}$$

For a 5 cps Gimbal System the following maximum stress levels are estimated to be

Roll Arm - 1200 psi

Pitch Arm - 2000 psi

Yaw Arm - 2000 psi

The buckling stress, f_c, for each arm is therefore

Roll Arm = 4800 psi

Pitch & Yaw Arm = 8000 psi

From ALCOA STRUCTURAL HANDBOOK[5] for long flat aluminum plates in edge compression

$$f_c = \frac{102 \times 10^6}{(1.63 \frac{S}{t})^2} \quad \text{psi.}$$

Solving this for each arm $S/_t$ ratio we get the following results.

$$\frac{S_r}{t_r} = R_r = 90$$

$$\frac{S_p}{t_p} = R_p = 69$$

$$\frac{S_y}{t_y} = R_y = 69$$

Therefore

$$W_r = \frac{4 S_r^2 L_r \rho}{R_r} = \frac{4 \times S_r^2 \times 52 \times .1}{90} = .231 S_r^2$$

$$W_p = \frac{4 S_p^2 L_p \rho}{R_p} = \frac{4 \times S_p^2 \times 215 \times .1}{69} = 1.245 S_p^2$$

$$W_y = \frac{4 S_y^2 L_y \rho}{R_y} = \frac{4 \times S_y^2 \times 295 \times .1}{69} = 1.711 S_y^2$$

or a = .231 b = 1.245 c = 1.711

$A = A'a = .147 \times .231 = .034$

$B = B'b = 2.865 \times 1.245 = 3.57$

$C = C'c = 10.41 \times 1.711 = 17.82$

The final total deflection equation for a 5 cps Gimbal System is therefore

$$\delta_T = \frac{\overset{(A)}{.0340}}{W_r^2} + \frac{\overset{(B)}{3.57}}{W_p^2} + \frac{\overset{(C)}{17.82}}{W_y^2}$$

Solving now for the minimum weight of each arm in terms of δ_T we get

$$W_r^2 = \frac{A + \sqrt[3]{BA^2} + \sqrt[3]{CA^2}}{\delta_T}$$

$$= \frac{.0340 + \sqrt[3]{3.57 \times (.034)^2} + \sqrt[3]{17.82 \times (.034)^2}}{\delta_T}$$

$$W_r^2 = \frac{.325}{\delta_T}$$

$$W_r = \frac{.569}{\delta_T^{\frac{1}{2}}}$$

$$W_p^2 = \frac{B + \sqrt[3]{AB^2} + \sqrt[3]{CB^2}}{\delta_T}$$

$$= \frac{3.57 + \sqrt[3]{(.034)(3.57)^2} + \sqrt[3]{17.82 \times (3.57)^2}}{\delta_T}$$

$$W_p^2 = \frac{10.438}{\delta_T}$$

$$W_p = \frac{3.23}{\delta_T^{\frac{1}{2}}}$$

$$W_y^2 = \frac{C + \sqrt[3]{AC^2} + \sqrt[3]{BC^2}}{\delta_T}$$

$$= \frac{17.82 + \sqrt[3]{(.034)(17.82)^2} + \sqrt[3]{(3.57)(17.82)^2}}{\delta_T}$$

$$W_y^2 = \frac{30.680}{\delta_T}$$

$$W_y = \frac{5.53}{\delta_T^{\frac{1}{2}}}$$

$$W_g = W_r + W_p + W_y = \frac{9.329}{\delta_T^{\frac{1}{2}}}$$

$$W_g^2 = \frac{87.00}{\delta_T}$$

$$\delta_T = \frac{87.00}{W_g^2} \qquad Q = 87.00 \qquad G = \frac{g}{4\pi^2} = 9.78$$

$$W_g = \frac{Qf^2}{6G} + \frac{f}{6G}\sqrt{Q^2f^2 + 36\,QGW_{pL}}$$

W_{pL} = 600 lbs (mockup spacecraft)

$$W_g = \frac{87 \times (5)^2}{6 \times 9.78} + \frac{5}{6 \times 9.78}\sqrt{(87)^2(5)^2 + 36 \times 87 \times 9.78 \times 600}$$

= 405 lbs

$$W_g = \frac{9.329}{\delta_T^{\frac{1}{2}}}$$

$$\delta_T^{\frac{1}{2}} = \frac{9.329}{405} = .023$$

$$W_r = \frac{.569}{\delta_T^{\frac{1}{2}}} = \frac{.569}{.023} = 25 \text{ lbs}$$

$$W_p = \frac{3.23}{\delta_T^{\frac{1}{2}}} = \frac{3.23}{.023} = 140 \text{ lbs}$$

$$W_y = \frac{5.53}{\delta_T^{\frac{1}{2}}} = \frac{5.53}{.023} = 240 \text{ lbs}$$

W_g = 405 lbs check

Since

$$W_r = .231\ S_r^2$$

$$S_r = \sqrt{\frac{25}{.231}} = 10.4 \text{ inches}$$

$$\frac{S_r}{t_r} = 90$$

$$t_r = \frac{S_r}{90} = \frac{10.4}{90} = .116 \text{ inch}$$

$$W_p = 1.245\ S_p^2$$

$$S_p = \sqrt{\frac{140}{1.245}} = 10.6 \text{ inches}$$

$$\frac{S_p}{t_p} = 69$$

$$t_p = \frac{S_p}{69} = \frac{10.6}{69} = .154 \text{ inch}$$

$$W_y = 1.711\ S_y^2$$

$$S_y = \sqrt{\frac{240}{1.711}} = 11.84 \text{ inches}$$

$$\frac{S_y}{t_y} = 69$$

$$t_y = \frac{S_y}{69} = \frac{11.84}{69} = .172 \text{ inch}$$

Arm Stress Levels:

Roll Arm:

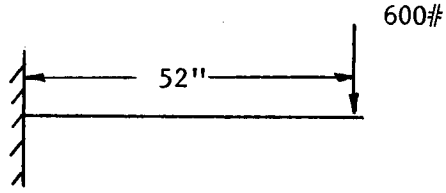

$$I_r = \frac{2}{3} S_r^3 t_r = \frac{2}{3} \times (10.40)^3 \times .116 = 87 \text{ inches}^4$$

$$f_b = \frac{MC}{I_r} = \frac{600 \times 52 \times 5.2}{87} = 1870 \text{ psi}$$

Pitch Arm:

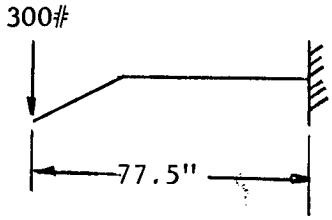

$$I_p = \frac{2}{3} S_p^2 t_p = \frac{2}{3} \times (10.6)^2 \times .154 = 122 \text{ inches}^4$$

$$f_b = \frac{MC}{I_p} = \frac{300 \times 77.5 \times 5.3}{122} = 1015 \text{ psi}$$

Yaw Arm:

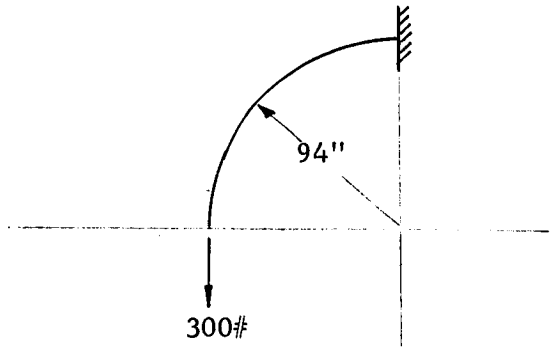

$$I_y = \frac{2}{3} S_y^2 t_y = \frac{2}{3} (11.84)^2 (.172) = 191 \text{ inches}^4$$

$$f_b = \frac{MC}{I_y} = \frac{300 \times 94 \times 5.92}{191} = 875 \text{ psi}$$

Mass Moments of Inertia: 5 cps Gimbal System

Each arm is considered to be a thin rod.

Roll Arm:

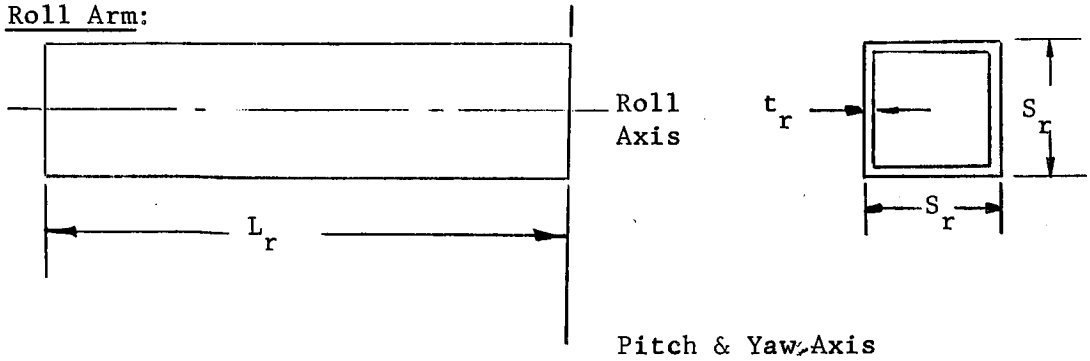

L_r = 52 inches S_r = 10.4 inches W_r = 25 lbs

$$J_r = \frac{M_r S_r^2}{3} = \frac{25}{3 \times 386} \times (10.4)^2 = 2.32 \text{ inch lb sec}^2$$

$$J_p = J_y = \frac{M_r L_r^2}{3} = \frac{25}{3 \times 386} \times (52)^2 = 65 \text{ inch lb sec}^2$$

Pitch Arm:

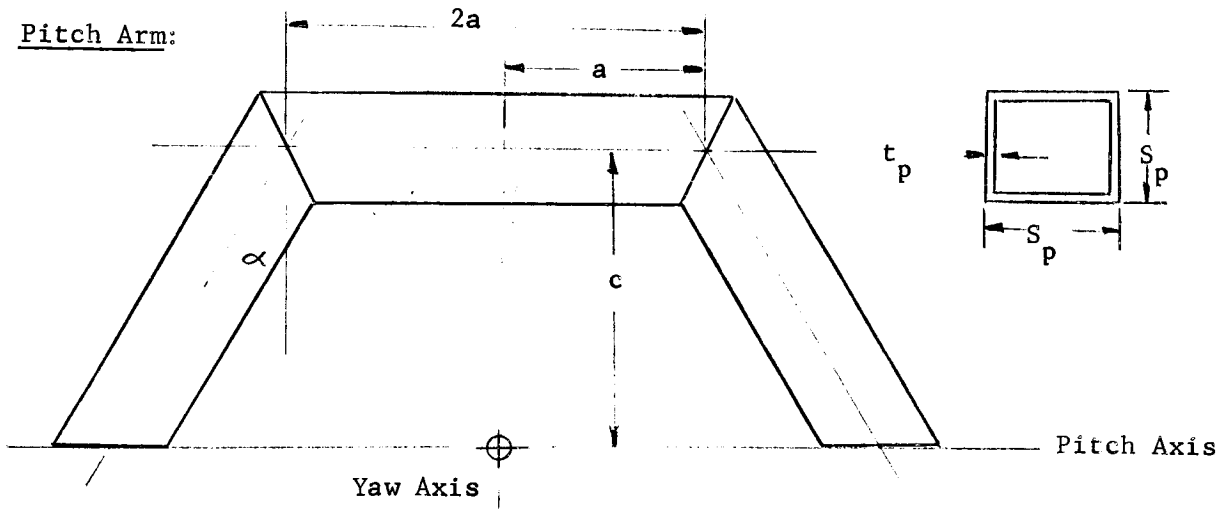

a = 47.5 inches c = 52 inches $\alpha = 30^o$

S_p = 10.6 inches W_p = 140 lbs

$$J_p = \frac{M_p}{a \cos \alpha + c} \left[\frac{c}{3} \left(c^2 + \frac{S_p^2}{2}\right) + a \cos \alpha \left(c^2 + \frac{S_p^2}{3}\right) \right]$$

$$= M_p \left[1699 + .24\, S_p^2 \right]$$

$$= \frac{140}{386} \left[1699 + .24 \times (10.6)^2 \right]$$

$$= 626 \text{ in lb sec}^2$$

$$J_y = \frac{M_p}{a \cos\alpha + c}\left[a\cos\alpha \left(c^2 + \frac{a^2}{3} + \frac{S_p^2}{6}\right) + c\left(a^2 + ac\tan\alpha + \frac{c^2}{3\cos^2\alpha} + \frac{S_p^2}{6}\right)\right]$$

$$= M_p\left[4240 + .167\, S_p^2\right]$$

$$= \frac{140}{386}\left[4240 + .167\,(10.6)^2\right]$$

$= 1545$ inch lb sec^2.

Jaw Arm:

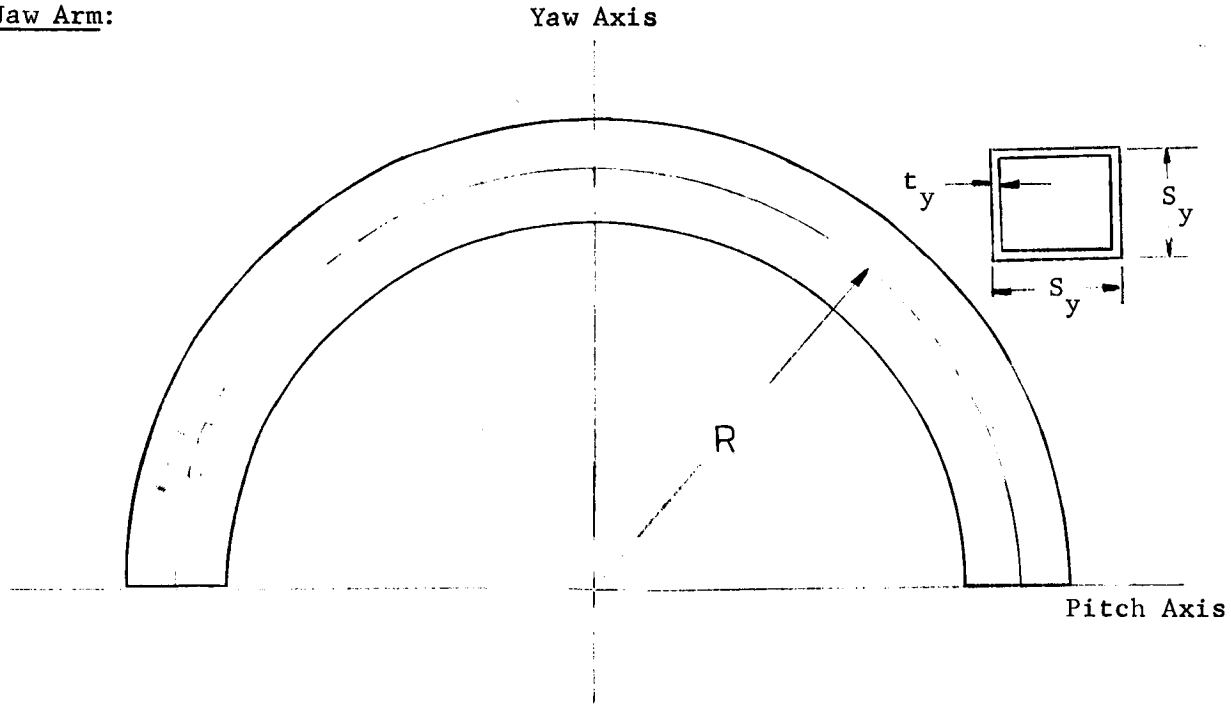

R = 94 inches

$\gamma = \frac{\rho}{g}$

W_y = 240 lbs

ρ = .1 #/inch^3

S_y = 11.84 inches

t_y = .172 inch

$$J_y = 2\pi \gamma S_y t_y R^3$$

$$= 2\pi \times \frac{.1}{386} \times 11.84 \times .172 \times (94)^3$$

$$= 2750 \text{ in lb sec}^2.$$

II. Cross Span Dolly

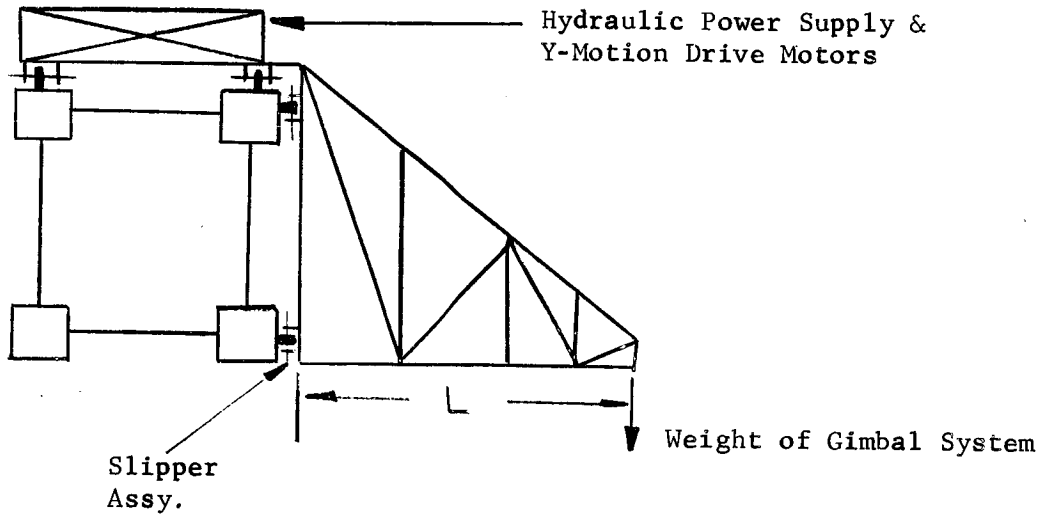

Considering the dolly as a single degree of freedom cantilever beam with a varying cross section under-going bending vibrations the stiffness can be determined by the following analysis.

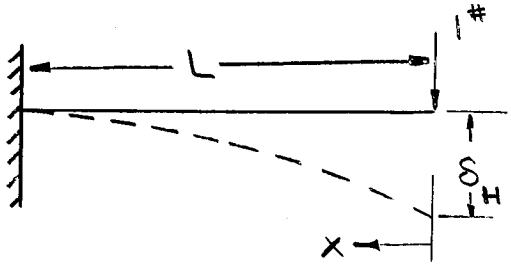

$I(x) = I_o\left(\frac{x}{L}\right)^2$ where I_o is the cross section moment of inertia at the base of the beam.

For a unit load:

$$\delta_H = \frac{1}{EI_o}\int_0^L \frac{x^2}{\frac{x^2}{L^2}}\,dx = \frac{L^3}{EI_o}$$

Since K =

$$K = \frac{EI_o}{L^3}$$

For L = 50 inches and E = 10^7 psi (Alum.)

$$K = \frac{10^7 I_o}{(50)^3} = 80\, I_o$$

For a single degree of freedom system

$$f = \frac{1}{2\pi}\sqrt{\frac{K}{m}}$$

Therefore

$$I_o = \frac{f^2\, 4\pi^2 m}{80}$$

For a 5 cps gimbal system m is as follows:

5 cps Gimbal System

Gimbal Payload (mockup spacecraft)	=	600 lbs
Gimbal Structure	=	405 lbs
C.G Correction Mechanism	=	198 lbs
Roll Arm Drive	=	62 lbs
Pitch Arm Drive	=	305 lbs
Yaw Arm Drive	=	668 lbs
		2,238 lbs

$$m = \frac{2238}{386} = 5.78 \text{ lb sec}^2/_{\text{inch}}$$

We find that we can design the dolly for a frequency much greater than that of the gimbal system, without adding much weight to the system. For a dolly frequency

f = 11 x 5 = 55 cps, we have:

$$I_o = \frac{(55)^2 \times 4\pi^2 \times 5.78}{80}$$

$$= 8{,}650 \text{ inches}^4$$

$$I_o = \frac{1}{2} Ad^2 \qquad d = 60 \text{ inches}$$

$$A = \frac{2I_o}{d^2} = \frac{2 \times 8{,}650}{(60)^2} = 4.8 \text{ in}^2$$

$W = 2 AL \rho K$

L = 50 inches

$\rho = .1\#/in^3$.

K = .3, shear member weight factor

W = 2 x 4.8 x 50 x .1 x 3

= 144 lbs = 150 lbs

Stress Check:

$$M_{max} = 2{,}238 \times 50 = 111{,}900 \text{ in lbs}$$

$$f_{b\,@\,base} = \frac{MC}{I_o} = \frac{111{,}900 \times 30}{8{,}650} = 388 \text{ psi}$$

III. CROSS SPAN AND VERTICAL TRUSSES

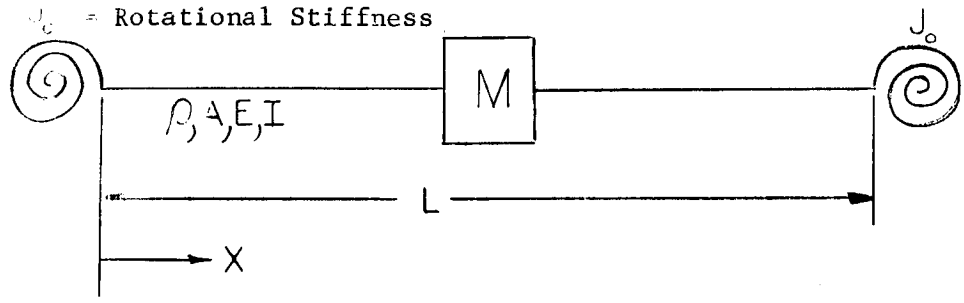

Consider the cross span as a uniform beam with a concentrated mass at the center, and supported at the ends by springs which oppose rotation of the ends, where the rotational stiffness, J_o, is provided by the vertical trusses.

Using Hamilton's principle* and the boundary conditions for the symmetric and asymmetric mode of vibration the frequency equation for each

---

* Housner G. W., Hudson D. E., Applied Mechanics Dynamics, D. Van Nostrand Co. Inc., July 1953 pg. 260.

Hamilton's principle states that the actual path followed by a dynamical process is such as to make the integral of (T-V) a minimum.

$$\delta \int_{t_1}^{t_2} [T - V] dt = 0$$

where T = total Kinetic Energy of system.

V = total Potential Energy of system.

mode can be obtained by a lengthy mathematical analysis. These equations are as follows:

Symmetric Mode:

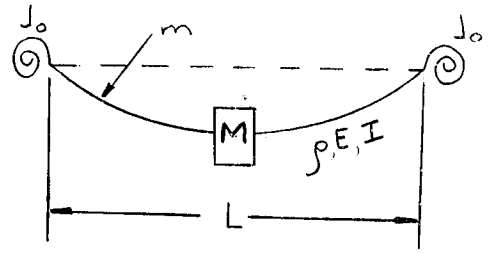

$$\frac{M}{m}\frac{\lambda}{2}\left(\tan h\ \frac{\lambda}{2} - \tan\frac{\lambda}{2}\right) + 2 + \frac{J_o L}{2EI}\left[\frac{M}{m}\left(1 - \sec\frac{\lambda}{2}\ \mathrm{sech}\frac{\lambda}{2} + \frac{2}{\lambda}\right.\right.$$

$$\left.\left.\left(\tan\frac{\lambda}{2} + \tan h\frac{\lambda}{2}\right)\right] = 0\right.$$

Asymmetric Mode:

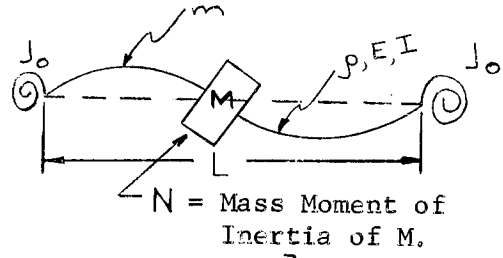

$$\sin\frac{\lambda}{2}\sin h\frac{\lambda}{2}\left[2 + \left[\left(\frac{\lambda}{2}\right)^3\frac{4N}{mL^2} - \frac{J_o L}{2EI}\left(\frac{2}{\lambda}\right)\right]\left[\cot\frac{\lambda}{2} - \coth\frac{\lambda}{2}\right]\right]$$

$$+ \frac{2J_o N}{EImL}\left(\frac{\lambda}{2}\right)^2\left(\cos\frac{\lambda}{2}\cos h\frac{\lambda}{2} - 1\right) = 0$$

The first eigen values, λ_1, of these equations were obtained by trial and error for various values of the parameters $\frac{J_o L}{2EI}$, $\frac{4N}{mL^2}$ and $\frac{M}{m}$. These results are shown in the following table.

Symmetric Mode

$\frac{JoL}{2EI_{cs}}$ \ $M/_m$	.2	1.0	5.0	10.0
0	2.887	2.384	1.719	1.463
.2	2.9917	2.4668	1.7787	1.5123
1.0	3.2767	2.6919	1.9366	1.6462
5.0	3.7827	3.0810	2.2047	1.8722
10.0	3.9688	3.2200	2.2990	1.9516
	4.250	3.440	2.446	2.072

λ_1

Asymmetric Mode

$\frac{JoL}{2EI_{cs}}$ \ $\frac{4N}{ML^2}$	.2	1.0	5.0	10.0
0	3.844	2.620	1.759	1.474
.2	3.8608	2.6303	1.7655	1.4850
1.0	3.9151	2.6637	1.7874	1.5036
5.0	4.0392	2.7373	1.8352	1.5438
10.0	4.0901	2.7683	1.8544	1.5607
	4.150	2.828	1.894	1.588

λ_1

These results were then used to plot curves showing the variance of λ_1 with the parameters.

Using the relationships $\omega = 2\pi f = \frac{\lambda^2}{L}\sqrt{\frac{EI}{mL}}$

$$I = \frac{1}{2} Ad^2$$

$$m = \frac{2 \rho ALK}{g}$$

we can arrive at an expression for λ_1 in terms of the desired frequency and the cross span configuration. This expression is

$$\lambda_1^2 = \frac{4\pi f L^2}{d} \sqrt{\frac{\rho K}{E g}}$$

Thus, after selecting the following values, a value of λ_1 can be obtained.

f = design frequency, cps

L = cross span length, inches

d = cross span depth, inches

ρ = .1 lb/in^3 (Aluminum)

E = 10^7 psi (Aluminum)

K = 3, truss shear member weight factor

g = 386 in/sec^2

With the value of λ_1 and a selected value of relative rotational stiffness, $\frac{J_o L}{2EI} = 5$, a value of $\frac{M}{m}$ or $\frac{4N}{mL^2}$ can be obtained from the curves plotted from the solution of the symmetric and asymmetric mode frequency equations.

With the cross span configuration established J_o of the vertical trusses can be determined*. Using this and the vertical truss designing

---

* $\frac{J_o L}{2EI_{cs}} = 5 \qquad J_o = \frac{10 EI_{cs}}{L}$

load condition of

$$J_o = \frac{3EI_{VT}}{b}$$

where $b \geq \frac{1}{2} L$

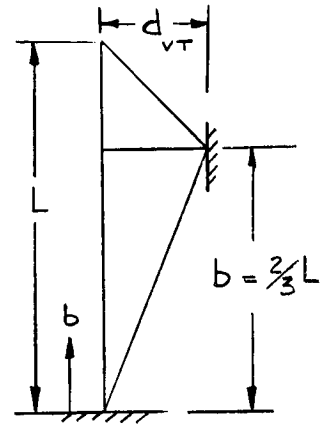

the section moment of inertia, I_{VT}, of the vertical truss could be determined. Then by picking a depth, d_{VT}, the weight can be obtained in the following manner.

$$I_{VT} = \frac{1}{2} A_{VT} d_{VT}^2 \qquad W = 2A_{VT} L_{VT} \rho K$$

$$A_{VT} = \frac{2I_{VT}}{d_{VT}^2}$$

Since calculations indicated that the symmetric mode was the designing mode* the following sample calculation is made for that mode.

---

* Based on the rough calculation of N, mass moment of inertia and of mass, M, with respect to the cross span centerline.

5 cps Simulator - 75' x 75' x 200'

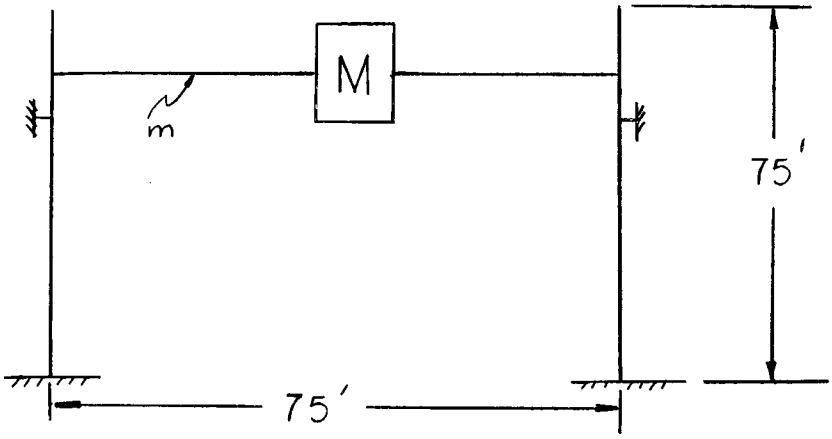

f = 5 cps ρ = .1#/in^3, K = 3, E = 10^7 psi.

M = mass of gimbal system + cross span dolly system

$$M = \frac{1638\# + 3964\#}{386} = \frac{5602\#}{386}$$

Selecting a depth of the cross span of 60 inches we get

$$\lambda_1^2 = \frac{4\pi f L^2}{d}\sqrt{\frac{\rho K}{Eg}}$$

$$\lambda_1^2 = \frac{4\pi \times 5 \times (900)^2}{60}\sqrt{\frac{.1 \times 3}{10^7 \times 386}}$$

$$\lambda_1 = 2.73$$

With $\frac{J_o L}{2EI_{cs}} = 5$ we get an $\frac{M}{m}$ ratio equal to 1.87.

Therefore since $\frac{M}{g} = W$ the weight of the cross span equals

$$W_{cs} = \frac{5602}{1.87}$$

$$W_{cs} = 3000 \text{ lbs}$$

$$A_{cs} = \frac{W_{cs}}{2L_{cs}k\rho}$$

$$= \frac{3000}{2 \times 900 \times 3 \times .1}$$

$$= 5.6 \text{ in}^2$$

$$I_{cs} = \frac{1}{2} A_{cs} d_{cs}^2$$

$$= \frac{1}{2} \times 5.6 \times (60)^2$$

$$= 10{,}008 \text{ in.}^4$$

Since $\frac{J_o L}{2EI_{cs}} = 5$

$$J_o = \frac{10EI_{cs}}{L}$$

$$= \frac{10 \times 10^7 \times 10{,}008}{900}$$

$$= 1110 \times 10^6 \text{ inch lb.}$$

$$J_o = \frac{3EI_{vt}}{b} \quad \text{for} \quad b \geq \frac{1}{2}L$$

for $b = \frac{2}{3}L = 600''$

$$I_{VT} = \frac{1110 \times 10^6 \times 600}{3 \times 10^7}$$

$$= 22{,}200 \text{ in}^4.$$

For a depth of vertical truss of 90 inches at 2/3's of it's height.

$$A_{VT} = \frac{2I_{VT}}{d_{VT}^2}$$

$$= \frac{2 \times 22{,}200}{(90)^2}$$

$$= 5.5 \text{ in}^2$$

$$W_{VT} = 2A_{VT}L_{VT}\rho K$$

$$= 2 \times 5.5 \times 900 \times .1 \times 3$$

$$= 2959 \text{ lbs}$$

APPENDIX B

TEST EQUIPMENT FOR MEASURING TORQUES GENERATED BY HUMANS WHILE TRACTIONLESS

The test equipment described in this appendix was used to provide tractionless support for the subject and to record the subject's angular velocity and torque output. The principal pieces of apparatus, including the smooth floor, the rotary air-bearing platform, the overhead torque handle and the chart recorder with amplifier are described in detail.

A smooth, flat work surface of adequate size was necessary for the operation of the air-bearing supported platform.

The air film between the bearings and the floor surface varied in thickness from .002 to .004 inches depending upon air supply flow rate and the load supported by the bearings. From previous experiments, it was known that minor surface protrusions caused serious interference with the bearings while minor surface indentations did not adversely affect the bearing's operation. The height of surface protrusions that caused interference was determined by the air film thickness between the bearing surfaces. Also, from previous experiments it was known that the pad type air thrust bearing having the standard 125$\surd$ RMS manufacturing finish could be operated satisfactorily if the surfaces were periodically wiped clean of oil and foreign particles.

After a thorough investigation of possible work surface materials including concrete, aluminum plate, plastic, ice, and expoxy, a poured-in-

place epoxy was selected on the basis of surface flatness, surface smoothness and cost. A small experimental sample proved that a low viscosity epoxy resin and a polyamide hardener could be mixed in one batch and be poured into place to provide a smooth, flat, and level work surface that would have sufficient hardness to avoid scratching and abrasion in normal use.

The floor area to be used in the Mechanical Laboratory had height variations up to 1.5 inches over 12 feet. A wooden bumper was fastened to the floor surrounding the test area and tooling plaster was used as a filler to provide an approximately level base for the epoxy. The plaster filler varying from 0.5 inches to 2.0 inches compensated for the slope of the lab floor. A sheet of epoxy, approximately 0.3 inches thick, was poured in place atop the plaster. In the fluid state, the epoxy flowed evenly over the plaster and a smooth, level, work surface was obtained.

Two problems were encountered with the epoxy surface technique. First, the fast-drying tooling plaster used for the filler set before it could be evenly worked in place, causing some plaster surface unevenness and hence, some variation in the thickness of the epoxy which covered it. The second problem (which may be related to the first) was the more noticeable. Part of the epoxy at one end of the work surface buckled free of the plaster surface and remained raised with an air gap existing between the plaster and the epoxy. This is believed to have been caused by the differential expansion between the plaster and the epoxy and the rigid

frame surrounding the epoxy which prevented outward expansion. Fortunately, this surface condition did not cover sufficient area to interfere with the test program.

The air-bearing supported platform was designed to provide continuous rotation about the vertical axis and translation in the horizontal plane bounded by the limits of the test area. The platform is shown in Figure B-1 with the circular support plate removed and rotated 90 degrees from its normal position.

The three upper air thrust bearings, shown in the figure, supported the upper plate on an air film and allowed it to rotate under nearly frictionless conditions. The three lower air thrust bearings, mounted at the ends of the arms and facing downard, supported the assembly on an air film above the floor. The air bearings were attached to the frame through spherical bearings which allowed them sufficient articulation to seek uniform air film thicknesses independent of structural deflections and opposing surface slopes.

The air-bearings were 9 inches in diameter with a .25 inch air supply port in the center. The air pressure requirements varied between 50 and 90 psi, depending upon the bearing load and the floor surface. To maintain a .004 inch air gap with a 300 lb. table load, air at 80 psi was used at the rate of 40 CFM. For these experiments shop air from the 110 psi source was provided. This air passed through a sintered metal filter to remove excess oil and water.

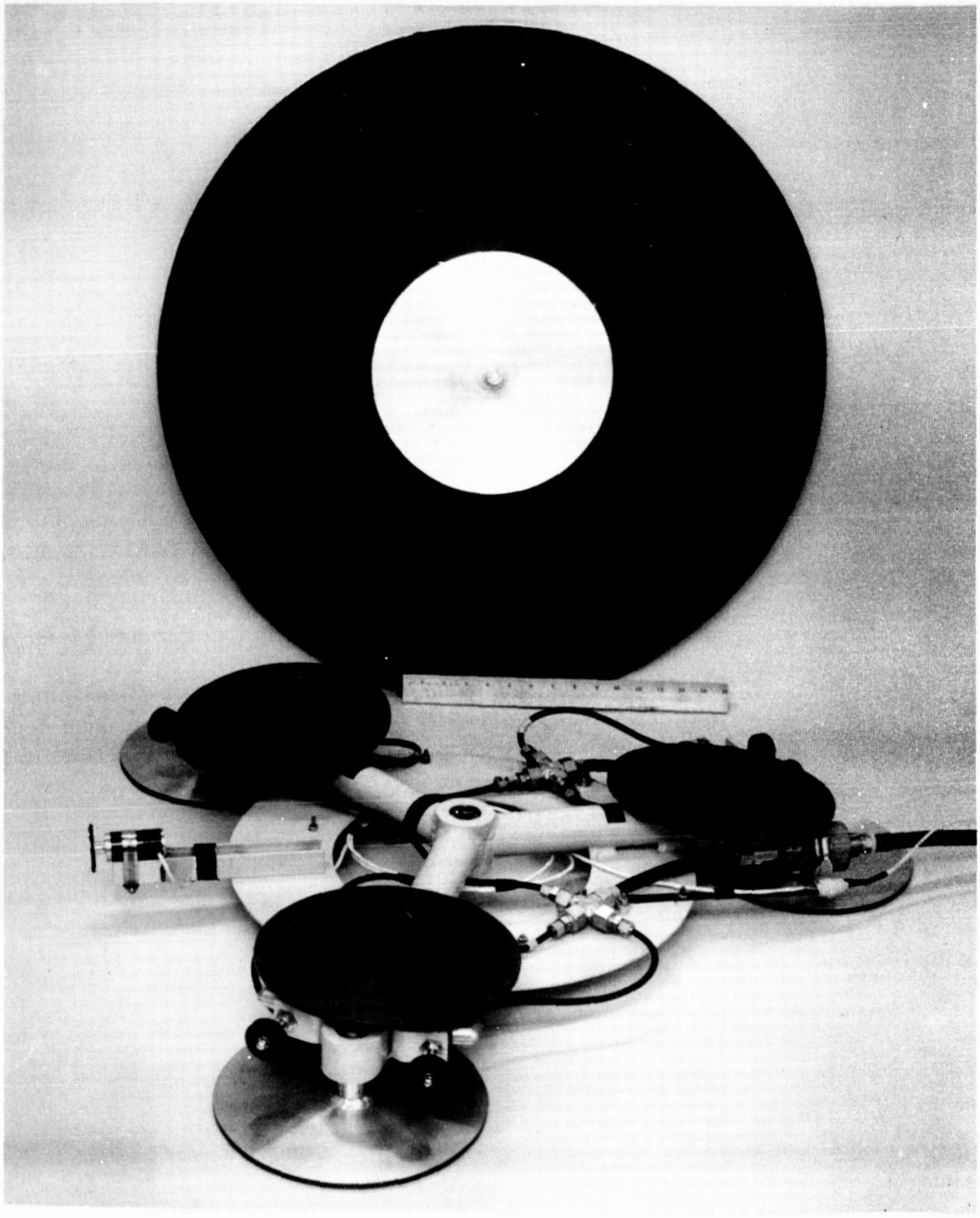

Figure B-1
AIR BEARING SUPPORTED ROTARY PLATFORM

A small ball bearing in the hub of the Rotary Platform received the axle which was butt welded to the bottom of the circular platform. While adding a small amount of friction torque, this bearing was necessary to maintain alignment between the circular plate and the frame.

The air supply hose was attached to the frame at the end of the arm on the right side of Figure B-1. The compressed air was distributed equally to the six bearings. Individual needle valves provided the capability to compensate for individual bearing differences. These valves also provided the capability for activating either upper or lower pads alone when the test equipment was used for either translation or rotation independently.

The bearing surfaces were manufactured to a 63 $\surd$ RMS finish with a .002 inch flatness. All bearing surfaces were given a .002 inch Martin Hardcoat finish. This electro-chemical finish provided a hard aluminum oxide surface that was very satisfactory in resisting abrasion.

A D.C. voltage generating tachometer mounted on the frame is shown between the bearings on the left side of Figure B-1. The rubber wheel of the tachometer contacted the underside of the circular plate to provide an output signal proportional to the differential angular velocity between the plate and the frame. This signal was linear in calibration tests up to 160 RPM.

The torque handle and its supporting structure are shown in Figure B-2. This assembly was securely mounted to the overhead structural

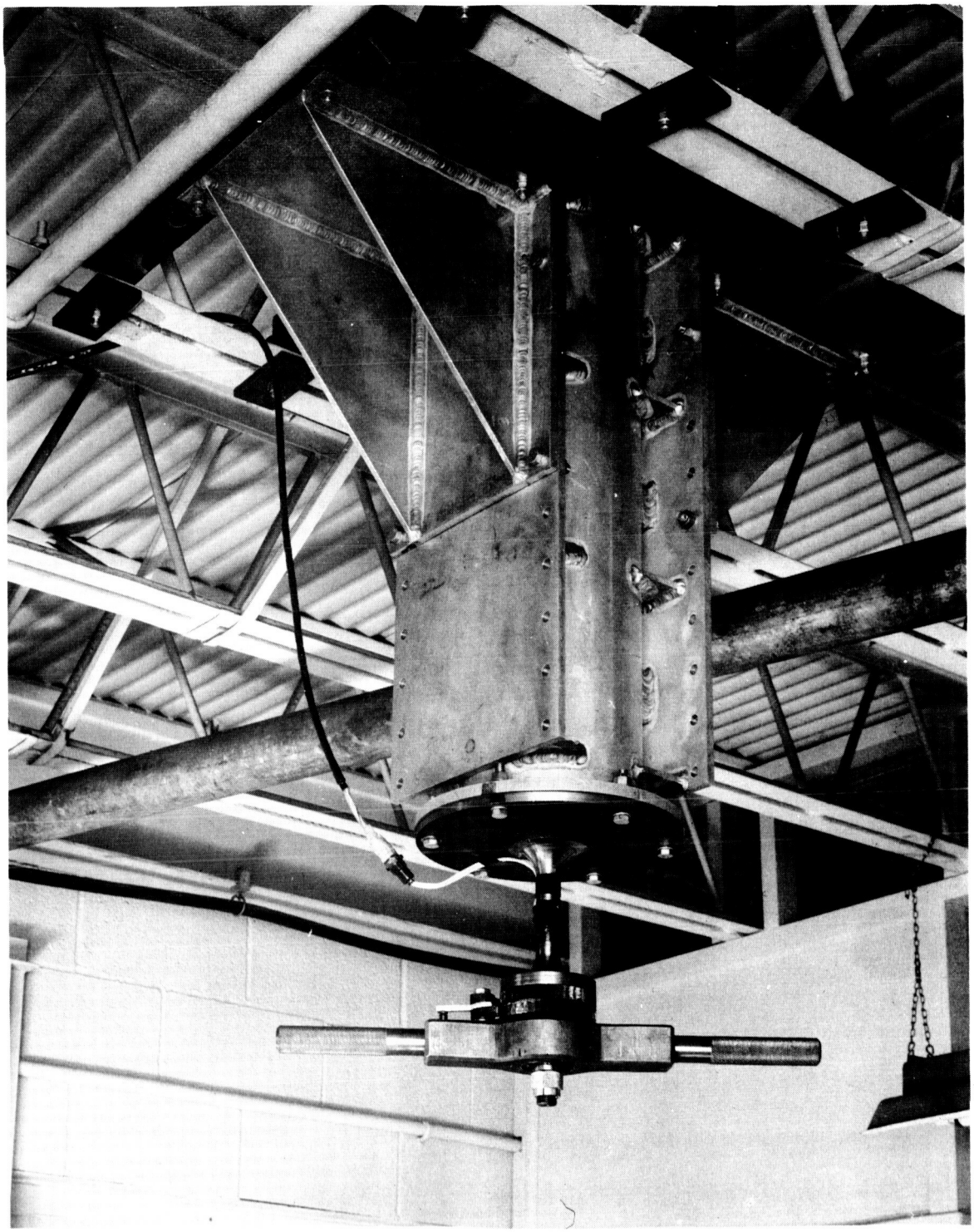

Figure B-2
TORQUE HANDLE AND SUPPORTING STRUCTURE

members of the building above the center of the test area.

The torque handle with a double set of angular contact ball bearings at its hub was free to rotate about a vertical axis through its center. The angular contact bearings provided both axial and radial load-carrying capabilities. As a safety precaution, the torque handle was designed to support the subject's weight to prevent injury in case the subject lost his balance during the tests. Appreciable axial bearing loads were developed in this manner.

Two ratchet wheels oriented in opposite directions were secured to the shaft above the torque handle. A spring loaded pawl selector on the torque handle permitted the selection of either clockwise or counterclockwise free rotation. Once the direction of free rotation was selected the pawl engaged the appropriate ratchet and prevented rotation of the torque handle in the opposite direction.

A strain-gage bridge located on the steel shaft directly above the ratchet wheels was designed to indicate the torsional strain and hence the torque exerted on the free end of the shaft by the test subject. The strain gages of the torsion bridge mounted on the surface of the shaft were oriented at 45 degrees to the axis of the shaft. In this manner the principal axis of the gage corresponded to the principal axis of torsional strain in the shaft. The torsional strain gage bridge was oriented for maximum sensitivity to torsional strain and minimum sensitivity to bending and axial strain. The torsion bridge was equally sensitive to either clockwise or counterclockwise applied torque.

The vertical plates of the support tube were bolted to the two box gussets shown in Figure B-1. A series of mounting holes spaced on 2.9 inch centers permitted torque handle height variations over a 12 inch range.

An extension tube 4.3 feet long was used to lower the torque handle for the Roll Axis tests. This 5.0 inch diameter tube with 10.0 inch diameter attachment plates welded to each end provided rigid support for the handle in the lower position.

A 2 by 6 feet pallet of 0.5 inch plywood was used to support the subject on top of the rotary platform in the Roll Axis test position. The weight of the subject held the pallet in place satisfactorily, making attachment between the pallet and the platform unnecessary.

A motion picture camera operating at 64 frames per second was used to film a limited number of the tests. These films were used to analyze the actions of the subjects both in slow motion and on a frame-by-frame basis. In a secondary capacity, the films were used to verify the tachometer calibration.

A CEC Model 5-124 Oscillograph Recorder with a CEC Model 1-127 Carrier Amplifier was used to record the torque and angular velocity traces on a known time scale. A four inch per second tape speed with tenth-of-a-second timing lines provided a clear record of the subject's torque and motion history.

The D.C. signal from the tachometer was attenuated to produce approximately a six inch trace deflection corresponding to 160 RPM of the

circular plate of the air-bearing platform. In calibration tests, the angular velocity trace was linear within 3% over the zero to 160 RPM range in both clockwise and counterclockwise rotation. The tachometer was calibrated using the electrical signal from a limit switch which was set to close contacts momentarily once per revolution. This electrical signal circuit was connected to one of the galvonometers of the oscillograph to produce a mark on the trace at the completion of each revolution of the circular plate of the air-bearing platform. These marks on the known time base of the recorder tape, provided the time per revolution and hence angular velocity data.

With a carrier voltage of 5.0 volts, the resistance change of the torsional strain gage bridge produced a four inch trace deflection corresponding to approximately 65 pound feet of torque on the torque handle. The amplification of the strain gage bridge signal was changed by known increments for various subjects to keep the torque trace deflection within a four inch range.

APPENDIX C

ANALYSIS OF SAMPLE TRACES ROLL AXIS TESTS

SUPINE TEST POSITION

The angular velocity and torque traces shown in Figure C-1 illustrate the basic shapes of the two traces recorded in this test series. The torque trace in all cases was a single pulse. This torque pulse generally resembled either a half sine or versine curve, depending upon the individual onset and decay characteristics. The characteristics of the peak of the torque pulse varied over a wide range from a narrow spike peak to a long duration pulse with a flat peak. In many cases, secondary peaks were observed either before or after the major peak of the torque pulse.

The angular velocity trace had the same shape as the time integral of the torque trace. Angular velocity as discussed in Section 4.2 was determined by the relationship.

$$\dot{\theta} = \frac{\int_o^t T\,dt}{I} \qquad (1)$$

where $\int_o^t Tdt$ is the integral of the torque trace over the period t.

This theoretical relationship assumes that the subject's body rotates as a rigid mass that does not change its moment of inertia during rotation. As discussed in Section 4.3, the subject neither remained perfectly rigid during rotation nor did his moment of inertia remain exactly

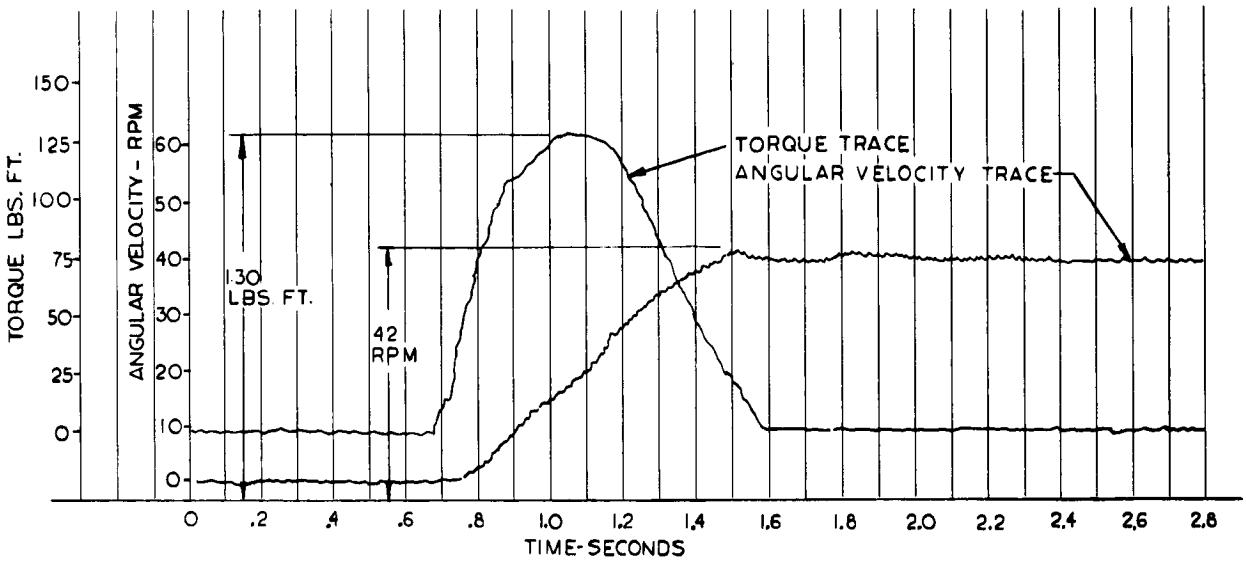

SUPINE TEST POSITION
FIG. C1

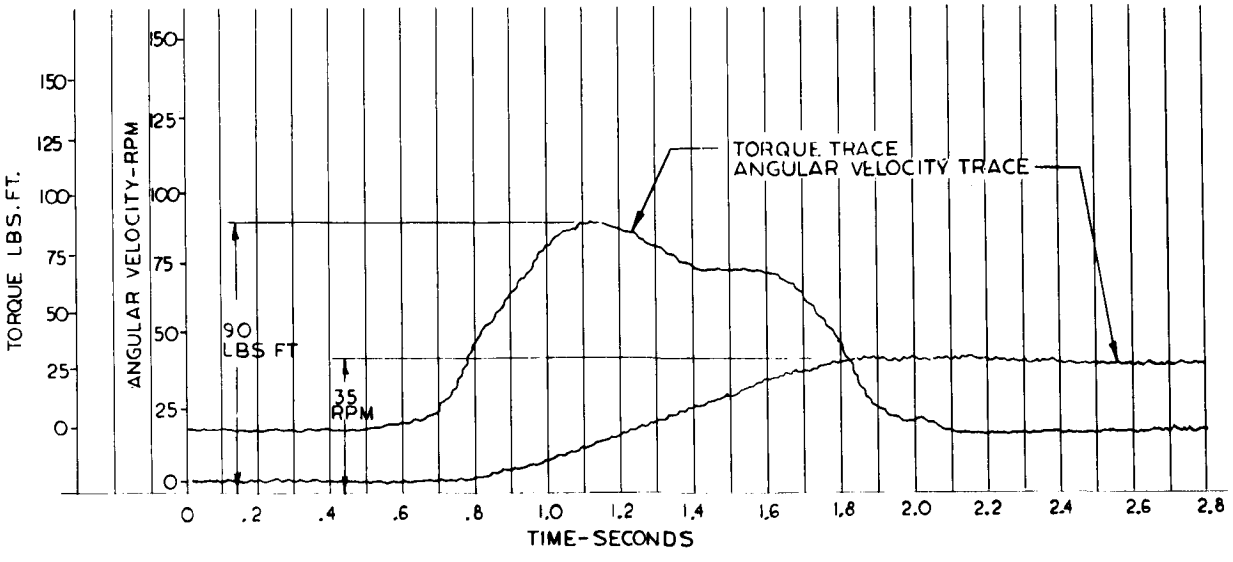

SUPINE TEST POSITION
FIG. C2

constant. Such deviations from the theoretical conditions caused those oscillations which were visible on the recorded angular velocity traces.

The torque trace shown in Figure C-2 illustrates a rather flat pulse of long duration. This trace having a total duration of 1.5 seconds is unusual in that the subject was able to maintain a torque level over 50 lb/ft for over 0.8 second. Generally the pulse had a narrow peak with a short duration on the order of .5 sec for torque greater than 50 lb/ft.

Figure C-3 shows a torque trace with a step in the decay phase while Figure C-4 shows a trace which has a step in the onset phase. Many traces having a step in the decay phase were encountered. These steps were caused by the combined movements of the subject's body in rotation and the subject's arms in maintaining contact with the torque handle. The subject was able to maintain the positive torque output until his body rotated between 90 to 135 degrees. Throughout the torque application phase the subject did not execute equal force with each hand. Depending upon the subject's physical coordination and rotary position, he was likely to pull or push harder first with one hand and then the other. In many cases this produced the minor peaks which were superimposed on the major torque pulse trace.

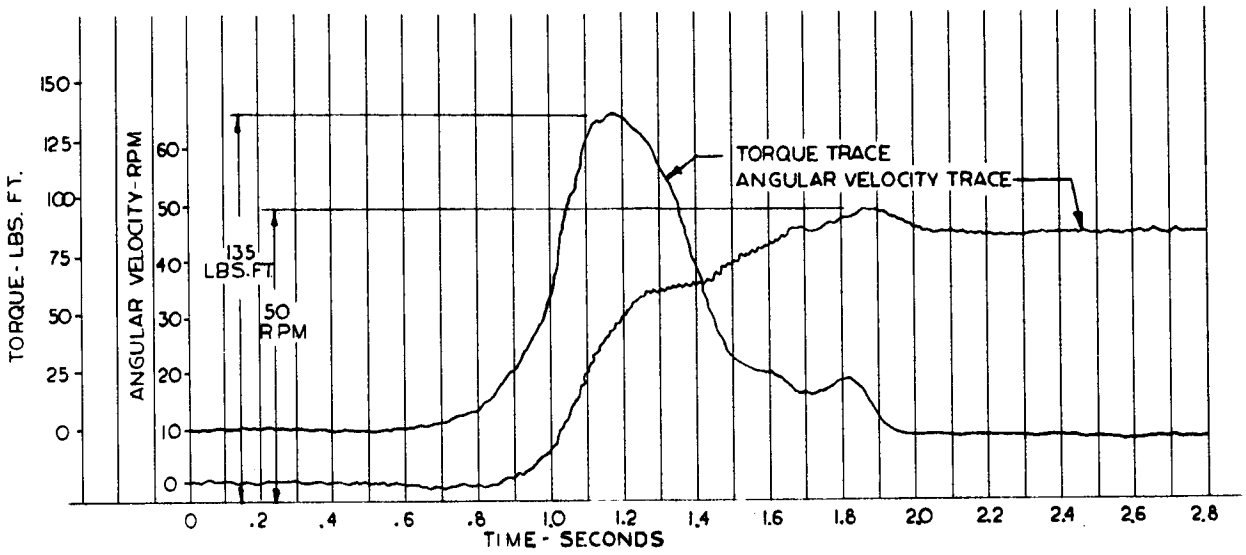

SUPINE TEST POSITION

FIG. C3

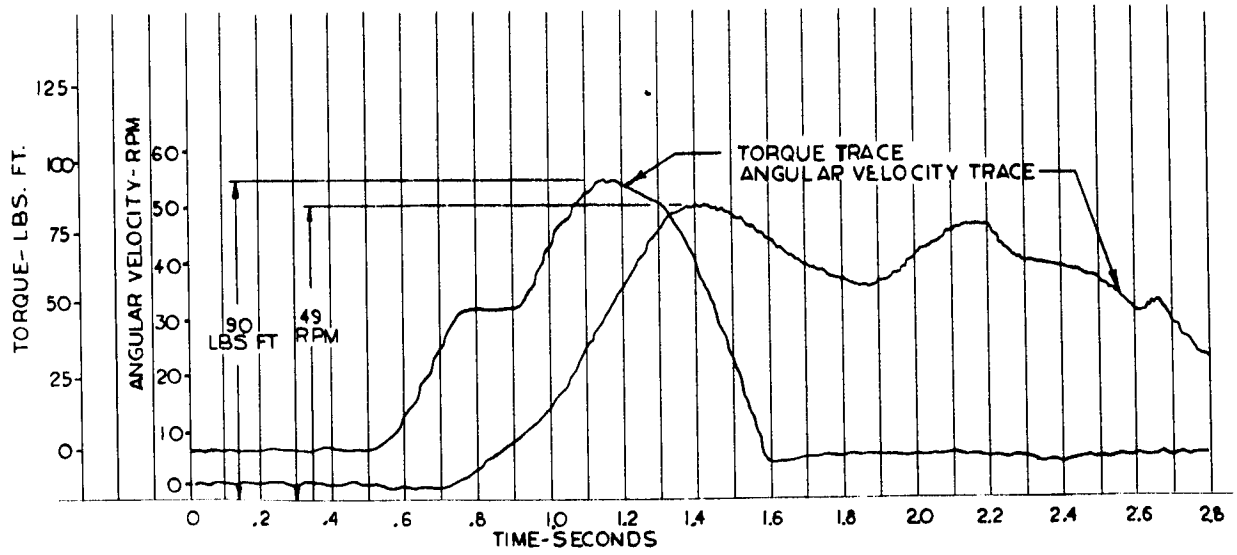

SUPINE TEST POSITION

FIG. C 4

Yaw Axis Tests - Standing Test Position

A typical torque pulse recorded in the standing position is shown in Figure C-5. The oscillatory pattern of the angular velocity trace is clearly seen in this figure. Following the angular velocity peak which was 102 RPM, there was a momentary decrease to 50 RPM followed by a low frequency oscillation in the area of 75 RPM.

Figures C-6 and C-7 demonstrate distinctly different patterns of torque application. In Figure C-6, the subject achieved a high torque level in the very short period of less than 0.2 seconds. The major part of the decay phase was also of short duration. In Figure C-7, the subject increased his torque application effort at a leisurely rate requiring over 0.7 seconds to reach the peak torque value.

A trace having a very low resultant angular velocity is shown in Figure C-8. This velocity trace was unusual for the standing position tests because there was practically no oscillation. This was due to the subject's ability to stabilize his center of gravity near the axis of rotation and to minimize torsional spring characteristics of the body in the standing position. The degree of difficulty in maintaining stabilization in the standing position increased as the angular velocity increased so it was not surprising that the relatively stable trace shown in Figure C-8 represented a very low angular velocity.

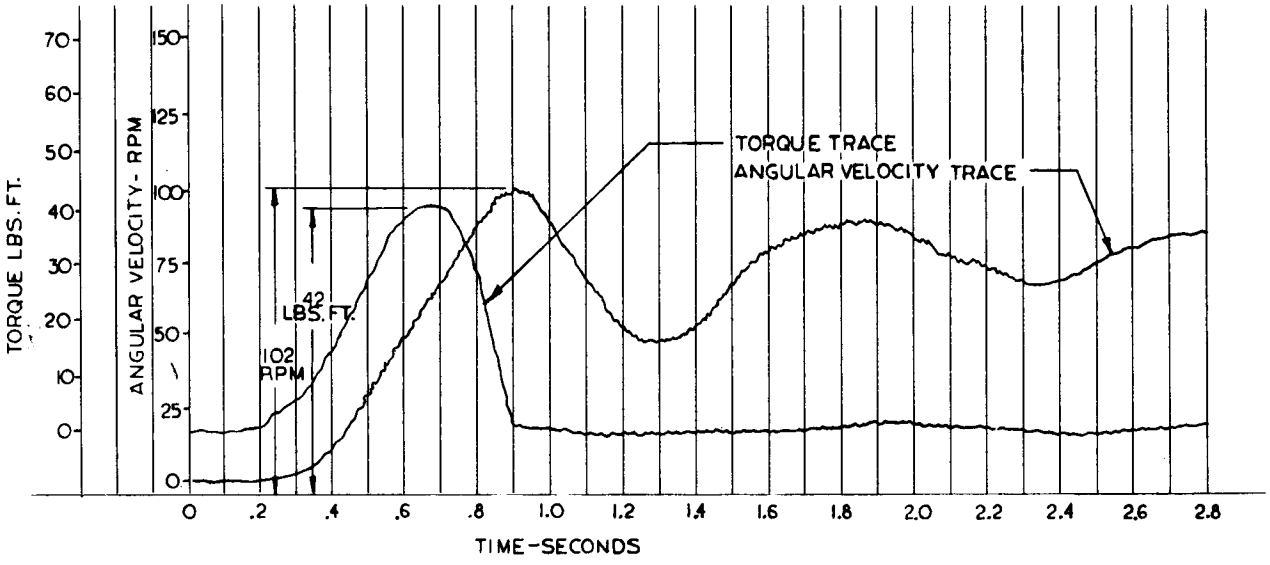

STANDING TEST POSITION
FIG. C5

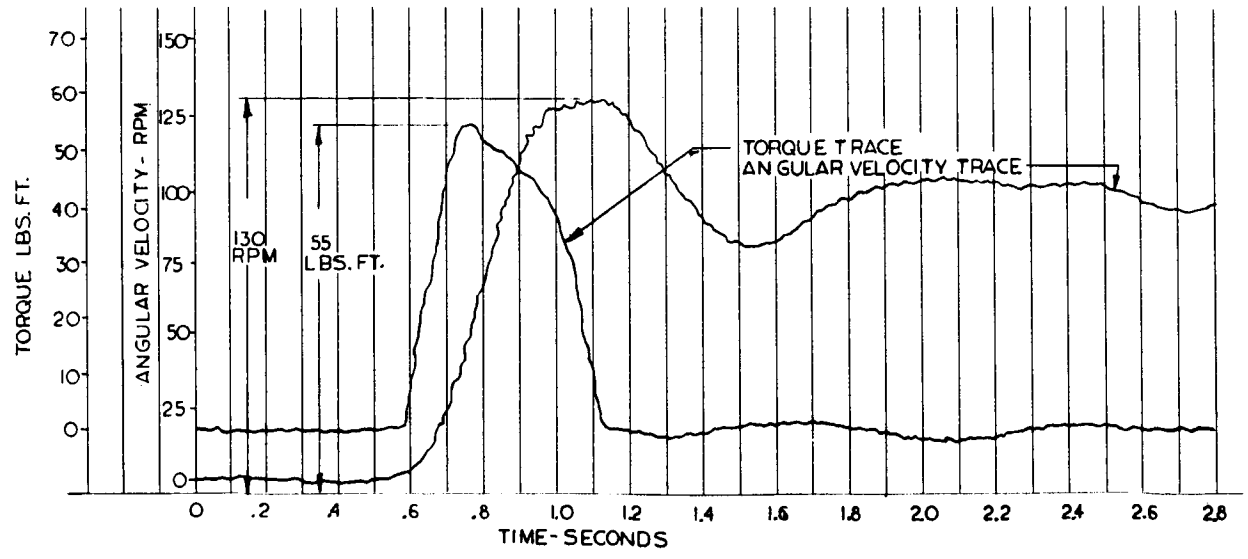

STANDING TEST POSITION
FIG. C6

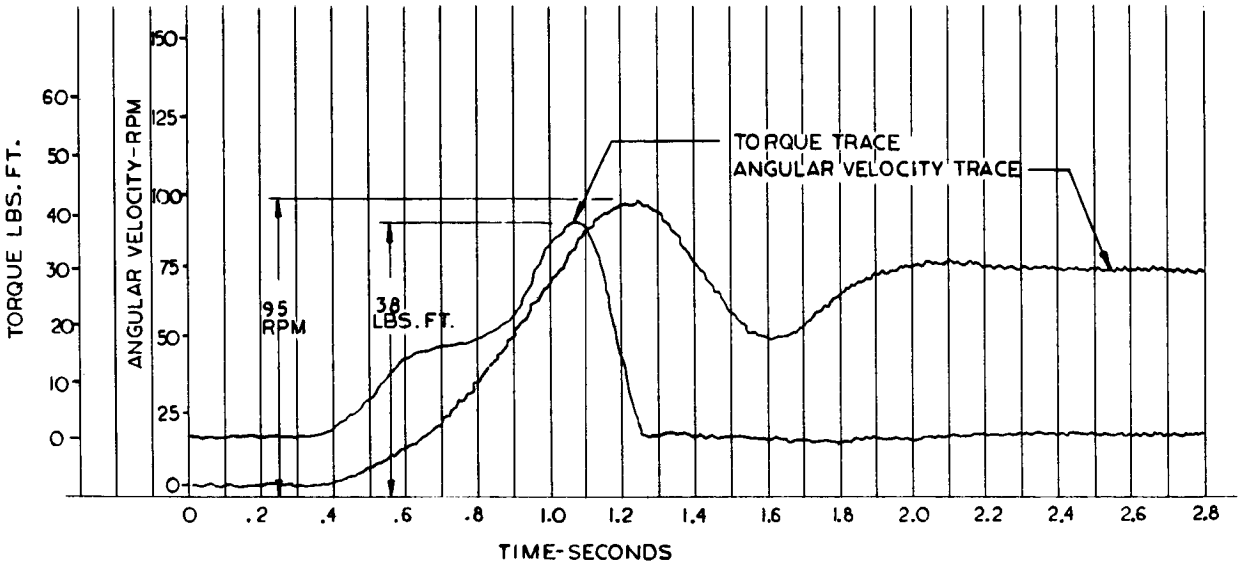

STANDING TEST POSITION

FIG. C7

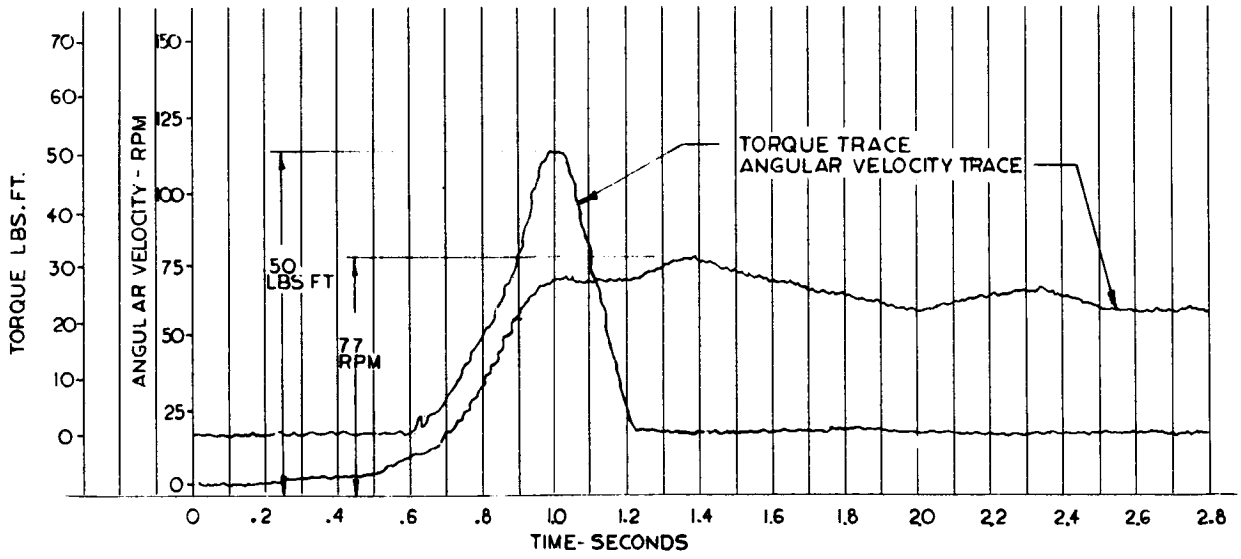

STANDING TEST POSITION

FIG. C8